MODELLING AND DETECTION OF FAULTS IN AXIAL-FLUX PERMANENT MAGNET MACHINES

By: Oladapo Omotade Ogidi

Thesis submitted to the Department of Electrical Engineering, University of Cape Town, in complete fulfilment of the requirements for the degree of Doctor of Philosophy

December 2015

Declaration

This dissertation is submitted to the Department of Electrical Engineering, University of Cape Town, in complete fulfilment of the requirements for the degree of Doctor of Philosophy. It has not been submitted before for any degree or examination at this or any other university. The author confirms that this thesis is based on his own work, save for which is duly referenced. Portions of this work have been published in peer reviewed journals and at refereed international conferences.

Acknowledgments

To the Blessed Trinity, my strength, a heart of worship.

To my esteemed supervisor, Prof Paul Barendse for his patience, guidance and technical contributions, a heart of gratitude.

To my co-supervisor, Prof Mohamed Khan for his support and encouragement, a heart of gratitude.

To Mr. Chris Wozniak and Mr. Philip Titus for their technical support and directions in the laboratory, thank you.

To my colleagues in the AMES research group, Department of Electrical Engineering, University of Cape Town, your valuable insights are highly appreciated.

To my family, especially my parents who toil that I may live, a heart of love.

Abstract

The development of various topologies and configurations of axial-flux permanent magnet machine has spurred its use for electromechanical energy conversion in several applications. As it becomes increasingly deployed, effective condition monitoring built on reliable and accurate fault detection techniques is needed to ensure its engineering integrity. Unlike induction machine which has been rigorously investigated for faults, axial-flux permanent magnet machine has not. Thus in this thesis, axial-flux permanent magnet machine is investigated under faulty conditions. Common faults associated with it namely; static eccentricity and interturn short circuit are modelled, and detection techniques are established. The modelling forms a basis for; developing a platform for precise fault replication on a developed experimental test-rig, predicting and analysing fault signatures using both finite element analysis and experimental analysis.

In the detection, the motor current signature analysis, vibration analysis and electrical impedance spectroscopy are applied. Attention is paid to fault-feature extraction and fault discrimination. Using both frequency and time-frequency techniques, features are tracked in the line current under steady-state and transient conditions respectively. Results obtained provide rich information on the pattern of fault harmonics. Parametric spectral estimation is also explored as an alternative to the Fourier transform in the steady-state analysis of faulty conditions. It is found to be as effective as the Fourier transform and more amenable to short signal-measurement duration. Vibration analysis is applied in the detection of eccentricities; its efficacy in fault detection is hinged on proper determination of vibratory frequencies and quantification of corresponding tones. This is achieved using analytical formulations and signal processing techniques.

Furthermore, the developed fault model is used to assess the influence of cogging torque minimization techniques and rotor topologies in axial-flux permanent magnet

machine on current signal in the presence of static eccentricity. The double-sided topology is found to be tolerant to the presence of static eccentricity unlike the single-sided topology due to the opposing effect of the resulting asymmetrical properties of the airgap. The cogging torque minimization techniques do not impair on the established fault detection technique in the single-sided topology. By applying electrical broadband impedance spectroscopy, interturn faults are diagnosed; a high frequency winding model is developed to analyse the impedance-frequency response obtained.

Contents

List of Tables

List of Figures

Nomenclature

ADC	Analog to Digital Converter
AFPM	Axial-Flux Permanent Magnet
AI	Artificial Intelligence
ANN	Artificial Neural Networks
BNC	British Naval Converter
CM	Condition Monitoring
COM	Common
CTMTs	Cogging Torque Minimization Techniques
CWT	Continuous Wavelet Transform
DAQ	Data Acquisition
DE	Dynamic eccentricities
DS	Double-Sided
DTFT	Discrete-Time Fourier Transform
DWT	Discreet Wavelet Transform
EIS	Electrical Impedance Spectroscopy
EPV	Extended Park's Vector
ESPRIT	Estimation of Signal Parameters via Rotational Invariance Technique
FEA	Finite Element Analysis
FEM	Finite Element Method
FFT	Fast Fourier Transform
FLS	Fuzzy Logic Systems
FSCW	Fractional Slot Concentrated Winding
GA	Genetic Algorithm
GAF	Generalized Ambiguity Function
GCD	Greatest Common Divisor
HF	High Frequency
HHT	Hilbert Huang Transform
IDWT	Inverse Discrete Wavelet Transform
IEPE	Integrated Electronics Piezo Electric
I/O	Input/Output
ISC	Interturn Short Circuit
ISO	International Standard Organization
MCSA	Motor Current Signature Analysis
MEC	Magnetic Equivalent Circuit
MMF	Magneto Motive Force
MUSIC	Multiple Signal Classification
MWFA	Modified Winding Function Approach
NI	National Instruments

PV	Park Vector
PM	Permanent Magnet
PWM	Pulse Width Modulation
PSD	Power Spectral Density
SE	Static Eccentricity
SNR	signal–to–noise ratio
SPWVD	smoothed pseudo Wigner-Ville distribution
SS	Single-Sided
STFT	Short-time Fourier Transform
TFR	Time Frequency Representation
UMP	Unbalanced Magnetic Pull
VA	Vibration Analysis
VI	Virtual Instrument
WFA	Winding Function Approach
WPD	Wavelet Packet Data
WT	Wavelet Transform
ZAM	Zhao-Atlas-Marks
2D	Two-Dimensional
3D	Three-Dimensional

List of Symbols

$x[n]$	Discrete time signal
$X[k]$	Discrete Fourier transform
N	Operator N
$w[n]$	window function
H	Hilbert transform
$E(t)$	Envelope of analytical signal
$\varphi(\xi,\tau)$	Transformation's Kernel
Q or N_s	Number of slots
p	Number of poles
g	Airgap length
g_{max}	Airgap length (maximum)
g_{min}	Airgap length (minimum)
$g_e(\varphi)$	Effective length of airgap in the presence of static eccentricity
D	Outer diameter of the AFPM machine
ϵ_s	Index for static eccentricity
γ	Deflection angle
β	Deflection angle
α_{skew}	Skewing angle
ψ^v	Flux linkage in harmonics, v
v	Space harmonic order
θ	Rotor position
s_{sk}	Skew pitch ratio
τ_p	Pole pitch ratio
$k^v{}_{sk}$	Skew pitch factor of harmonics, v
$k^v{}_p$	Winding pitch factor of harmonics, v
$k^v{}_d$	Winding distribution factor of harmonics, v
T_{cogg}	Cogging torque
T_r	Total torque ripple
T_{MMF}	Torque ripple due to MMF harmonics
T_{av}	Average Torque
T_{max}	Maximum torque
T_{min}	Minimum torque
m	Number of phase
k	Integer constant
q	Slots per pole per phase
f_{SE}	Static eccentricity fault frequencies
f_1	Fundamental frequency in line current
f	Frequency of line current

R_{XX}	Correlation matrix
R_{XY}	Mutual correlation matrix
E	Mathematical expectation
Hi	Mathematical conjugation
B	Magnetic flux density
$\mathcal{F}(\theta, t)$	Airgap MMF
$\mathcal{F}_1$	Stator MMF
$\mathcal{F}_2$	Rotor MMF
$\Lambda(\theta, t)$	Airgap permeance
t	Time
M_1	Mutual inductance
L	Inductance
V	Stator voltage
I	Stator current
i_f	Fault current
R	Stator resistance
r_f	Fault resistance
T_e	Electromagnetic torque
i_d	d-axis current
i_q	q-axis current
L_d	d-axis inductance
L_q	q-axis inductance
v_{sh}	Slot harmonics
f_s	Sampling frequency
f_v	Frequencies of space harmonics, v
$x(t)$	Continuous time signal
$y(t)$	Hilbert transform of $x(t)$
$\vec{x}(t)$	Analytical signal
$i(t)$	Current signal
f_{ISC}	ISC fault frequencies
$\bar{\imath}(t)$	Hilbert modulus of current signal
$\emptyset_v$	Phase angle of space harmonics, v
$\emptyset_1$	Phase angle of fundamental harmonics
$\emptyset_{ISC}$	Phase angle of ISC fault harmonics
E	EMF of stator
F_n	Normal component of magnetic force
F_t	Tangential component of magnetic force
B_n	Normal component magnetic flux density
B_t	Tangential component magnetic flux density
B_m	Analytical expression of B_n
m_0	Mode number
f_{m_0}	Natural frequency at different modes

K_r	Lumped stiffness of stator
M_r	Lumped mass of stator
F_2	Frequency of the second magnetic force harmonic
F_{line}	Vibrating frequencies related to the line current/voltage
w_r	Rotor angular velocity

Chapter 1
Introduction

1.1 Introduction

Renewable energy and energy-efficient devices have been proposed as sustainable solutions to environmental pollution caused by fossil fuel and the challenges of its depleting reserve. In providing and improving these solutions, innovations need to be explored and accelerated in the development of electric machines since loads coupled to them account for over 60% of the world's electrical energy utilization and they are the key electromechanical energy converters in prevalent renewable applications such as wind turbines and electric vehicles. Traditionally, induction machines have been extensively deployed in these applications but due to advancements in power electronics converters and permanent magnet (PM) materials, other electrical machine configurations have also been developed and are increasingly being deployed. Prominent among these configurations is the axial-flux permanent magnet machine. The 'axial-flux machine' refers to the propagation of flux in the axial rather than the radial direction. The use of permanent magnets in combination with the axial-flux configuration leads to a combined concept referred as the 'axial-flux permanent magnet' (AFPM) machine. It has been found to be a more adequate and competitive solution in applications where the machine length is limited by the space, or where it is possible to integrate the rotor directly into the driven machinery, and also, where variable speed, torque and power densities are prime. Thus, AFPM machines are now widely used in a variety of applications, from power generation to transportation, wherever axial compactness coupled with high torque density and high efficiency is

required such as; hybrid electric vehicles, wind energy generation, high and low speed power generators, ship and aircraft propulsion, combined heat and power, washing machines, etc. Despite the noteworthy development of AFPM machine and its increasing applications, it has not been rigorously studied for fault diagnosis. Fault investigations will aid in maintaining its engineering integrity and developing condition monitoring (CM) strategies, thus guaranteeing improved performance, increased life time and lower cost of operation.

1.2 Problem Statement

The studies of electric machine behaviour during abnormal conditions due to the presence of faults and the possibility to detect such abnormalities in real-time is a challenge to electrical engineers and researchers. The methods available for analysing and diagnosing faults in electric machines have shortcomings. Some of these methods include current analysis, axial-flux monitoring, temperature monitoring, chemical analysis, noise and vibration analysis. Flux monitoring is expensive and invasive but gives qualitative information on the state of health of electrical machine. Although expensive sensors or specialised tools are required by vibration analysis (VA), it remains the most established and commonly used approach for detecting mechanical faults. Electrical quantities such as current and voltage are readily measured by tapping into the existing transducers (voltage and current transformers) that are already installed as part of the protection, control or instrumentation system. As a result, current monitoring is non-invasive and cheap, thus, the method known as motor current signature analysis (MCSA), based on stator current monitoring is also commonly used for detecting faults. However, it has poor fault discriminatory ability. Both VA and MCSA are usually based on Fourier transform, in particular, the fast Fourier Transform (FFT) since it is easy to implement and represents the spectra understandably. However the applications where AFPM machines are deployed are characterized by transients, making the FFT method suffer in reliably when detecting faults since it is unable to

accurately represent signals with non-periodic components and also requires long period of signal acquisition to ensure high frequency resolution. Also, PM machines are typically designed with non-overlapping concentrated windings, a winding configuration inherently rich in voltage and current harmonics content. Thus it becomes more difficult and demanding to detect faults in them using MCSA as the harmonics overshadow vital and potential fault signatures. These are challenges to overcome in developing reliable fault detection techniques in AFPM machine.

1.3 Aim and Objectives

The aim of this thesis is to analyse fault types, failure modes and develop fault detection techniques for AFPM machine to reduce downtime and ensure engineering integrity.

The objectives are:

1. Survey renewable energy industry where electrical machines are deployed for current trends and future outlook.
2. Investigate the common faults associated with AFPM machines, their causes and frequency of occurrence.
3. Analyse and investigate the 3D electromagnetic behaviour of a healthy and faulty AFPM machine by means of finite element analysis (FEA).
4. Model machine fault scenarios and identify the parameters which are most sensitive to the particular fault.
5. Determine the most suitable signal processing technique for a particular fault.
6. Establish baseline and criteria for fault detection and discrimination.
7. Explore the impact of different rotor configurations and their tolerance for faults.
8. Develop a procedure for condition monitoring and fault prediction strategies for AFPM generators.

9. Obtain valuable indices for further improvements in design to reduce fault occurrence.

1.4 Research Questions

The research questions answered in this thesis are:

1. What are the indicators of PM machine faults?
2. What is the level of information richness of these indicators?
3. How credible are these indicators to prevent false alarms?
4. How can discrimination between faults be realized?
5. What advanced signal processing techniques can be used for detection during non-stationary operation?
6. How can prompt detection of faults be realized before the initiation of failure actions?
7. Which rotor configuration provides the greatest immunity to faults?
8. How will the answers to Q1-7 influence the factors to be considered when selecting most appropriate condition monitoring technique for AFPM machines?

1.5 Scope

This thesis focused on the frequent and typical fault types associated with the AFPM machine namely; static eccentricity (SE) and interturn short-circuits (ISC). The effects of these faults on current, torque and vibration are investigated and discrimination between faults is sought. Indices for fault type, degree and detection are introduced; derived through simulation and experimentation. The impact of different rotor configuration and cogging torque minimization techniques is also explored and the ability to diagnose during transient condition is investigated.

1.6 Research Outputs

The refereed conference (C) and peer-reviewed journal (J) publications from this thesis are:

C1. Ogidi, O.O.; Barendse, P.S.; Khan, M.A., "Development of a test rig for eccentricity fault studies on an axial-flux permanent magnet (AFPM) wind generator," *International Conference on Electrical Machines (ICEM'14),* Berlin, Germany, Sept 2014.

C2. Ogidi, O.O.; Barendse, P.S.; Khan, M.A., "Detection of Static Eccentricity Faults in AFPM Machine with Asymmetric Windings using Vibration Analysis," *International Conference on Electrical Machines (ICEM'14)* Berlin, Germany, Sept. 2014.

C3. Ogidi, O.O.; Barendse, P.S.; Khan, M.A., "Effects of Rotor Topologies on Axial-Flux Permanent Magnet Machine under Static Eccentricities" *IEEE Energy Conversion Congress and Expo (ECCE'15)*, Montreal, Canada, Sept 2015.

C4. Ogidi, O.O.; Barendse, P.S.; Khan, M.A., "The Detection of Interturn Short Circuit Faults in Axial-Flux Permanent Magnet Machine with Concentrated Windings" *IEEE Energy Conversion Congress and Expo (ECCE'15)*, Montreal, Canada, Sept 2015.

C5. Ogidi, O.O.; Barendse, P.S.; Khan, M.A., "Detection of Interturn Short Circuit Faults in Axial-Flux Permanent Magnet Machines Using Electrical Impedance Spectroscopy" *IEEE Energy Conversion Congress and Expo (ECCE'16)*, Milwaukee, US, Sept 2016 (*Submitted*).

J1. Ogidi, O.O.; Barendse, P.S.; Khan, M.A, "Detection of Static Eccentricity Faults in AFPM Machine with Concentrated Windings Using Vibration Analysis" *IEEE Transactions on Industry Applications* Nov/Dec 2015.

J2. Oladapo Omotade Ogidi, Paul S. Barendse, Mohamed A. Khan, Fault Diagnosis and Condition Monitoring of Axial-Flux Permanent Magnet Wind Generator, *Electric Power Systems Research* (*Accepted*).

J3. Ogidi, O.O.; Barendse, P.S.; Khan, M.A., "Effects of Rotor Topologies on Axial-Flux Permanent Magnet Machine under Static Eccentricities" *IEEE Transactions on Industry Applications* (*Submitted*)

J4. Ogidi, O.O.; Barendse, P.S.; Khan, M.A., "The Detection of Interturn Short Circuit Faults in Axial-Flux Permanent Magnet Machine with Concentrated Windings" *IEEE Transactions on Industry Applications* (*Submitted*)

1.7 Organisation and Scientific Contributions of the Thesis

The research constituted an overall approach to the modelling and detection of faults in AFPM machine. Naturally, such an approach involves the task of reviewing relevant literatures, surveying industry standards, trends and practical implementation of faults in a specific and controllable manner. After inducing such faults, then follows testing, measurement, and the actual detection becomes a challenge. However, the chapters in this thesis are not arranged to follow the actual historical course of the study but a flow based on the modelling techniques and method of fault diagnostics adopted.

Chapter 2 presents the overview, rationale, theory development and analysis of fault detection methods and condition monitoring (CM) strategies used in electric machines. The merits and demerits of various methods are identified. It concludes by justifying the use of the methods applied for fault detection in this thesis.

In chapter 3, the common faults associated with AFPM machines are discussed. The development of an experimental rig for fault investigations and online CM system of the prototypes used in experimentation is also presented. The realizations of the developments are in-situ capability, accuracy of the fault replication techniques, integrity of the measuring instrumentation and measurement procedures.

In chapter 4, background of AFPM machine topologies is provided and the state-of-the art in detecting SE in AFPM machine is presented in the introduction. SE in AFPM machines is modelled using 2D-plane and finite element analysis (FEA). Subsequently, the influence of rotor topologies and various cogging torque minimization techniques on torque and current harmonics in the presence of SE is investigated. Detection

technique is proposed for SE using MCSA and discrimination from other rotor faults is sought. Finally, an alternative spectral estimation technique to FFT is investigated for the MCSA method.

The detection of ISC is presented in chapter 5. The state-of-the art in the detection of ISC faults in PM machines is presented in the introduction. Using FEA and mathematical formulations, the machine performance is predicted and subsequently verified experimentally. Attention is paid to fault-feature extraction and fault discrimination. Using frequency and time-frequency techniques, the fault-features are tracked in steady and transient conditions respectively.

In chapter 6, SE is detected using VA. In the introduction, a critical review of VA for fault detection in electrical machine is presented. VA is perused as an alternative to MCSA since SE is mechanical related. Vibratory tones triggered by the fault are tracked in both stationary and non-stationary conditions using signal processing techniques and detection techniques are proposed.

The feasibility of electrical impedance spectroscopy (EIS) to detect ISC is investigated in chapter 7. An experimental scheme for performing the EIS and the algorithm for determining the impedance-frequency response are presented. Impedance-frequency response of both healthy and ISC scenarios are obtained and a high frequency (HF) winding model is derived to analyse the impedance-frequency response obtained.

Finally, chapter 8 concludes this thesis by summarizing the main findings and presenting some concluding remarks. Some directions for future research are recommended.

Chapter 2
Fault Diagnosis and Condition Monitoring of Electrical Machines

2.1 Introduction

This chapter presents a review of the state-of-the-art in fault diagnostic strategies and condition monitoring of electrical machines. First, it discusses the basis and need for online fault diagnostics for electrical machines. It then presents a review of the commonly monitored fault-indicating parameters and their methods of analysis alongside the guiding philosophy. The benefits and drawbacks associated with various fault-indicating parameters and their methods of analysis are identified. The theoretical development of these methods for both stationary and non-stationary conditions of machine operation are also discussed. It concludes by identifying the best fault-indicating parameters to be monitored and the methods to be used to diagnose the faults to be investigated.

2.2 Basis and Benefits of Condition Monitoring

Electrical machines are designed to have electrical and mechanical symmetry in the stator and rotor for better coupling and higher efficiency. A fault condition will influence this symmetrical property and induce abnormal symptoms during operation such as; mechanical vibration, excessive temperature increase, irregular airgap torque,

acoustic noise, instantaneous output power variation, change in voltage, change in current, speed variations, increased losses, higher torque pulsation and lower average torque [1]-[6]. These abnormal symptoms have been known to have specific patterns pertaining to the machine conditions and severity, such as particular frequency, duration, amplitude, variance, degree and phase. Based on monitoring and analysing the expected symptoms and their specific patterns, many fault detection techniques have been proposed [5]-[7]. These techniques have mostly been applied to induction machines [2],[5],[8]-[10], but few have been on applied to PM machines, thus presenting an opportunity to better understand the impact of the faults specific to AFPM machines with the intention of the detecting them before occurrence. As the deployment of AFPM machines increase [11]-[12], an effective and efficient fault diagnostic strategy is needed to ensure safe and reliable operation [5]. Some of the identified benefits of condition monitoring are [1]-[3], [5]-[7]:

- Early detection of deterioration to avoid catastrophic failure;
- Accurate damage evaluation to enable cost-effective maintenance practice (proactive maintenance);
- Increased energy availability or reduced downtime and maintenance costs;
- Root cause analysis to recommend improvements in component design or equipment operation and control strategies.

2.3 Fault Indicators in Electrical Machines

Generally, online CM and diagnosis require the sensing and analysis of signals that contain specific information (symptoms) which is characteristic of the degradation process, problem, or fault to be detected. Due to the wide variety of physical phenomena to be found in electric machines, several fields of science and technology need to be considered when designing and developing competitive monitoring and diagnostic systems. For example, Fig.2.1 [13] illustrates the complexity of the

interactions of physical phenomena characteristic of a general electromagnetic energy converter structure. Electrical, mechanical, thermal, fluid flow and motion interact in a complex manner, as depicted in the figure. Various parameters belonging to these fields may be found to be suitable fault indicators for an electrical machine [1], [4]-[7]. Some of the indicators are given in Table 2.1 [14], being representative of any type of electrical machine, providing useful information for possible fault identification. It presents the following:

1. Type of instrumentation required to monitor some machine parameters.
2. The degree of accuracy of fault indication that may be obtained when relying on a specific parameter.
3. The level of expertise an operator needs in order to interpret the recorded data.
4. How invasive a dedicated sensor for each fault indicator would be.
5. Possible means of analysis (signal processing techniques).

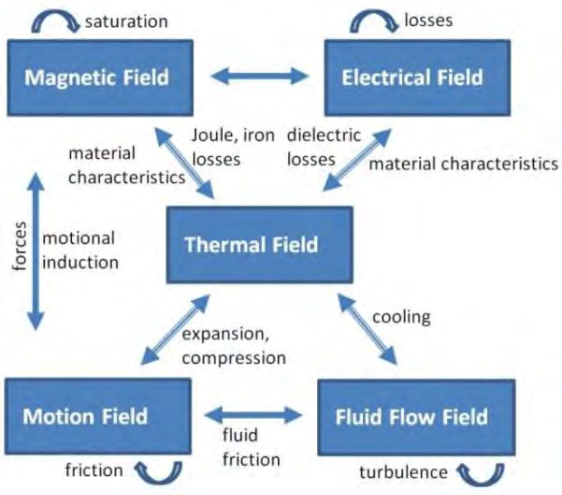

Fig.2.1. Interactions of physical phenomena characteristic for a general electromagnetic energy converter structure

Table 2.1. Fault indicators in electrical machines

Parameter	Measurement device	Potential information richness	Intrusive to Electrical machine	On/Off line	Operator skill required	Measurement frequency	Measured as part of control strategy	Possible means of analysis
Current	Hall effect transducer	Average	No	On	High	Continuous	Yes	RMS trending, phase relationship, spectrum analysis, statistical methods
Voltage	DVM	Average	No	On	High	Continuous	Yes	RMS trending, phase relationship, spectrum analysis, statistical methods
Flux	Search coil Hall effect device	Very High	Yes and No	On	High	Hourly	No	RMS trending, time analysis, spectrum analysis, statistical methods
Force	Dynamometer	Very High	No	On	High	Continuous	No	RMS trending, time analysis, spectrum analysis, statistical methods
Vibration	Accelerometer	High	Yes and No	On	Expert	Hourly	No	spectrum analysis, statistical methods
Acoustics	Microphone	High	No	On	Expert	Hourly	No	RMS trending, spectrum analysis, statistical methods
Temperature	a. Hand-held probe	Low	Yes and No	Off	Low	Monthly or on suspected deterioration (SD)	No	Trending
	b. Thermal paint	Low	Yes	Off	Low	Monthly or on SD	No	Visual inspection
	c. Thermocouple	Average	Yes	On	Average	Continuous	Yes	Trending
	d. Infrared-red camera	High	No	On	Expert	Monthly or on suspected deterioration	No	Visual inspection and trending
Instantaneous angular speed	Encoder	Average	No	On	High	Continuous	Yes	Peak to peak variation
Torque	Torque sensors (magneto-elastic, piezoelectric, strain gauge)	High	No	On	Expert	Continuous	Yes and No	RMS trending, spectrum analysis, statistical methods

In [5], [7], [15]-[20], these parameters are generally categorised as:

1. Mechanical: vibration, acoustic noise, speed fluctuations.
2. Electrical: voltage, current.
3. Electromagnetic: flux, electromagnetic leakage fluxes, surges, and partial discharges, torque.
4. Others: temperature, oil particle, gas in oil analysis etc.

Operators of electric machines pay special attention to the temperature monitoring since the basic rule is that 'every additional 10°C causes a winding to deteriorate twice as fast as when the operation takes place in the allowable temperature range', [7] which represents a very serious concern for the healthy operation of machines. Other components of electrical machines may be irreversibly affected by higher temperatures; the case of magnets in a PM machine is a good example. The magnetic characteristics of PMs are temperature-dependent and a high temperature may lead to irreversible demagnetisation of the magnets [18], [21]. Temperature monitoring devices such as thermal imaging are installed to monitor temperatures and to look for abnormally hot spots [22]. Vibration monitoring has historically been the foundation of most online condition monitoring programs [17], [23]-[29] but new techniques such as those involving spectral analysis of the electric line current powering the motor are now of significant interest [5]. The main problem concerning the monitoring of vibration is that it requires expensive sensors and may sometimes be invasive, requiring transducers to be fitted in or around the machine, with an obvious interruption to operation. This may be a practical problem in terms of machine design and approval by the manufacturer, operator, or safety legislation authority [19]. Intrusiveness and cost is also a drawback to some other parameters, for instance, rotor speed, torque and flux.

To date, current monitoring is the most attractive to CM strategy [5]-[6], [9]-[10]. It makes use of the winding as the search coil and the needed transducers are usually installed by default for machine control or protection purposes. As a consequence, a

variety of techniques based on current spectrum are applied to today's cost-effective microprocessor hardware platforms in order to accurately diagnose impending failures of electrical machines. Despite the success of current monitoring at diagnosing faults, some drawbacks are [27]-[29]:

1. Ineffective discrimination between different faults, since abnormalities and time harmonics may end up generating similar signatures.
2. The current spectrum is influenced not only by fault conditions but also by other factors, including the supply, static and dynamic load conditions, noise, machine geometry, and these conditions may lead to errors in fault detection.
3. In order to facilitate the successful detection of rotor faults during steady state operation, a large supply current needs to flow. This large current is usually obtained by monitoring the machine while it is running under full load conditions. There are certain situations, however, when this requirement is impractical, for example, if the machine has been taken off-line or removed to a workshop environment.

2.4 Methods of Analysing the Fault Indicators

Fault analysis and detection techniques have been developed for the indicators discussed in the previous section using different methods. The methods adopted in literature and industry to derive them can be grouped into four categories namely; signal-based, model/simulation-based, machine theory-based and artificial intelligence-based [5]. The sub-types of each category are listed in Fig.2.2 [1]-[10], [14]-[20]. The theoretical development of these methods is examined in this section.

2.4.1 Signal-Based

The signal-based method is the most extensively used and it makes use of standard and advanced digital signal processing techniques for both steady-state and transient regimes of machine operation. It is used to find a simple and effective transform of the

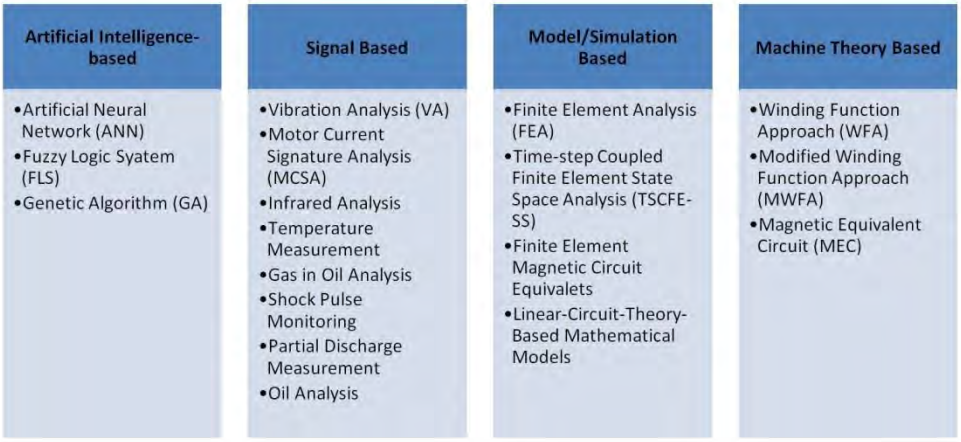

Fig.2.2. Methods of analysing fault indicators in electrical machines

original signal. The important information contained in the signal can be shown and the dominant features can be extracted for fault detection. Standard digital techniques are applied in the frequency domain, assuming a stationary signal, and in the joint time-frequency domain for non-stationary signals. Standard signal processing techniques such as discrete Fourier transform (DFT), fast Fourier transform (FFT) and short-time Fourier transform (STFT) have been used for fault detection and condition monitoring of electric machines for decades [30]-[34]. The FFT is the typical tool applied under stationary conditions to implement the Fourier transform and extract harmonics or frequency components in a machine parameter (usually line current) being monitored. There has been a substantial amount of research on the development of various steady-state condition monitoring techniques utilizing the Fourier transform [1]-[10], [14]-[20], [30]-[34]. However, in electric machines, most multi-components (distorted) waveforms are transients or time-varying and are usually as a result of load or supply voltage or current steep changes [5], [35]-[36]. Transient signals are short time events, whose time behaviour cannot be predicted and are totally varying in nature, both in time, frequency and other parameters. A variety of alternative schemes to analyse the properties of non-stationary signals have been developed to improve the description of their frequency domain content. Each of these techniques has its own particular domain of application which addresses certain problems, but not all, encountered in

the analysis of non-stationary signals [5], [10]. The domain of analysis is time-frequency and there are two basic approaches to its analysis. The first approach is to initially cut the signal into slices in time, and then to analyse each of these slices separately to examine their frequency content; mapping of a one dimensional signal $x(t)$ to a two dimensional function of the time and frequency and therefore are able to provide a true time-frequency representation $TFR\ (x: t, f)$ of signal $x(t)$ [36]. Another approach is to first filter different frequency bands, and then cut these bands into slices in time and analyse their energy content. The first of these approaches is used for the construction of the STFT, the Wigner-Ville distribution (WVD) and its variant, smoothed pseudo Wigner-Ville distribution (SPWVD), while the second leads to filter-bank methods and to the wavelet transform (WT). The signal processing technique will be discussed in further detail in the proceeding subsections.

2.4.1.1 Fourier Transform

In steady state, non-parametric spectral estimation using Fourier transform is commonly applied to transform the signal to the frequency domain for further analysis [35]. In signal processing, the Fourier transform $X(f)$ of a continuous time signal $x(t)$ is commonly defined as in (2.1), the discrete counterpart of the Fourier transform is the discrete-time Fourier Transform (DTFT). The DTFT of a discrete time signal $x[n]$, is a function of continuum of frequencies, unlike the continuous case, the DTFT is always periodic with period 2π. A transform of a discrete-time signal that is a function of finite number of frequencies is called a discrete Fourier transform (DFT). The DFT can be viewed as "discretization in frequency" of the DTFT. The discrete Fourier transform $X[k]$ of the sampled signal $x[n]$, where $k = 0, 1, \dots N-1$ is given in (2.2).

$$X(f) = \mathfrak{F}\{x(t)\} = \int_{-\infty}^{\infty} x(t) e^{-j2\pi ft}\, dt \tag{2.1}$$

$$X[k] = \sum_{n=0}^{N-1} x[n] e^{-j\left(\frac{2\pi}{N}\right)kn} n \tag{2.2}$$

The direct evaluation of $X[k]$ requires N^2 multiplications, this can result in a great deal of computation if N is large. However, using the fast Fourier transform FFT algorithm to compute $X[k]$ requires an order of $(Nlog_2N)/2$ multiplications. This is a significant decrease in the N^2 multiplications required in DFT computation, thus the FFT is a computationally-efficient method for determining the DFT of $x[n]$ [36]. The FFT improved the computational efficiency of the Fourier transform of a signal represented by discrete data points. However, despite the functionality of the Fourier transform, especially in regard to obtaining the spectral analysis of a signal, there are several shortcomings to this technique. The first of these is the inability of the Fourier transform to accurately represent functions that have non-periodic components that are localized in time or space, such as transient impulses. This is due to the Fourier transform being based on the assumption that the signal to be transformed is periodic in nature and of infinite length. Another deficiency is its inability to provide any information about the time structure of a signal, as results are averaged over the entire duration of the signal [35]-[40]. This is a problem when analyzing signals of a non-stationary nature, where it is often beneficial to be able to acquire a correlation between the time and frequency domains of a signal. There is also the problem of spectral smearing or leakage. It substantially affects the results obtained by conventional spectral analysis, but this can be overcome and the quality of the signal improved by multiplying the signal data with a suitable window function $w[n]$; as given in (2.3). The worst shortcoming of the Fourier transform is its limitation in its resolving power, requiring long observation intervals in order to achieve acceptable accuracy and reduced leakage. However, it is simple, robust and gives accurate information about the frequency components of a signal. Thus, it remains industry standard in processing and analysing signals in steady-state.

$$y[n] = x[n] \cdot w[n] \tag{2.3}$$

2.4.1.2 Parametric Method

As previously explained non–parametric spectral estimators such as FFT are greatly limited in that they require long observation intervals in order to achieve acceptable accuracy and reduced leakage. For data sets of short duration, these conventional techniques are not useful, and an alternative approach has been developed. The parametric (model based) spectral estimation, which has proven useful in extracting high resolution frequency spectra from relatively short data sets, providing the structure of the signal is known (*a priori* knowledge) [41]-[48]. The components of a known order related structure can be accurately tracked and extracted from a background of noise and components of an unknown structure. The basic principle is that if a signal depends on a finite set of parameters, then all of its statistical properties including its power spectrum can be expressed in terms of these parameters. This is done using parametric models that relate to the eigenvector decomposition of the correlation matrix to estimate the discrete part of the spectrum [42]. In [43], it was first observed that the zeros of the z–transform of the eigenvector corresponding to the minimum eigenvalue of the covariance matrix, lie on the unit circle, and their angular positions correspond to the frequencies of the sinusoids. In a later development in [45], it was shown that the eigenvectors might be divided into two groups, namely, the eigenvectors spanning the signal space and eigenvectors spanning the orthogonal noise space. The eigenvectors spanning the noise space are the ones whose eigenvalues are the smallest and equal to the noise power. One of the most important techniques, based on the approach in [43] is the separation of the data into noise and signal subspaces namely; the multiple signal classification (MUSIC) [44]-[45] and estimation of signal parameters via rotational invariance technique (ESPRIT) respectively [46]-[47]. The comparison of the two different parametric methods is presented in [48] as shown in Table 2.2; ESPRIT is superior to MUSIC. Parametric spectral estimators have been applied in geophysical seismology, speech technology (speech recognition, coding or compression), communications (code-timing estimation), radar and sonar systems

(localization with sensor array, synthetic aperture radar imaging and feature extraction) and electromagnetics (resonant frequency of cavity) [45]-[47]. Lately, its applications are emerging in power system applications [49]-[50].

2.4.1.3 Short–Time Fourier Transform

The STFT is the most widely used method for analysis of non-stationary signals and can play the role of "benchmark" or a tool for comparison of accuracy of new investigated methods [51]-[55]. It is based on a simple and intuitive concept: the conventional Fourier transform gives no information about the time location of the spectral peaks, because its basis functions are not localized in time. In order to extract such information, one breaks the time–localized signal into smaller time fragments and Fourier–analyze each of the time segments. The sum of such partial spectra shows the time variation of the spectral content of a given signal in time. Temporal window function as in STFT is also applied for different parametric methods in order to obtain time– frequency representations of signals in [53]. When trying to improve the time resolution, it is possible to choose smaller time intervals but up to a certain limit, when the segment spectrum becomes meaningless and without any relation to the true spectral content of the signal. In the case of parametric methods, which allow exact spectral estimation based on very short data sequences, such limitation affects less the results. The problem with the STFT technique is that it provides constant resolution for all frequencies since it uses the same window with constant width for the analysis of the entire signal. This means that if a good frequency resolution using windows is desired,

Table2.2. Comparison between ESPRIT and MUSIC

Method	**Computational Cost**	**Accuracy**	**Risk of False Estimates**
MUSIC	High	High	Medium
ESPRIT	Medium	Very High	None

it would compromise the time resolution [14], [27], [53]. Furthermore, there are no orthogonal bases existing for the STFT, thus difficult to obtain a fast and effective algorithm to calculate the STFT.

2.4.1.4 Hilbert Transform

The Hilbert transform technique is useful for analysing instantaneous frequency content of a signal [54]-[56]. Consider how a real signal $x(t)$ is transformed into the corresponding analytical signal $q[n]$ in (2.4)-(2.8). The Hilbert transform $y(t) = H\{x(t)\}$ of the signal $x(t)$ is obtained using (2.4), where the principle value of the integral is used. Thus, the complex analytical signal $z(t)$ is obtained from both $x(t)$ and y(t) and the envelope $E(t)$ of the analytical signal are derived in (2.6). Now the discrete version of the Hilbert transform of the sampled signal $x[n]$ is given by (2.7). From the Hilbert signal, the instantaneous magnitude of the analytical signal which reflects how much energy changes with time can be created. The fundamental component is therefore shifted to the DC value, and can be removed from the magnitude of the analytical signal by subtracting the mean in (2.8), resulting in the signal $q[n]$.

$$y(t) = \frac{1}{\pi}\int_{-\infty}^{\infty} \frac{x(\tau)}{\tau - t} d\tau \tag{2.4}$$

$$z(t) = x(t) + jy(t) \tag{2.5}$$

$$E(t) = |x(t) + jy(t)| \tag{2.6}$$

$$z[n] = x[n] + jy[n] = x[n] + jH_d\{x[n]\} \tag{2.7}$$

$$q[n] = abs\big(hilbert(x)\big) - mean\left[abs\big(hilbert(x)\big)\right] \tag{2.8}$$

2.4.1.5 Cohen-Class Distributions

The Cohen-class distribution yields a time-frequency energy density. Cohen distribution is a generalized form of phase-space distribution from which all other time-frequency distributions may be derived. Since energy is a quadratic function of a signal,

it distributes the energy of a signal over time and frequency. The general form of the Cohen's class of distributions for a signal *x(t)* is given in (2.9) [57], where *φ(ξ,τ)* is the transformation's kernel that defines the transformation. This equation can be rewritten in terms of the generalized ambiguity function (GAF), A (*ξ, τ: φ*), [59] in (2.10) and GAF is defined in (2.11). For a multi-component signal, the elements of the GAF corresponding to auto-terms are mainly located around the origin, while the interference components are located away from the origin, at a distance proportional to the time-frequency distance between auto-terms. Therefore time-frequency distribution that selects a region around the origin in the ambiguity domain, and reduces to zero away from the origin is suited for analysing machine signals that are time-changing. Well known techniques are WVD, SPWVD, Choi-Williams etc. The WVD has good concentration of time-frequency plane but support areas of the signal do overlap each other, thus interference appears on the time-frequency plane rendering imperfect information about the energy distribution of the signal in the time-frequency domain, and an atomic decomposition of a signal based on the WVD does not exist. Improvement methods such as the Choi-Williams and cone-shaped distribution has been proposed to overcome these shortcomings, however reduction of interference results in reduced frequency resolution [56]-[57]. A TFR technique, Zhao-Atlas-Marks (ZAM) distribution has been proposed to resolve the problem of cross-term artifacts [57] while enabling high frequency resolution and has been applied to electric machine fault diagnosis in [56], [58]. Like the WVD and Choi Williams, it yields a time-frequency energy density while reducing the presence of cross-term interference.

$$D(t,\omega;\varphi) = \iiint e^{j(\xi\mu-\tau\omega-\xi t)}\varphi(\xi,t).f\left(\mu+\frac{\tau}{2}\right)f^*\left(\mu-\frac{\tau}{2}\right)d\mu d\tau d\xi \tag{2.9}$$

$$D(t,\omega;\varphi) = \frac{1}{4\pi^2}\iint A(t,\omega;\varphi)e^{-j(\xi t+\tau\omega)}\ d\xi d\tau \tag{2.10}$$

$$A(\xi,t;\varphi)=\varphi(\xi,\tau)\int_{-\infty}^{\infty}f\left(\mu+\frac{\tau}{2}\right)f^{*}\left(\mu-\frac{\tau}{2}\right)e^{-j\xi\mu}d\mu$$

$$=\frac{\varphi(\xi,\tau)}{2\pi}\int_{-\infty}^{\infty}F\left(v+\frac{\xi}{2}\right)F^{*}\left(v-\frac{\xi}{2}\right)e^{-jv\tau}dv \qquad (2.11)$$

2.4.1.6 Wavelet Transform

Advanced signal processing techniques such as wavelet algorithms can be applied to implement wavelet transform (WT) to localise and identify short time dynamic phenomena [60]-[65]. The WT can be used for multi-scale analysis of a signal through dilation and translation, to extract the time-frequency characteristics of a signal more effectively than the previously discussed methods. Thus in this sub-section, its underlying theory is examined. The signal $x(t)$ is considered non-stationary and the WT technique is discussed further.

i. Continuous Wavelet transform

The continuous wavelet transform (CWT) of $x(t)$ is a time-scale method of signal processing that can be defined as the sum over all time of the signal multiplied by the shifted, scale version of the wavelet function $\psi(t)$ is given by (2.12), where $\psi^{*}(t)$ denotes the complex conjugates of the mother wavelet $\psi(t)$. The parameter a represents the scale (contraction or dilation) index which is the reciprocal of frequency and it is the distance between the center of the wavelet function and it's crossing on the time axis. The parameter b is the shift (translation); it governs the movement of the wavelet function along the time axis. In CWT, the mother wavelet is dilated and translated continuously on a real number system.

$$T(a,b)=\frac{1}{\sqrt{a}}\int_{-\infty}^{\infty}x(t)\psi^{*}\left(\frac{t-b}{a}\right)dt \qquad (2.12)$$

ii. Discrete Wavelet Transform

The Wavelet series was introduced as a sampled version of CWT for implementation on the computer, however required a considerable amount of resources. It also suffers redundancy when attempting to reconstruct the signal. The

discrete wavelet transform (DWT) was introduced to overcome the shortcomings of the wavelet series [51]. The DWT reduces computational time and is much easier to compute. The most common discretization is dyadic, given in (2.13), where a and b is replaced by 2^j and $2^j k$ respectively. An efficient way of implementing this is using filter schemes which was developed by Mallat in 1988 [51]-[52], [65].

$$WT(j,k) = \frac{1}{\sqrt{2^j}} \int_{-\infty}^{\infty} x(t)\psi^*\left(\frac{t-2^j k}{2^j}\right) \tag{2.13}$$

iii. One stage filtering: Approximation and Detail

For many signals, the low frequency content is the important part; it gives the signal identity, while the high frequency contents impart flavour. In wavelet analysis, the approximations are the high-scale, low frequency components of the signal. The details are the low-scale, high frequency components. The most basic filter process is depicted in Fig.2.3. The original sampled signal $x[n]$ passes through two complementary filters and emerges as two signals. If this operation is applied on a real digitized signal such as $x[n]$, twice as much data is obtained. To overcome this problem down-sampling is introduced [66].

iv. Multiple level decomposition

The wavelet decomposition process can be iterative, with successive approximations being decomposed in turn, such that the signal is decomposed into lower resolution components as illustrated in Fig.2.4. If f_s (in samples per second) is the sampling frequency used to capture the signal $x[n]$, then the detail space d_j contains information concerning signal components whose frequencies are included in certain intervals as given in (2.14), where $k = 1{:}\,n$, n is the number of decomposition level, and f_s is the sampling frequency. The approximation space a_n includes low frequency components of the signal which belong to the interval in (2.15). The decomposed components can be reconstructed or synthesized to obtain the original signal with-out loss of information using inverse discrete wavelet transforms (IDWT). Since the

wavelet decomposition process involves filtering and down-sampling; the reconstruction process involves up-sampling and filtering [66].

$$f(d_j) \in \left[2^{-(k+1)} \cdot f_s,\ 2^{-k} \cdot f_s\right] \tag{2.14}$$

$$f(a_n) \in \left[\ 0, 2^{-(n+1)} \cdot f_s\right] \tag{2.15}$$

v. Selection of Mother Wavelet

There are several wavelets with different mathematical properties that have been developed. The wavelets include infinite support wavelets such as; Gaussian, Mexican Hat, Morlet and Meyer, and wavelets with compact support such as; the Haar, Daubechies, Coiflet, Symlets and Biorthogonal. In some fields of science, some families show better results for particular applications. In the case of compactly supported wavelets, these are high order mother wavelets (with a large number of coefficients) and lower-order mother wavelets. Low order wavelets result in overlap between adjacent frequency bands. The Daubechies mother wavelet is commonly used in the DWT to analyse induction machine faults [61]-[64].

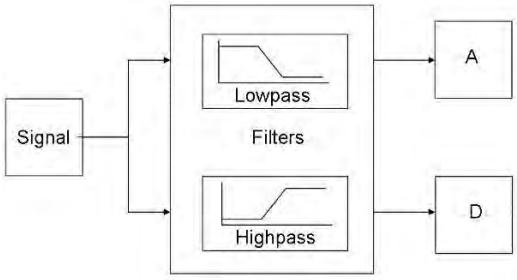

Fig.2.3. Wavelet filtering

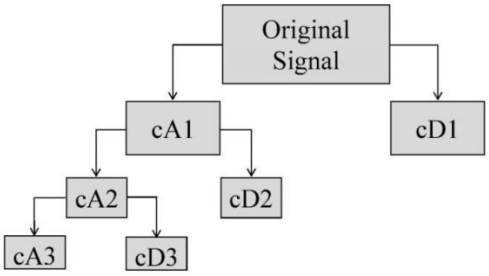

Fig.2.4. Wavelet decomposition

2.4.2 Model and Simulation-Based

The basis of any reliable fault diagnosis method of electrical machines is precise performance analysis under both healthy and faulty conditions. Modelling of faulty machines is the first step of this procedure and has considerable effect on the accuracy of the results. Thus, approaches that consider all effective characteristics of machines such as the finite element method (FEM) are reliable for investigating faulty machines [5]. The typical computer-based tool for analysing electrical machine is the finite element analysis (FEA). It has also been widely used as an analysis and design tool in many Engineering disciplines such as structures, computational fluid mechanics and electromagnetic problems [67]-[68]. FEA is the implementation of FEM to solve a certain type of problem using computer programmes or software. The problem could be mechanical, structural, electromagnetic etc. FEM on the other hand is a mathematical model (which is the result of an idealization of an actual physical problem considered) for solving ordinary and elliptic partial differential equations via a piecewise polynomial interpolation scheme using numerical techniques [68]-[70]. Therefore when FEA is applied to an electromagnetic problem like an electrical machine, it uses numerical techniques to solve and analyse the equations describing its magnetic field. These governing equations (2.14)-(2.17), generally known as Maxwell's equations, are partial differential equations subjected to boundary conditions, describing the macroscopic properties of the medium being considered [68]-[69]. These equations cannot be solved in closed analytical form. While in general, an exact analytical solution cannot be obtained for the posed mathematical model in closed analytical form, the exact solution of the mathematical model does exist. The solution is unique and an approximation of this exact solution can be obtained with very high accuracy using numerical techniques such as Newton Raphson method. This can be implemented by the solvers in FEA. The major advantage of the FEA is that the physical geometries are modelled mathematically, and using computer tools, numerical techniques can be employed to give precise electromagnetic solutions. At present,

several commercial 2D/3D finite element software packages are available and can be applied to PM machine design. However, applying FEA to magnetic field analysis often requires many repetitions of geometrical modelling, solving and post-processing; a time-consuming task. Although, the symmetrical characteristics of the machine may be used to model a quarter or half of the complete machine, this simplification cannot be used in the case of a faulty machine since faults alter the symmetry of electric machines. Also, the software is primarily not designed for fault investigations, therefore, its effective utilization for fault depends on the skills of the user.

$$\nabla \times \mathrm{E} = -\frac{\partial \mathrm{B}}{\partial t} \qquad \text{Faraday's law} \qquad (2.14)$$

$$\nabla \times \mathrm{H} = -\frac{\partial \mathrm{D}}{\partial t} + \mathrm{J} \qquad \text{Maxwell} - \text{Ampere} \qquad (2.15)$$

$$\nabla . \mathrm{D} = \rho \qquad \text{Gauss's law} \qquad (2.16)$$

$$\nabla . \mathrm{B} = 0 \qquad \text{Gauss's law} - \text{magnetic} \qquad (2.17)$$

2.4.3 Machine-Theory Based

Since electrical machines are electromagnetic device, the best possible way to analyse it is to obtain the electromagnetic field distribution of the machine [5]. This requires a solution of Poisson's or Laplace's or Maxwell's equation, which even for the best computer today is an enormous task considering the structure of even the simplest machines. Analysing machines with field solvers to identify fault signature would be inordinately time consuming. Describing electric machines as a group of coupled magnetic circuits provide a time-saving way of obtaining their operational characteristics; this is the basis of the machine-theory approach [72]-[74].

2.4.3.1 Winding Function Approach (WFA)

Electrical machine circuit elements are usually inductances and resistances. The former is difficult to compute because it varies with rotor position and also, with magnetic saturation. The winding and modified winding function approach

(WFA/MWFA) provides the necessary tool to compute these inductances. It provides a computationally efficient way to estimate inductances from the machine winding and airgap data; because the winding structure dictates the magneto motive force (MMF) inside a machine and the airgap, the bulk of the permeance; flux, flux linkage and inductance can easily be computed using the method. However, the approach is far from being accurate since it neglects critical factor in evaluating machine parameters by making the following assumptions [5], [72]:

1. Flux crosses the airgap radially or axially in a radial and axial flux machine respectively (axial and radial flux is negligible respectively);
2. Saturation is negligible;
3. Average core saturation is included using Carter's coefficient to adjust airgap length;
4. Eddy current, friction and windage losses are neglected;
5. The magnetic material has infinite permeability;
6. Slot effects are negligible.

2.4.3.2 Magnetic Equivalent Circuit (MEC)

The magnetic equivalent circuit method uses another approach to model electric machines. The approach can be considered as a reduced FE method because it takes into account approximately accurate machine geometry, stator and rotor leakages, and linear and non-linear magnetic characteristics of machine cores [75]-[77]. This makes it more accurate than the WFA method. The machine to be analysed is divided into three segments; the stator (yoke, teeth, windings), the rotor (yoke, teeth, windings) and the airgap. The analysis can be performed in two ways [76]; indirect and direct. In the indirect way, machine performance are analysed by considering linear magnetic cores to calculate inductances. On the other hand, it may be applied directly to analyse machine performance without calculating inductances. Changes in parameters can then be evaluated to determine machine faults and severity. Although the method is less

accurate than the FE method, it offers a better advantage of faster computational speed.

2.4.4 Artificial Intelligence-Based

Artificial intelligence (AI) is the study of the system conditions through the use of computational models to recognise patterns. These patterns are determined by performance specifications, past observations, expert knowledge or even simulation of a system model. Once trained, the system is able to rapidly recognise pattern similarities and classify new information accordingly. In electric machine fault diagnostic applications, it consists of templates or patterns distinguishing acceptable and unacceptable operations that are then compared to the system observation to determine if a fault has occurred. Popular AI techniques are expert systems (ES), artificial neural networks (ANN), fuzzy logic systems (FLS) and genetic algorithms (GA). They have been integrated into each other and also with other traditional techniques [78]. It has numerous advantages over conventional fault diagnostic approaches in electric machines [78]-[80]. Besides offering improved performance, the technique is easy to extend and modify. These can be made adaptive by the incorporation of new data or information. AI techniques are slowing replacing the human interface for the monitoring of electric machine faults giving rise to the concepts of automated diagnosis. There is a significant opportunity to add intelligence to machines, providing a level of communication and diagnostic capability. The intelligence can be built into the machine's terminal box so that the overall package requires no more space. The major disadvantage is that the success of fault detection depends on the initial training data and only faults represented in the training can be diagnosed. In addition, the volume of training is extensive [5].

2.5 Electrical Impedance Spectroscopy

Electrical impedance spectroscopy (EIS) has been applied to diagnose insulation failure in electrical machines [81]-[84]. It basically involves the excitation of stator windings with high frequency signals, whereby insulation condition may be determined from the impedance response obtained from measured voltage and current signal at the frequencies of excitations. Most impedance spectroscopy applications make use of commercial impedance analyzers which may be very expensive. However, in some papers, EIS has been performed with laboratory built hardware [85]-[86]. Using algorithms and software programming, the characteristics of the impedance response can be evaluated and the state of health of insulation is determined.

2.6 Points of Reference in Developing Fault Detection Techniques and CM Strategies for AFPM Machines

After a critical review of fault indicators in electric machines and methods of their analysis in this chapter, the following factors are identified as points of reference in developing appropriate fault detection techniques and CM strategies for AFPM machine:

1. Applicability based on fault type and applications where the machine is deployed.
2. High reliability of sensors, instrumentation and data acquisition system.
3. Cost competiveness.
4. Non-invasiveness.
5. Accurate and reliable diagnosis.
6. Quantification of the severity of the problem.
7. Computational intensity and accuracy of the signal processing techniques.

2.7 Conclusions

The methods of analyzing fault-indicating parameters in electric machines, and in particular, parameters relevant to AFPM machines have been discussed. The signal-based method is best suited for its advantages such as; cost-saving, non-invasive monitoring and in-situ detection of faults, therefore enabling the points of reference highlighted in section 2.6. Others such as the model/simulation-based and machine-theory-based may perform well in analyzing the performance of electric machines under faulty conditions, but are limited in extracting fault signatures and detecting them in real-time. AI can recognize faults in real-time but characteristics or patterns of faults must have been initially determined and set to train its network for successful online implementation. Thus, the advantages of AI are limited in this thesis since the objectives are to determine such fault characteristics. The signal-based method, employing MCSA and VA for electrical and mechanical faults is most suitable to characterize faults using signal processing techniques in both frequency and time-frequency domain. Both strategies may complement each other for better and reliable fault diagnosis in AFPM machines. In addition, for a better understanding of the electromagnetic behaviour of the AFPM machine topologies under fault conditions, FEA is implemented for fault modelling and detection.

2.7 References

[1] Y. Wenxian, H. N Chong and J. Jiesheng, "Fast individual harmonic extraction: An efficient tool for wind turbine condition monitoring," IEEE International Conference on Electrical Machines and Systems (ICEMS), 2011.

[2] M. El Hachemi Benbouzid, "A review of induction motors signature analysis as a medium for faults detection," IEEE Transactions on Industrial Electronics. Vol. 47, pp. 984-993, October 2000

[3] W. Yang, P. Tavner, C. Crabtree and M. Wilkinson, "Cost effective condition monitoring for wind turbines," IEEE Transactions on Industrial Electronics 2010, Vo. 57, No. 1, pp. 263−271.

[4] S. Nandi and H.A. Toliyat, "Detection of rotor slot and other eccentricity related harmonics in a three phase induction motor with different rotor cages", IEEE Conference Proceedings of International Conference on Power Electronic Drives and Energy Systems for Industrial Growth–PEDES '98, Perth, Australia, Nov. 30-Dec. 3, 1998, Vol. 1, pp. 135-140.

[5] Hamid Toliyat, S. Nandi, S. Choi, H. Meshdin-Kelk, Electrical machines: Modeling, condition monitoring and fault diagnosis. CRC Press, Taylor and Francis Group, Boca Raton, USA, 2013.

[6] S. Nandi, H. A Toliyat, and X. Li, “Condition monitoring and fault diagnosis of electrical machines – A review”. IEEE Transactions on energy conversion. Vol. 20, no. 4, pp. 719 – 729, December, 2005.
[7] D. E Crawford, “A mechanism of motor failures”, 12th IEEE Electrical and Electronics Insulation Conference, Institute of Electrical and Electronics Engineers, Inc., New York, NY, pp. 126- 129, 1975.
[8] S. M. Mirimani, A. Vahedi, and F. Marignetti, “Effect of inclined static eccentricity fault in single stator–single rotor axial flux permanent magnet machines,” *IEEE Trans. Magn.*, vol. 48, no. 1, pp. 143–149, Jan. 2012.
[9] Nandi, S., Toliyat, H.A., Xiaodong Li, ‘Condition monitoring and fault diagnosis of electrical motors-a review’, *IEEE Transactions on Energy Conversion*, Vol. 20, Issue 4, pp. 719-729, 2005.
[10] Yao Duan; Toliyat, H., "A review of condition monitoring and fault diagnosis for permanent magnet machines," *Power and Energy Society General Meeting, 2012 IEEE* , vol., no., pp.1,4, 22-26 July 2012.
[11] A. Parviainen, “Design of axial-flux permanent magnet low-speed machines and performance comparison between radial-flux and axial-flux machines”, PhD dissertation, Acta Universitatis Lappeenrantaensis, 2005.
[12] Giulii Capponi, F.; De Donato, G.; Caricchi, F., "Recent Advances in Axial-Flux Permanent-Magnet Machine Technology," *Industry Applications, IEEE Transactions on* , vol.48, no.6, pp.2190,2205, Nov.-Dec. 2012.
[13] Driesen, J., 2000, ‘Coupled electromagnetic-thermal problems in electrical energy transducers’, Doctoral Thesis, Leuven, May, 2000, 216 p.
[14] Payne, B.S., Husband, S.M., Ball, A.D., 2002, ‘Development of condition monitoring techniques for a transverse flux motor’, *International Conference on Power Electronics, Machines and Drives–PEMD ‘02 (IEE Conference Publication No. 487)*, Bath, UK, June 4-7, 2002, pp. 139 144.
[15] Thorsen, O.V.; Dalva, M., "Failure identification and analysis for high-voltage induction motors in the petrochemical industry," *Industry Applications, IEEE Transactions on* , vol.35, no.4, pp.810,818, Jul/Aug 1999.
[16] W. T. Thomson, ‘A review of on-line condition monitoring techniques for three-phase squirrel-cage induction motors–past, present and future’, 2nd IEEE International Symposium on Diagnostics for Electrical Machines, Power Electronics and Drives–SDEMPED ‘99, Gijon, Spain, Sept. 1-3, 1999, pp. 3-17.
[17] SpectraQuest, ‘Machinery Fault Simulator’, SpectraQuest Inc., Available on web at: www.spectraquest.com.
[18] M. Negrea, P. Jover, A., Arkkio, ‘A comparative investigation of electrical parameters for fault detection and condition monitoring in induction motors–stator winding current and electromagnetic flux’, 17th International Conference on Electrical Machines–ICEM ’06, Sept. 2–5, 2006, Chania, Crete Island, Greece, on CD, 6 p.
[19] P. Tavner, and J. Penman, ‘Condition Monitoring of Electrical Machines’, Research studies press LTD, 1987. ISSN/ISBN: 0-86380-061-0, 302 p.
[20] P. J. Tavner, A. F. Anderson, ‘Core faults in large generators’, IEE Proceedings on Electric Power Applications, Vol. 152, Issue 6, 2005, pp. 1427-1439.
[21] M. Negrea, A. Arkkio, T. Jokinen, M. Hakuli, M., ‘Thermal analysis of a permanent magnet synchronous motor’, 3rd IEEE International Symposium on Diagnostics for Electrical Machines, Power Electronics and Drives–SDEMPED ‘03, Grado, Italy, Sept. 1-3, 2001 pp. 517-522.
[22] J. Malinowski, J. McCormick, ‘AC induction motor specifications-an update on currently available procedures and options’, Conference Record of the 2002 Annual Pulp and Paper Industry Technical Conference, Toronto-ON, Canada, June 17-21, 2002, pp. 181-189.
[23] R. Lisner and P. L. Timar, “A new approach to electric motor acoustic noise standards and test procedures,” IEEE Trans. Energy Convers., vol. 14, no. 3, pp. 692–697, Sep. 1999.

[24] G. H. Jang and D. K Lieu, “Vibration reduction in electric machine by interlocking of the magnets,” IEEE Trans.Magn., vol. 29, no. 2, pp. 1423– 1426, Mar. 1993.
[25] M. Tsypkin, “Induction motor condition monitoring: vibration analysis technique - a twice line frequency component as a diagnostic tool,” IEEE International Electric Machines & Drives Conference (IEMDC), 2011.
[26] Project UpWind, Condition Monitoring for Wind Turbines. Report as deliverable 7.1.1, WP7 condition monitoring contract no.: 019945 (SES6). European Commission, Dec. 2005.
[27] Climente-Alarcon, V.; Antonino-Daviu, J.A.; Vedreno-Santos, F.; Puche-Panadero, R., "Vibration Transient Detection of Broken Rotor Bars by PSH Sidebands," *Industry Applications, IEEE Transactions on* , vol.49, no.6, pp.2576,2582, Nov.-Dec. 2013.
[28] Seshadrinath, J.; Singh, B.; Panigrahi, B.K., "Investigation of Vibration Signatures for Multiple Fault Diagnosis in Variable Frequency Drives Using Complex Wavelets," *Power Electronics, IEEE Transactions on* , vol.29, no.2, pp.936,945, Feb. 2014.
[29] Seshadrinath, J.; Singh, B.; Panigrahi, B.K., "Vibration Analysis Based Interturn Fault Diagnosis in Induction Machines," *Industrial Informatics, IEEE Transactions on* , vol.10, no.1, pp.340,350, Feb. 2014.
[30] Ahmed, I., Supangat, R., Grieger, J., Ertugrul, N., and Soong, W.L.: ‘A baseline study for on-line condition monitoring of induction machines’. Australasian Universities Power Engineering Conf., AUPEC, Brisbane, Australia, 2004.
[31] Bellini, A., Filippetti, F., Franceschini, G., Tassoni, C., and Kliman, G.B.: ‘Quantitative evaluation of induction motor broken bars by means of electrical signature analysis’, IEEE Trans. Ind. Appl., 2001, 37, pp. 1248–55.
[32] Kliman, G.B., Premerlani, W.J., Yazici, B., Koegl, R.A., and Mazereeuw, J.: ‘Sensorless, online motor diagnostics’, IEEE Comput. Appl. Power, 1997, pp. 39–43.
[33] Siau, J., Graff, A., Soong, W.L., and Ertugrul, N.: ‘Broken bar detection in induction motors using current and flux spectral analysis’, Aust. J. Electr. Electron. Eng., 2004, 1, (3), pp. 171–177.
[34] Supangat, R.; Ertugrul, N.; Soong, W.L.; Gray, D.A; Hansen, C.; Grieger, J., "Detection of broken rotor bars in induction motor using starting-current analysis and effects of loading," *Electric Power Applications, IEE Proceedings* - , vol.153, no.6, pp.848,855, November 2006.
[35] M. Abdesh Shafiel Kafiey Khan, "Wavelet Based Diagnosis and Protection of Electric Motors," pp. 256-282.
[36] Edward W Kamen, *Fundamentals of Signals and systems using the web and matlab*. New Jersey: Prentice Hall, 2000.
[37] E. Sedjic and J. Jiang, ‘Comparative study of three time–frequency representations with applications to a novel correlation method,’ Proc. of IEEE International Conf. on Acoustics, Speech, and Signal Processing (ICASSP), Montreal, May 17–21, 2004, Vol. 2, pp. 633–636.
[38] A. Siddique, "A Review of Stator Fault Monitoring Techniques of Induction Motors," IEEE Transactions on Energy Conversion, VOL. 20, NO. 1, pp. 106-114, 2005.
[39] B.K.N Rao, Handbook of Condition Monitoring 1st Edition. Oxford: Elsevier Science LTD, 1996.
[40] M Pineda-Sanchez, M Riera-Guasp , J. Roger-Folch , E Hurtado-Perez, and J. Perez-Cruz , "Improved Resolution of the MCSA Method Via Hilbert Transform, Enabling the Diagnosis of Rotor Asymmetries at Very Low Slip," IEEE Transactions on Energy Conversion, pp. 52 - 59 , 2009.
[41] Swami A., *Cumulant–Based Approach to the Harmonic Retrieval and Related Problems*, IEEE Transactions on Signal Processing, Vol. 39 , Iss. 5, 1995, pp. 1099–1108.
[42] Therrien C. W., *Discrete Random Signals and Statistical Signal Processing*, Englewood Cliffs, New Jersey, Prentice Hall PTR, 1992.
[43] Pisarenko V. F., T*he retrieval of harmonics from a covariance function*, Geophysics J. Roy. Astron. Soc., Vol. 33, 1973, pp. 347–366.

[44] Schmidt R. O., *Multiple emitter location and signal parameter estimation*, Proc. RADC Spectrum Estimation Workshop, Griffiss AFB, NY, 1979, pp. 243–258.
[45] Stoica P., Nehorai A., *Performance comparison of subspace rotation and Music–like methods*, IEEE Trans. Acoust. Speech, Signal Processing, No. 39, 1991, pp. 446–453.
[46] Roy R., Kailath T., *ESPRIT – Estimation of Signal Parameters via Rotational Invariance Techniques*, IEEE Transactions on Acoustics, Speech, and Signal Processing, Vol. ASSP– 37, 1989, pp. 984–995.
[47] Rao B. D., Hari K. V. S., *Performance Analysis of ESPRIT and TAM in determining the direction of arrival of plane waves in noise*, IEEE Trans. on Acoustics, Speech and Signal Processing, Vo. 37, No. 12, 1989, pp. 1990–1995.
[48] Zbigniew Leonowicz, 'Parametric methods for time–frequency analysis of electric signals', Phd thesis, Politechnika Wrocławska, Wroclaw University of Technology, Poland, 2007.
[49] El Bouchikhi, E.H.; Choqueuse, V.; Benbouzid, M.E.H., "A parametric spectral estimator for faults detection in induction machines," *Industrial Electronics Society, IECON 2013 - 39th Annual Conference of the IEEE* , vol., no., pp.7358,7363, 10-13 Nov. 2013.
[50] Boqiang Xu; Liling Sun; Lie Xu; Guoyi Xu, "An ESPRIT-SAA-Based Detection Method for Broken Rotor Bar Fault in Induction Motors," *Energy Conversion, IEEE Transactions on* , vol.27, no.3, pp.654,660, Sept. 2012.
[51] P.S Barendse, "The application of advanced signal processing techniques to the condition monitoring of electrical machine drive systems," Cape Town, 2007.
[52] B.S Prabhu, Dynamic Analysis of Rotating Systems and Appplications. Brentwood: Multi- Sxience Publishing, 2008.
[53] Cohen L., Time–Frequency Analysis, Englewood Cliffs, NJ, Prentice–Hall, 1995.
[54] Leonowicz Z., Łobos T., Ruczewski P., Szyma´nda J., Analysis of distorted signals using HOS, International Journal for Computation and Mathematics in Electronic Engineering COMPEL (Great Britain), Vol. 17, Issue 5/6, 1998, pp. 602–611.
[55] Bracale A., Carpinelli G., Lauria D., Leonowicz Z., Łobos T., Rezmer J., Spectrum estimation of non–stationary signals in traction systems, Proceedings of the International Conference on Power Systems. (ICPS 2004), Kathmandu, Nepal, Nov 3–5, 2004, Vol. 1, 821–826.
[56] S. Rajagopalan, José A. Restrepo, José M. Aller, T. G. Habetler, and R. G. Harley, "Selecting Time-Frequency Representations for Detecting Rotor Faults in BLDC Motors Operating Under Rapidly Varying Operating Conditions," in *Proc. 32nd Annual Conference of the Industrial Electronics Society (IECON 2005),* 2005, pp. 2579-2584.
[57] Y. Zhao, L. E. Atlas, and R. J. Marks II, "The use of cone-shaped kernels for generalized time-frequency representations of non-stationary signals," *IEEE Trans. on Acoustics, Speech, and Signal Process*., vol. 38, no. 7, pp. 1084-1091, 1990.
[58] Rajagopalan, S.; Habetler, T.G.; Harley, R.G.; Restrepo, J.A; Aller, J.M., "Non-Stationary Motor Fault Detection Using Recent Quadratic Time-Frequency Representations," *Industry Applications Conference, 2006. 41st IAS Annual Meeting. Conference Record of the 2006 IEEE* , vol.5, no., pp.2333,2339, 8-12 Oct. 2006.
[59] L. Cohen and T. E. Posch, "Generalized ambiguity functions," in Proc. *IEEE International Conference on Acoustics, Speech, and Signal Processing, ICASSP '85*, 1985, pp. 1033–1036
[60] F. Auger, P. Flandrin, P. Goncalvès, and O. Lemoine, Time-frequency toolbox for use with MATLAB, CNRS France/Rice University, 1996.
[61] M Riera-Guasp, J Antonino-Daviu, M Pineda-Sanchez, R Puche-Panadero, and J Perez-Cruz, "A general Approach for the Transient Detection of Slip-Dependent Fault Components Based on the Discrete Wavelet Transform," IEEE Transaction on Industrial Electronics, pp. 4167 - 4180, December 2008.

[62] J Antonino-Daviu, M Riera-Guasp, Folch J.R, and M Pilar Molina Palomares, "Validation of a new method for Diagnosis of Rotor Bar failures via Wavelet Transform in Industrial Induction Machines," IEEE Transaction on industrial applications, pp. 990-996, 2006.
[63] S.H Kia, H Henao, and Gerard-Andre Capolino, "Diagnosis of Broken-Bar Fault in Induction machines using Discrete Wavelet Transform without Slip estimation," IEEE Transaction on industrial applications, pp. 1395 -1404, 2009.
[64] J. Pons-Llinares, J. Antonino-Daviu, J. Roger-Folch, and D. Morinigo-Sotelo, "Eccentricity diagnosis in Inverter - Fed Induction Motors via the Analytic Wavelet Transform of transient currents," in XIX International Conference on Electrical Machines (ICEM), Rome, 2010 , pp. 1 – 6.
[65] A. Bellini, F. Filippetti, C. Tasson, and G.-A. Capolino, "Advances in Diagnostic Techniques for Induction Machines," IEEE Transactions on Industrial Electronics , pp. 4109 - 4126 , 2008.
[66] M Misiti, Y Misit, G Oppenhiem, and J-M Poggi, Wavelet Toolbox User's Guide.: The Mathworks, 1996.
[67] M. Amrhein and P. T. Krein, "Three-dimensional magnetic equivalent circuit framework for modeling electromechanical devices," *IEEE Trans. Energy Convers.*, vol. 24, no. 2, pp. 397–405, Jun. 2009.
[68] Silvester, P. P.; and Ferrari, R. L.: Finite Elements for Electrical Engineers. Second ed., Cambridge Univ. Press, 1990.
[69] S. J. Salon, *Finite Element Analysis of Electrical Machines*. Norwell, MA: Kluwer, 1995.
[70] M. Amrhein and P. T. Krein, "Force calculation in 3-D magnetic equivalent circuit networks with a Maxwell stress tensor," *IEEE Trans. Energy Convers.*, vol. 24, no. 3, pp. 587–593, Sep. 2009.
[71] Design of Axial-Flux Permanent-Magnet Low-Speed Machines and Performance Comparison between Radial-Flux and Axial-Flux Machines. Asko Parviainen. Ph.D Thesis. Lappeenranta University of Technology. Isbn 952-214-029-5, Isbn 952-214-030-9 (Pdf), Issn 1456-4491.
[72] X. Luo, Y. Liao, H. A. Toliyat, A. El-Antably and T. A. Lipo, "Multiple coupled circuit modeling of induction machines," IEEE Trans. Ind. Appl., vol. 31, no. 2, pp. 311-318, Mar/Apr. 1995.
[73] H. A. Toliyat, M. S. Arefeen and A. G. Parlos, "A method for dynamic simulation of air-gap eccentricity in induction machines," IEEE Trans. Ind. Appl., vol. 32, no. 4, pp. 910-918, Jul./Aug. 1996.
[74] H. A. Toliyat and T. A. Lipo, "Transient analysis of cage induction machines under stator, rotor bar and end ring faults," IEEE Trans. Energy Convers., vol. 10, no. 2, pp. 241-247, June 1995
[75] P. Campbell, "The magnetic circuit of an axial field DC electrical machine," IEEE Trans. Magn., vol. 11, no. 5, pp. 1541–1543, Sep. 1975.
[76] S. A. Saied, K. Abbaszadeh, and M. Fadaie, "Reduced order model of developed magnetic equivalent circuit in electrical machine modeling," IEEE Trans. Magn., vol. 46, no. 7, pp. 2649–2655, Jul. 2010.
[77] K. Yamazaki, A. Suzuki, M. Ohto, T. Takakura, and S. Nakagawa, "Equivalent circuit modeling of induction motors considering stray load loss and harmonic torques using finite element method," IEEE Trans. Magn., vol. 47, no. 5, pp. 986–989, May 2011.
[78] Siddique, A; Yadava, G. S.; Singh, B., "Applications of artificial intelligence techniques for induction machine stator fault diagnostics: review," *Diagnostics for Electric Machines, Power Electronics and Drives, 2003. SDEMPED 2003. 4th IEEE International Symposium on* , vol., no., pp.29,34, 24-26 Aug. 2003.
[79] F. Pilippetti. G. Fraanceschini. and C. Tassoni, -A survey of AI techniques approach for induction machines on-line diagnostic," in *Proc.PEMC'96,* vol. 2, Budapest, Hunghary, 1996,pp. 314-318
[80] Abdelhadi, B.; Benoudjit, A; Nait-Said, N., "Application of genetic algorithm with a novel adaptive scheme for the identification of induction machine parameters," *Energy Conversion, IEEE Transactions on*, vol.20, no.2, pp.284,291, June 2005.

[81] Neti, P.; Grubic, S., "Online broadband insulation spectroscopy of induction machines using signal injection," in *Energy Conversion Congress and Exposition (ECCE), 2014 IEEE* , vol., no., pp.630-637, 14-18 Sept. 2014.
[82] Shilei Ma; Boggs, S., "50+ Years of impedance measurement and spectroscopy, and implementation of virtual spectroscopy based on finite element analysis," in *Electrical Insulation Magazine, IEEE* , vol.30, no.1, pp.25-31, January-February 2014.
[83] Burkanudeen, A.; Ramesh, P., "Novel latent epoxy curing agent for secondary insulation in electrical rotors and stators," in *Dielectrics and Electrical Insulation, IEEE Transactions on* , vol.19, no.5, pp.1791-1798, October 2012.
[84] David, E.; Lamarre, L., "Influence of rise time on dielectric parameters extracted from time domain spectroscopy in the context of generator stator insulation," in *Dielectrics and Electrical Insulation, IEEE Transactions on* , vol.12, no.3, pp.423-428, June 2005.
[85] Arellano-Padilla, J.; Sumner, M.; Gerada, C., "On-line detection of stator winding short-circuit faults in a PM machine using HF signal injection," *Electrical Machines, 2008. ICEM 2008. 18th International Conference on* , vol., no., pp.1,8, 6-9 Sept. 2008.
[86] Seilmeier, M.; Ebersberger, S.; Piepenbreier, B., "HF Test Current Injection-Based Self-Sensing Control of PMSM for Low- and Zero-Speed Range Using Two-Degree-of-Freedom Current Control," *Industry Applications, IEEE Transactions on* , vol.51, no.3, pp.2268,2278, May-June 2015.

Chapter 3
Development of a Test-Rig for Fault Investigations

3.1 Introduction

Early detection of faults is important to improve the availability and cost-effective maintenance of electrical machines. During online CM, fault diagnosis using fault detection techniques is established when distinguishable instantaneous features of the machine deviate from the healthy operational case. Information on the healthy operational case is typically a set of baseline data with which the real-time machine information is compared to. However, the fault detection techniques must have been hitherto established using machine theory and signal processing techniques. Therefore in this chapter, a test-rig for developing fault detection techniques in AFPM machine is developed. The main features of the rig are related to ease and correctness of the fault implementation, isolation of faults, in-situ capability and reliability of the measurement procedure. Firstly, the faults that are typical to AFPM machines are identified.

3.2 Faults in AFPM Machines

It is discussed in chapter 2, that fault detection in rotating electrical machines has received an intense amount of research interest since the 1980s [1]-[4]. With advances in digital signal processing hardware and software, electric drives, measuring sensors and instrumentation, the topic of fault diagnosis remains attractive and critical to the operation of electric machines, and significant progress has been made. However,

AFPM machines have not been rigorously studied for faults although there has been some works published on fault diagnostics for radial-flux PM machines [5]-[12]. Increase in their applications [13]-[20] warrants investigation into their behaviour under faulty conditions with an aim to develop fault detection techniques and CM strategies. AFPM machine faults are broadly classified into electrical or mechanical faults as presented in Table 3.1. Stator winding short circuits and static eccentricity have been are identified as frequently occurring [9], [21]-[23] and are therefore investigated. These are replicated on a prototype in a controllable manner. The techniques used to replicate them while ensuring no damage is caused during fault investigations are discussed in the succeeding chapters, where each investigated fault is modelled and analysed.

3.3 Architecture of the Rig

The success of online CM is hinged on the reliability of fault detection techniques. To guarantee this, accurate fault replication techniques to extract machine information in order to distinguish acceptable from unacceptable operations is needed. Thus, this section advances fault diagnostics for AFPM machines by developing a platform for precise replication of faults to ensure accurate and reliable analysis of fault signatures. The development of the test-rig is predicated on four objectives namely:

1. Reliability and accuracy of sensors, instrumentation and the data acquisition hardware.
2. In-situ capability of the data acquisition system.
3. Integrity of the measurement procedure.
4. Accurate replication of faults.

In view of the aforementioned objectives, the following standards were established for the test rig shown in Fig.3.1-3.2:

1. Ability to test a very wide range of machine shapes and sizes.

2. The drive must be able to operate at the speed and torque rating of the prototype investigated.
3. The drive needs to be able to operate in three different modes of operation namely;
    a) Speed control; to rotate the prototype at desired speeds.
    b) Torque control; to apply the desired torque to the shaft of the prototype.
    c) Position control; to 'step' the prototype at a required angle (operates as a stepper motor).
4. The torque transducer should have sufficient resolution to measure cogging torque and the capacity to measure maximum torque produced by the machine under investigation.
5. Flexibility to vary the induced faults to the desired degree.
6. Versatility to support a change the AFPM from a double-sided to a single-sided topology.
7. Ability to monitor speed, torque vibration, current and voltage signals.

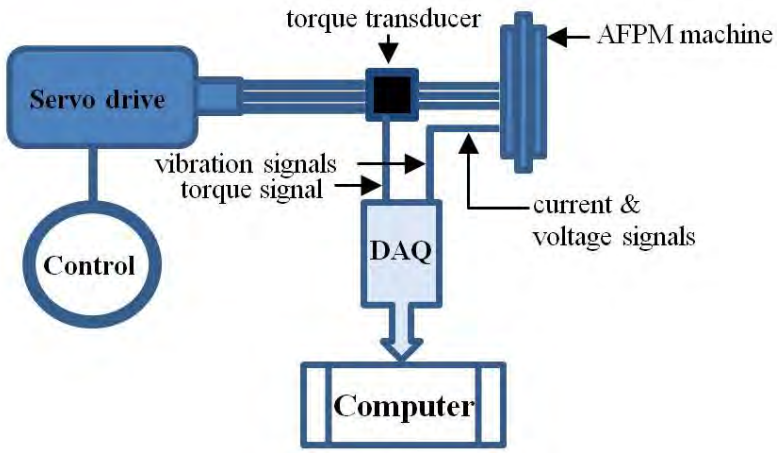

Fig.3.1. Architecture of the test rig

Table3.1. Common fault Types in AFPM machines

FAULTS	ELECTRICAL	MECHANICAL				
Types	Winding faults	Core or lamination	Magnet damage: *Broken/displaced PMs*	Eccentricity	Broken/misaligned Shaft	Bearing Faults
Sub-types	Short circuit ϕ-ϕ,3-ϕ,ϕ-grd inter – turn  Open circuit High impedance	–	– 	Static Dynamic	–	– 
Parts of generator affected	Stator	Stator Rotor	Rotor	Rotor	Shaft Rotor	Shaft Rotor
Frequency of occurrence	Frequent	Very Rare	-	Frequent	Rare	Frequent
Severity (danger and damage)	High	Cata-strophic	Medium	Low	Medium	Medium

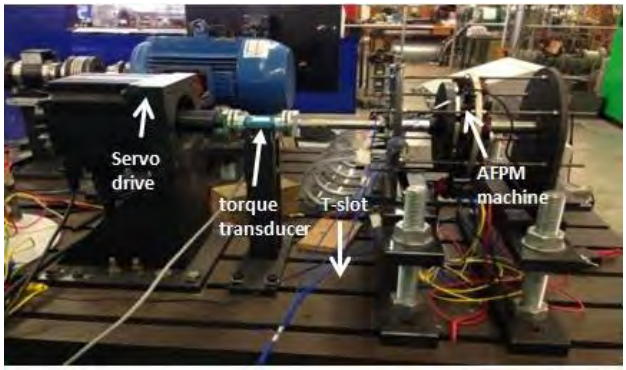

Fig.3.2.The test-rig showing key components

3.3.1 Machines Investigated

The machines analysed for faults are the surface-mounted PM, iron core, single-sided (single-rotor, single-stator) and double-sided (double-rotor, double-stator) topologies. The machine data is provided in Table3.2. Both topologies are 10p/12s machines with parallel stator teeth or trapezoidal slots and fractional slot concentrated winding (FSCW) shown in Fig3.3a. The rotor shaft is shown in Fig.3.3b. The rotor can be modified offline by mounting discs with different PM shapes as shown in Fig.3.4.The PM configurations are used to reduce cogging torque. The prototypes were coupled-to and mechanically aligned to a servo drive, with both rigidly mounted to a test bed with T-slots as seen in Fig.3.2. The winding configuration (shown in Fig.3.3a) provides advantages of ease of winding and accessibility to the inter-turn/inter-coil regions. The slot/pole combination is chosen in the design [24] because it is susceptible to low cogging torque since its lowest common multiple is large, thus it is commonly used in PM machines design [24]-[27]. It has the number of poles p and slots Q differ by two, i.e., $Q \pm p = 2$, making it very appropriate for medium to high speed applications in order to avoid high frequency problems in the machine core and control [26]-[27]. The slot/pole combination necessitates the employment of the FSCW configuration, a winding type inherently rich in current harmonics because the slots per pole per phase, $q < 1$ [27]-[28]. However, the FSCW configuration has advantages of short end regions,

ease of manufacturing, large self-inductance, low fault probability of coil-coil short circuit, high flux weakening capacity, high efficiency, high power and torque density [28].

Table3.2. Machine data

Parameters	**Value**
Rated Power	450W
Nominal Speed	600rpm
Nominal Torque	7Nm
Number of Turns/Phase	120
Pole Pair	5
Number of slots	12
Outer Diameter	180mm
Axial Length	27mm
Length of airgap	1.5mm
Inertia	0.048Kg/m^2
Stator Resistance (L-N)	0.40Ω
Stator Inductance (L-N)	7.4mH

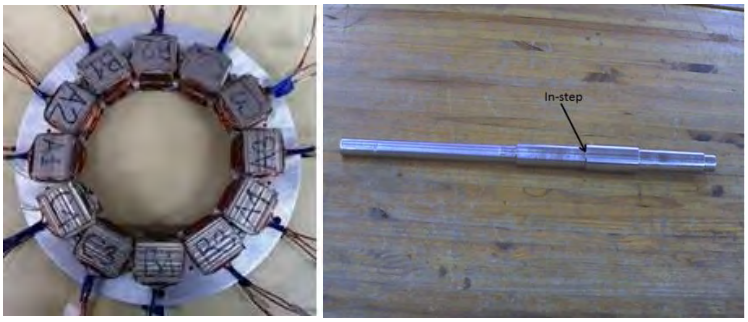

a b

Fig.3.3. (a) Stator core with coil windings (b) rotor shaft

a b c

Fig.3.4. Various PM rotor topologies; (a) equal PM pole (b) alternating PM pole (c) skewed PM pole

3.3.2 Servo Drive

This serves as both the prime mover and regenerative breaking in generating and motoring mode of the machine respectively. It has good stepping resolution required for measuring cogging torque and sufficient rated output power while configured to operate in motor or generator mode. A 3kW rated machine is chosen for the drive since the maximum torque and speed of the AFPM machine is 10Nm and 600rpm respectively. The data for the servo drive is given in Appendix A.

3.3.3 Measuring Instrumentation and Data Acquisition System

In chapter 2, the parameters which provide useful information for fault detection in electric machines are identified. Consequently, VA and MCSA are deemed fit as adequate diagnostic strategies for fault detection in AFPM machines. They both can analyse mechanical, electromechanical and electrical parameters which are critical in determining the state of health of machine. Thus, speed, torque, vibration, voltage and current signals are chosen and acquired for processing and analysis. The measuring instrumentation transducers and data acquisition (DAQ) system are described in this sub-section.

3.3.3.1 Current and Voltage Transducers

The current and voltage measurements were achieved using LEM modules (LEM is a transducer trademark that uses the Hall Effect principle) to provide the necessary isolation/transformation between the primary power circuit (machine output) and secondary side, the data acquisition device. The transducers have good linearity and response time (less than $1\mu s$ and $40\mu s$ for current and voltage transducer respectively); fast enough to process signals during transients.

3.3.3.2 Vibration

The ceramic shear piezoelectric accelerometer shown in Fig.3.5 is the transducer used to measure the vibration signals. It is an Integrated Electronics Piezo Electric (IEPE) which incorporates built-in, signal-conditioning electronics. The built-in electronics converts the high-impedance charge signal which is generated by the piezoelectric sensing element into a low-impedance voltage signal that is readily transmitted, over ordinary two-wire or coaxial cables. The IEPE sensors require constant excitation, which was provided for by the circuitry of the vibration DAQ used. There is an analogue pre-filter, before the analogue-digital converter (ADC) to eliminate the aliasing frequency components that may appear in the low frequency range. The features of the accelerometers are presented in Appendix A. The parameter to be monitored is the absolute vibration of the machine housing. The stud mounting method is ideal for obtaining high frequencies but the machine structure surfaces is curved and rough, thus making the surface not adequate for this type of mounting method. As a result, the adhesive mounting method using an aluminium mounting base as shown in Fig.3.5, was employed. The aluminium base, is 'hard coated' to provide electrical isolation to eliminate ground loops and reduce electrical interference that may be propagating from the surface of the machine under investigation. The accelerometer was riveted to a side of the aluminium base while the other side was fixed to the surface of the machine using adhesives.

3.3.3.3 Torque and Speed

Accurate torque measurements are vital for determining the performance of an electrical machine. Load cells are more commonly used to measure the torque of an electrical machine. The prime mover will be mounted on bearings, to allow free movement in the radial direction and the load cell connected to a side of the machine to measure the torque applied to its shaft. However, this method is not very accurate and has the inherent problem of varying the offset due to the stiffness of the entire

structure. A brushless in-line torque transducer overcomes these challenges and can measure the torque very precisely, thus, it was chosen for the test rig. To mitigate or reduce the effect of misalignment on the torque readings, the transducer is connected to the prime mover and the machine under test via rigid couplings to allow for radial and axial misalignment tolerance without introducing unwanted vibrations. A 15Nm DR-2112 in-line torque transducer by Lorenz-Messtechnik [29] was selected. The accuracy is 0.01 Nm, sufficient to measure low cogging torque values of small PM machines. The torque transducer also provided speed information as an analogue output.

3.3.3.4 DAQ: Voltage and Current Input

The current and voltage outputs of the LEM modules were fed to the input ports of the National Instrument® (NI) DAQ NI-9200 16-bit simultaneous analogue input voltage module. The module provides sixteen differential analogue input channels with a $\pm$10V input range. Each channel contains terminals for positive and negative signals and a common terminal COM which is internally connected to the isolated ground reference. The module protects each channel from overvoltage. The incoming current or voltage signal is buffered and conditioned by an instrumentation amplifier and then sampled by a 16-bit analogue to digital converter (ADC). The voltage module was used for voltage, current, torque and speed data acquisition.

3.3.3.5 DAQ: Vibration Input

The voltage signals obtained from the accelerometers are fed into the input ports of a DAQ device, NI-9234 24-bit analogue input module. It provides a dc power (excitation) and anti-aliasing filters for the accelerometers as seen in Fig.3.6. This module provides four BNC analogue input channels with $\pm$5V input range. The ADC used in the module is 24-bit delta-sigma.

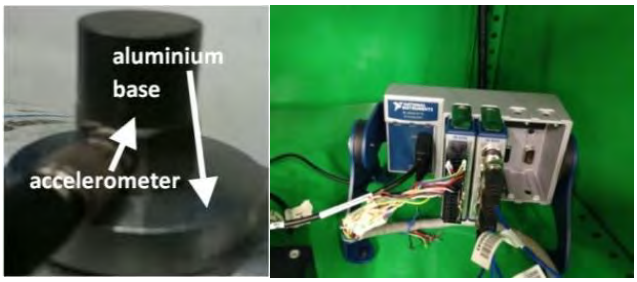

Fig.3.5. Accelerometer as mounted (left) and DAQ hardware (right)

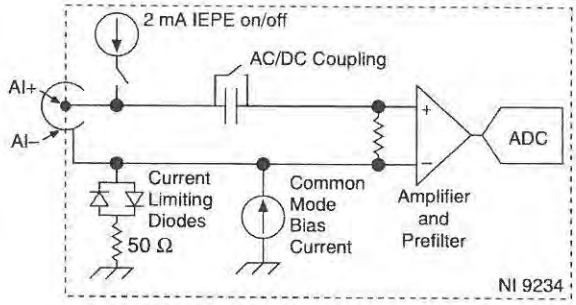

Fig.3.6. NI-9234 input circuitry

3.3.3.6 DAQ Chassis

The modules; NI-9251 and NI-9200 were seated on a 4-slot NI compaqDAQ-9178USB. The chassis contains four general purpose 32-bit counters built in and can run the four hardware-time analogue I/O, digital I/O or counters operations simultaneously. This permits simultaneous acquisition of currents, voltages, torque, speed and vibration signals.

3.3.3.7 DAQ Software

The LabView 2013 32bit software is the programming interface for the hardware discussed. This is a platform and development environment for a visual programming language by National Instruments®. A LabView virtual instrument (VI) was created using a DAQ assistant to read and display the captured signals for real-time monitoring. The DAQ assistant settings are configured to the input terminal connection, physical

channel, and appropriate type of measurement and scaling for the DAQ hardware system.

3.4 Signal Measurement and Trending

A series of baseline measurements were taken at different speeds and load levels. Harmonics of the stator current in the *abc*-reference frame and vibration signals were analysed. The quality of measurement was established by ensuring the following:

1. Proper mounting of sensors and transducers.
2. Integrity of transducers and DAQ hardware cabling system.
3. Correct measurement range to avoid saturated signals.
4. Sufficient number of samples and adequate sampling rate to detect the actual rate of change of the measured parameter for both steady state and transient studies.
5. Repeated measurements and trending to determine the baseline data. Correlation was established between historical trends and new data obtained in establishing the baseline.

Details of the experimental and measurement protocols relating to this thesis are given in Appendix B.

3.5 Conclusions

Typical faults in AFPM machines have been identified. The chapter also details the state-of-the art in hardware, software and basic functionalities a rig must meet for real-time fault diagnosis. The development of the rig is to ensure precise replication of various faults and reliable acquisition of machine signals for processing. It serves as a tool for analysing fault signatures associated with AFPM machines and the platform for developing various CM schemes. The effectiveness is seen in the experimental results in the succeeding chapters. The signal measurements obtained from the test

procedures for the healthy condition is the baseline data on which the faulty signals are benchmarked and analysed.

3.6 References

[1] S. Pöyhönen, M. Negrea, A. Arkkio, H. Hyötyniemi and H. Koivo, “Fault diagnostics of an electrical machine with multiple support vector classifiers,” *17th IEEE International Symposium on Intelligent Control–ISIC* Vol. 1, pp. 373-378, Oct. 2002

[2] S. Nandi, H. Toliyat, and X. Li, “Condition monitoring and fault diagnosis of electrical motors-a review,” *Energy Conversion, IEEE Transactions on*, vol. 20, no. 4, pp. 719 – 729, dec. 2005

[3] Hamid Toliyat et al., Electrical machines: Modeling, condition monitoring and fault diagnosis. CRC Press, Taylor and Francis Group, Boca Raton, USA, 2013

[4] P. Vas, Parameter estimation, condition monitoring, and diagnosis of electrical machines. Oxford, U.K.: Clarendon, 1993

[5] Yao Duan; Toliyat, H., "A review of condition monitoring and fault diagnosis for permanent magnet machines," *Power and Energy Society General Meeting, 2012 IEEE* , vol., no., pp.1,4, 22-26 July 2012

[6] B. Ebrahimi and J. Faiz, “Diagnosis and performance analysis of three phase permanent magnet synchronous motors with static, dynamic and mixed eccentricity,” *Electric Power Applications, IET*, vol. 4, no. 1, pp. 53 –66, January 2010

[7] Bon-Gwan Gu; Jun-Hyuk Choi; In-Soung Jung, "Development and Analysis of Interturn Short Fault Model of PMSMs With Series and Parallel Winding Connections," *Power Electronics, IEEE Transactions on*, vol.29, no.4, pp.2016,2026, April 2014

[8] Ebrahimi, B.M.; Faiz, J.; Roshtkhari, M.J., "Static-, Dynamic-, and Mixed-Eccentricity Fault Diagnoses in Permanent-Magnet Synchronous Motors," *Industrial Electronics, IEEE Transactions on* , vol.56, no.11, pp.4727,4739, Nov. 2010

[9] D. Dorrell, M. Popescu, and D. Ionel, “Unbalanced magnetic pull due to asymmetry and low-level static rotor eccentricity in fractional-slot brushless permanent-magnet motors with surface-magnet and consequent-pole rotors,” *Magnetics, IEEE Transactions on*, vol. 46, no. 7, pp. 2675 –2685, july 2010

[10] J. Li, Z. Liu, and L. Nay, “Effect of radial magnetic forces in permanent magnet motors with rotor eccentricity,” *Magnetics, IEEE Transactions on*, vol. 43, no. 6, pp. 2525 –2527, june 2007

[11] W. le Roux, R. G. Harley, and T. G. Habetler, “Detecting rotor faults in low power permanent magnet synchronous machines,” *Power Electronics, IEEE Transactions on*, vol. 22, no. 1, pp. 322 –328, jan. 2007

[12] L. Romeral, J. Urresty, J.-R. Riba Ruiz, and A. Garcia Espinosa, “Modeling of surface-mounted permanent magnet synchronous motors with stator winding interturn faults,” *Industrial Electronics, IEEE Transactions on*, vol. 58, no. 5, pp. 1576 –1585, may 2011

[13] Giulii Capponi, F.; De Donato, G.; Caricchi, F., "Recent Advances in Axial-Flux Permanent-Magnet Machine Technology," *Industry Applications, IEEE Transactions on*, vol.48, no.6, pp.2190,2205, Nov.-Dec. 2012.

[14] Zhaoqiang Zhang; Matveev, A.; Nilssen, R.; Nysveen, A., "Ironless Permanent-Magnet Generators for Offshore Wind Turbines," *Industry Applications, IEEE Transactions on* , vol.50, no.3, pp.1835,1846, May-June 2014

[15] Vansompel, H.; Sergeant, P.; Dupre, L.; van den Bossche, A., "Axial-Flux PM Machines With Variable Air Gap," *Industrial Electronics, IEEE Transactions on* , vol.61, no.2, pp.730,737, Feb. 2014.
[16] Ping Zheng; Jing Zhao; Ranran Liu; Chengde Tong; Qian Wu, "Magnetic Characteristics Investigation of an Axial-Axial Flux Compound-Structure PMSM Used for HEVs," *Magnetics, IEEE Transactions on* , vol.46, no.6, pp.2191,2194, June 2010
[17] Kamper, M.J.; Rong-Jie Wang; Rossouw, F.G., "Analysis and Performance of Axial Flux Permanent-Magnet Machine With Air-Cored Nonoverlapping Concentrated Stator Windings," *Industry Applications, IEEE Transactions on* , vol.44, no.5, pp.1495,1504, Sept.-Oct. 2008.
[18] J. F. Gieras, R. J. Wang and M. J. Kamper, Axial flux permanent magnet brushless machines. Kluwer academic publishers, Dordrecht, The Netherland, 2004.
[19] Kobayashi, Y. Doi, K. Miyata and T. Minowa, "Design of the axial-flux permanent magnet coreless generator for the multi-megawatts wind turbine" *EWEA European Offshore Wind Conference & Exhibition*, Stockholm, Sweden, Sep. 2009.
[20] Siemens Press Release. (2012, Sep. 19) [Online]. Siemens industry presents new gearless direct drive wind generator [Accessed July 2013].
[21] D. N. Mbidi, K. van der Westhuizen, R. Wang, M. J. Kamper, and J. Blom, "Mechanical design considerations of a double stage axial-flux PM machine," *IEEE IAS Conf*., vol. 1, pp. 198–201., 2000.
[22] S. M. Mirimani, A. Vahedi, and F. Marignetti, "Effect of inclined static eccentricity fault in single stator–single rotor axial flux permanent magnet machines," *IEEE Trans. Magn.*, vol. 48, no. 1, pp. 143–149, Jan. 2012
[23] Di Gerlando, A; Foglia, G.M.; Iacchetti, M.F.; Perini, R., "Evaluation of Manufacturing Dissymmetry Effects in Axial Flux Permanent-Magnet Machines: Analysis Method Based on Field Functions," *Magnetics, IEEE Transactions on* , vol.48, no.6, pp.1995,2008, June 2012
[24] Wanjiku, J.; Khan, M.A.; Barendse, P.S.; Pillay, P., "Influence of Slot-Openings and Tooth Profile on Cogging Torque in Axial-Flux PM Machines," *Industrial Electronics, IEEE Transactions on* , vol.PP, no.99, pp.1,1
[25] Magnussen, F.; Lendenmann, H., "Parasitic Effects in PM Machines With Concentrated Windings," *Industry Applications, IEEE Transactions on* , vol.43, no.5, pp.1223,1232, Sept.-oct. 2007
[26] Haodong Yang; Yangsheng Chen, "Influence of Radial Force Harmonics With Low Mode Number on Electromagnetic Vibration of PMSM," *Energy Conversion, IEEE Transactions on* , vol.29, no.1, pp.38,45, March 2014
[27] A. M. El-Refaie, M. R. Shah, J. P. Alexander, S. Galioto, K. K. Huh, and W. D. Gerstler, "Rotor end losses in multi-phase fractional slot concentrated winding permanent magnet synchronous machines," *IEEE Trans. Ind. Appl.*, vol. 47, no. 5, pp. 2066–2074, Sep.–Oct. 2011.
[28] R. Di Stefano and F. Marignetti, "Electromagnetic analysis of axialflux permanent magnet synchronous machines with fractional windings with experimental validation," *IEEE Trans. Ind. Electron.*, vol. 59, no. 6, pp. 2573–2582, Jun. 2012
[29] Lenze Servo Systems. (March 2010). Technical document [Online].Available:http://www.lenze.com/lenze.com_en_active/020_Products/020_Servo_drives/020_Servomotoren/Produktfamilie_Servomotoren.com.jsp?cid=0b0164e0800906ad

Chapter 4

Influence of Rotor Topologies and Cogging Torque Minimization Techniques on AFPM Machine under SE

4.1 Introduction

There are numerous topologies are associated with the AFPM machine. Some of these have been identified in [1]-[7]. From their physical outlook in Fig.4.1; the various topologies can be broadly classified in terms of the following; stator-rotor arrangement, stator type, method of PM integration to the rotor and method of PM arrangement on the rotor as shown in Table 4.1. The merits and demerits of these topologies are then presented. Key features in their design are the large aspect ratio (ratio of outer diameter to axial length) and rotor structural mass which accounts for half of the total active mass. These make AFPM machine susceptible to eccentricities; which can impair its performance, cause structural imbalance, mechanical stress and strains on bearings [8]. The maximum allowable manufacturing tolerance for SE in permanent magnet (PM) machines is 10%, above this, cases may be considered as faults [9]-[10]. SE is a condition of unequal airgap between stator and rotor. It occurs due to manufacturing imperfections such as unbalanced mass and bearing tolerance, or may be caused by shaft bow and bearing damage [11]-[12], resulting in unbalanced magnetic pull (UMP), vibrations, winding loosening, insulation fretting, stator-rotor rub and damage [8]-[16].

Table4.1. Some AFPM machine topologies

Topologies	Advantages	Disadvantages
Stator-rotor arrangement		
(a) Single-sided structure	Fewer PM is utilized, simple construction	Lower torque production, axial force is taken by bearing disc stiffness, poor winding utilization
(b) Double-sided structure i. Internal rotor or ii. Internal stator	Larger torque possible with a little increase in rotor diameter, better winding utilization	Lacks robustness and mechanical strength especially at high speed of operation. Requires larger volume of PMs
Stator type		
(a) Slotted stator core	Small air gap, low magnet volume	Large iron losses
(b) Slotless stator core	Flux ripples, cogging torque and saturation of core are eliminated. Hysteresis and eddy current losses do not exist	Higher magnet and copper volume are required
Method of integrating the PMs to the rotor		
(a) Surface-mounted (exterior) PM type	Ease of manufacturing	Not suitable for very high speed operation, PMs are exposed to factors causing demagnetisation
(b) Interior permanent magnet type	Saliency effect; hence reluctance torque, protection against demagnetisation and corrosion	Difficult to manufacture, higher cost
Method of arranging PMs on rotor face		
(a) N-N or S-S	Reduced end windings length, hence lower copper cost	Larger iron losses, difficult to assemble
(b) N-S	Results in lower iron losses	Effective only in iron-core type, long end windings and hence, higher copper losses

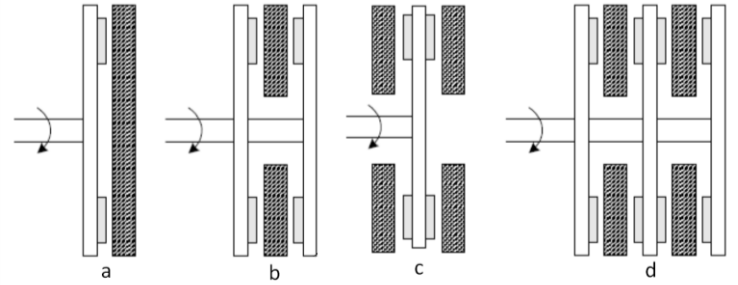

Fig.4.1. Rotor topologies of AFPM machine: (a) single-sided, (b) double-sided (inner stator), (c) double sided (inner rotor), (d) multi-stack

In [17]-[23], SE exacerbates cogging therefore cogging torque minimization techniques are investigated. However, the effects of these techniques on MMF harmonics and overall torque response are not considered. In [12], superposition of field functions was used to analytically evaluate the field and global quantities of the AFPM machine. Finite element analysis (FEA) is then used to investigate the field shapes and identify the parameters. This approach helps to analyse the effect of rotor dissymmetry on the circulation of current among winding parallel path. Though the technique gives insight into the behaviour of the machine, it cannot detect faults in real-time. In [13]-[15], the effects of static eccentricity on AFPM machine using finite elements analysis are studied. Results reveal unbalance in magnetic forces and torque. In [9], reduced magnitudes of induced EMF on the stator coils adjacent to the region with increased airgap are observed. The results were verified experimentally but the detection methods are offline since individual stator coils need to be floating for measurement of back EMF. Non-invasive diagnostic techniques are identified in [10]-[11], [16], phase current monitoring is identified as an alternative for condition-based maintenance due to lower cost and ease of measurement. Sideband frequencies are proposed as an index for eccentricity diagnosis but the prototype investigated is a radial-flux topology with a distributed winding configuration [11]. The larger amplitudes of dynamic eccentricities (DE) are used to discriminate it from SE. However,

some of the frequencies coincide with other rotor fault frequencies such as shaft misalignment and broken magnets frequencies etc. [16], [24].

In this chapter, using FEA and experimental verification, the following are investigated:

1. The effects of cogging torque minimization techniques (CTMTs) namely; magnet skewing and magnetic pole arc alternation, on current harmonics and torque ripple. Their impact on machine performance in the presence of SE is studied since they are widely applied in the design of PM machines.
2. The effect of SE on line current for fault detection; space harmonics are examined alongside the sideband components.
3. The impact of SE on single-sided and double-sided rotor topologies.
4. To propose a parametric signal processing technique as an alternative to the FFT in extracting SE fault features.

4.2 Effect of the CTMTs and Rotor Topologies on Harmonics

The three PM configurations used on the rotor disc for CTMT are shown in Fig.3.4. They are; equal PM pole, alternating PM pole and skewed PM poles. The fitting skew angle and magnetic pole width for both skewed and alternating PM pole respectively, both used as configurations to minimize cogging torque, are derived for the prototype in [25]. The pole-arc ratio and skewing angle per slot-pitch is given in Table 4.2. The full design details are given in [25]. The mathematical analysis of cogging and the effects of CTMTs on cogging torque are well documented in literature [20]-[23], [26]. Magnet skewing and alternating pole arc are two popular methods used to reduce cogging torque [22]. Due to manufacturing difficulty and expenses associated with skewing, alternating PM arc width is used as an alternative. The alternating PM arc width technique is similar to magnet skewing as it diminishes cogging torque harmonics using similar principles [20], but the determination of an appropriate pole arc width for

Table 4.2. PM Configurations on the prototypes

Rotor Topologies	Conventional Technique	Cogging Torque Minimization Techniques	
	Equal PM Pole	Skewed PM Pole	Alternate PM Pole
Single-Sided	0.80	$3^{o}\ \alpha_{skew}$	0.61-0.80
Double-Sided	0.80	$3^{o}\ \alpha_{skew}$	0.61-0.80

the alternate poles is difficult in design [20]. The DS topology is derived to overcome the increasing aspect ratio as the power rating in the SS topology increases [1]. In this section, the impact of CTMTs and rotor topologies on flux linkage ψ^{v} and winding factor $k^{v}{}_{w}$, where v is the harmonic order, is examined since both flux linkage and winding factor are good indicators of MMF harmonic content.

4.2.1 CTMTs

The flux due to PMs which links all the windings gives the flux linkage for each phase under no-load. Considering high harmonics, flux linkage per phase is described in (4.1), where $\hat{\psi}_{PM}$ is the peak PM flux linkage of the vth harmonic and θ is the rotor position in electrical degrees.

$$\psi_{ph}(\theta) = \sum_{v}^{\infty} \hat{\psi}^{v}{}_{PM} \sin v\theta \qquad (4.1)$$

Since skewing changes the relative position between the stator slots and rotor PMs across the circumference of AFPM machine, the magnetic field distribution varies. Thus taking into account the skewing effect, the flux linkage for each harmonic order due to the PMs is deduced in (4.2) under the following assumptions:

1. The origin of the general reference frame is taken to be at the center of the machine
2. The circumferential variation of the saturation due to skewing is neglected.

Using the *xyz* coordinate system in Fig.4.2, the flux linkage in (4.2) is over the active radius of the machine, $-0.5D \leq z \leq 0.5D$. Thus, the vth harmonic of the PM flux-

linkage of a machine with skewing can be described in (4.3), where k_{skv} is the skewing factor due to PMs for vth harmonic as described in (4.4) [27]. The harmonic components of the flux linkage in (4.3) may be reduced by k_{skv} using skewed or alternating PM pole, thus making flux density more sinusoidal in the airgap.

$$\psi^{v}(\theta) = \hat{\psi}^{v}{}_{PM} \sin v\theta \tag{4.2}$$

$$\hat{\psi}^{v}{}_{sk}(\theta, z) = k^{v}{}_{sk} \hat{\psi}^{v}{}_{PM} \sin v\theta \tag{4.3}$$

$$k^{v}{}_{sk} = \frac{\sin\left(v\frac{s_{sk}\pi}{\tau_p\ 2}\right)}{v\frac{s_{sk}\pi}{\tau_p\ 2}} \tag{4.4}$$

where s_{sk} is skewing pitch ratio and τ_p is pole pitch

4.2.2 Rotor Topologies

As a consequence of the dual airgap in the DS topology, it becomes amenable to multilayer winding layers (four) compared with double layer in the SS topology. Therefore, by going from two to four layers, the synchronous winding factor is improved as a result of decrease in the distribution factor, k_{dv} in (4.5) [28]-[30].

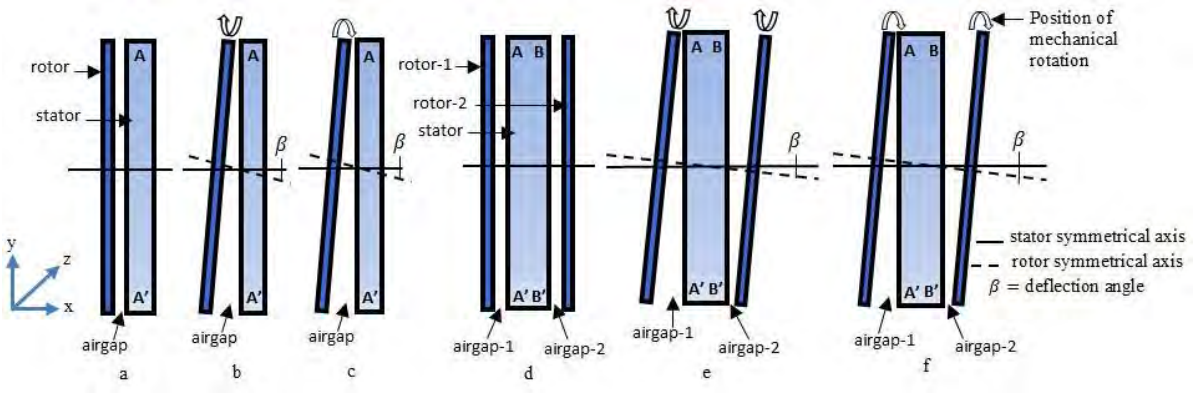

Fig.4.2. AFPM machine in 2D plane: (a-c) SS topology, (d-f) DS topology

In a FSCW, k_{dv} cannot be simply defined; however using voltage phasor k_{dv} is deduced in [27], [29] for various layers and slot/pole combinations. For example, the winding factor of the fundamental harmonic in the double layer winding of the prototype reduces from 0.067 to 0.0173 in the four layer windings for the fundamental harmonic component. Consequently, a combination of CTMTs with multilayer winding of the DS topology may result in larger reduction of $k^v{}_w$.

$$k^v{}_w = k^v{}_p k^v{}_d k^v{}_{sk} \tag{4.5}$$

4.3 Modelling of SE in AFPM Machine

4.3.1 2D Analytical

SE is a condition in which the axis of the rotor overlaps with its rotational axis but is deflected from that of the stator [9], [12]. The center line of the shaft is positioned at a constant offset from the stator, causing a time-invariant non-uniform airgap. The phenomenon of SE in AFPM machines is more penetrating than in the radial-flux type because it is inherently a 3D and complex geometry; as such the physical modelling of SE is difficult. However, a 2D plane in Fig.4.2 is used in this paper to reduce the scale of the geometry and to provide a bases for precise replication of the fault in FEA and experimentation. The machines under investigation are the surface-mounted PM, iron core stator, SS, and DS as shown in Fig.4.2. The SS topology has a rotor disc and single airgap while the DS topology has two airgaps and two rotor discs which rest on a common shaft. The healthy state is shown for SS and DS in Fig.4.2a&Fig.4.2d respectively, the airgap length, g is uniform along the axial direction (*x*-coordinate) and around the circumference (*y*-coordinate) of the stator. Here, the symmetrical axis of the rotor coincides with that of the rotor, irrespective of mechanical rotation. However, in event of occurrence of SE, the rotor shaft experiences a deflection and the symmetry of the rotor deviates from the stator's by an angle, β and the airgap varies in axial

length from small to large around the circumference of the stator. This variation is fixed in space, that is, it is independent of the position of mechanical rotation as indicated in Fig.4.2b-c for SS and Fig.4.2e-Fig.4.2f for DS. For this reason, permeance varies axially across the machine circumference from maximum to minimum in the regions of minimum to maximum airgap respectively. In the DS topology, Fig.4.2e-Fig.4.2f, the deflection of one rotor is conversely reflected on the other, in equal proportion. This causes the minimum reluctance seen by a stator face to experience a corresponding maximum reluctance on the opposite face since the rotor discs rest on a common shaft. Fig.4.3 (not drawn to scale) illustrates the worst possible scenario of the resulting asymmetric airgap due to SE. Here, mechanical clearance ceases to exist and the rotor disc starts to make contact with the stator. Thus, (4.6)-(4.8) is derived from the geometry, where D is the diameter of the rotor disc, γ and g_{max} are the resulting deflection angle and airgap length respectively. The increase in g is a consequence of the deflection length r which is directly proportional to β, with the greatest possible limit reached in (4.6) and (4.7). Therefore irrespective of the diameter of an AFPM machine, its deflection length from its axis is within the limits of the air-gap, i.e., the variation in air-gap length caused by SE is $g_{min} \geq 0 \leq 2g \geq g_{max}$ and the deflection length $r \leq g$. It can be measured in (4.9) as a percentage ratio of the deflection length to the length of the ideal airgap and the effective length of airgap caused by SE is expressed in (4.10), where φ is time-invariant spatial position. In practice, though $4g \ll (D + x)$ in (4.8), when $\gamma \gg 0$ significant SE factor given in (4.9) will result. Furthermore, since $0 < x$ and $0 < y$ in Fig.4.8, leakage flux will occur. These effects of SE on the magnetic field are better accounted for in FE computation using this 2D model in 3D finite element analysis (FEA).

$$g_{min} = g - r = 0 \tag{4.6}$$

$$g_{max} = g + r = 2g \tag{4.7}$$

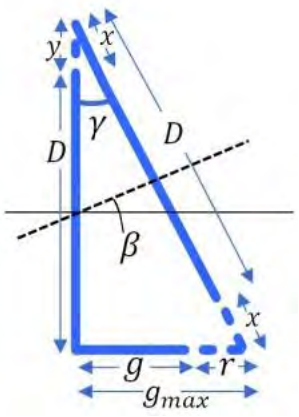

Fig.4.3. A cross-section of the asymmetric airgap

$$\frac{4g}{(D+x)} = \sin\gamma \tag{4.8}$$

$$\epsilon_s = \frac{r}{g} \times 100\% \tag{4.9}$$

$$g_e(\varphi) = g(1 \pm \epsilon_s) \tag{4.10}$$

4.3.2 3D FEA

The basis of any reliable fault diagnosis method for electric machines is precise performance analysis under both healthy and faulty conditions. Modelling of the fault is imperative in understanding and diagnosing the condition. Thus approaches that consider all effective characteristics of machines, such as FEA are reliable for investigating faulty machines [31]. The major advantage of FEA is that physical geometries can be modelled mathematically and numerical techniques can be employed to give precise electromagnetic solutions. Although at present, commercial 2D/3D FEA software packages are primarily not designed for fault investigations, their effective application for fault analysis can be skilfully achieved. Cedrat's Flux® is the commercial FEA software used to analyse the AFPM machine topologies under both healthy and faulty scenarios. Based on the analytical model, SE is replicated using the

geometric parameters of the experimental machine in chapter 3. The FEA takes into account significant practical parameters such as, saturation, leakage flux, finite permeance of magnetic materials, teeth and slotting effects. For a healthy machine, the FEA could be done by modelling a part of the geometry and applying periodicity since electrical machines have symmetrical characteristics. However, such simplification cannot be used in the case of SE since it alters the symmetrical properties of the machine. Thus, full geometrical modelling is performed using 3D FEA since the AFPM machine is inherently a 3D geometry.

4.4 Implementation of SE Faults

The axial magnetic force and pressure between the rotor and stator is very high, thus restraint of the rotor inclines due to SE as seen in Fig.4.2 is difficult. To practically implement the fault, the stator was housed on a flange which was fitted onto a rigid external frame. The flange is adjustable and its position on the external frame can be varied to obtain SE by displacing the stator axis from the rotor axis at an angular offset (illustrated in Fig.4.1) corresponding to the desired degree of SE. The rotor shaft was also designed with an in-step to rest the rotor disc and prevent the rotor from moving towards the stator (both shaft and rotor discs are shown in Fig.3.4). A fillet gauge was used to measure the resulting airgap variation to ensure accuracy. The rotor structure was not altered; thus the method eliminated the possibility of straining the bearing and inducing other faults during experimentation. The test rig developed in chapter 3 was the platform used for the fault replication.

4.5 Evaluation of Electromagnetic and Electrical Quantities

The effect of the CTMTs and rotor topologies under healthy and SE conditions on machine performance is determined by evaluating electrical and electromagnetic quantities. Using the Fourier transform and power spectrum density (PSD), the

harmonics present in the line current of the machine are extracted for both healthy and SE scenarios under various load conditions and at different speeds in the *abc* reference frame. Inductance and torque are also obtained from both FEA and experimentation to quantify the performance of the various rotor topologies and CTMTs. Since skewing decreases the rms value of the EMF fundamental wave as a result of reduced winding factor, the current and torque ratings are kept the same for both topologies and the three magnet configurations to provide a common template for the investigation.

4.5.1 Torque Ripple

4.5.1.1 Impact of CTMTs and Rotor Topologies on Torque Ripple under Healthy Condition

The effect of the various CTMTs on load torque is shown in Fig.4.4-4.5. The torque response is unidirectional and has both constant and periodic components. The periodic component is a function of time, superimposed on the offset and it is the cause of the pulsation. Results are obtained using (4.11)-(4.12) [32], where T_{av} is average torque, T_{cogg} is cogging torque, T_r is the total torque ripple and T_{MMF} is ripple due to MMF harmonics. At rated torque, the two CTMTs effectively reduced T_{MMF} in the equal PM pole configuration as shown in Fig.4.5, from 21.5% to 11.5% in the alternate PM pole and 11% in the skewed PM pole configuration in the SS topology. In the DS topology, the torque ripples obtained are 16%, 8.2% and 4.8% for the equal PM pole, alternate PM pole and skewed PM pole configuration respectively. The DS topology is more effective at reducing torque ripples due to MMF harmonics than the SS topology in combination with the CTMTs. The current harmonic components responsible for this are examined in the next section.

$$T_r(\propto) = \frac{T_{max} - T_{min}}{T_{av}} \tag{4.11}$$

$$T_{MMF} = T_r(\propto) - T_{cogg} \tag{4.12}$$

4.5.1.2 Impact of Rotor Topologies and CTMTs on Torque Ripple under SE Conditions

The torque response for both SS and DS topologies using the skewed PM pole is shown in Fig.4.6 and Fig.4.7 respectively. In the presence of SE, T_{MMF} in the SS topology increased with the degree of SE for all three PM configurations. The CTMTs do not prevent SE from impairing on machine performance but they reduce the impact; lower torque ripples are derived. However, no torque ripple effect due to SE is manifested in the DS topology. The inductances have been computed in FEA to closely examine this effect. Fig.4.8 shows the stator unsaturated inductances associated with the coils in the rotor position with minimum airgap length for the SS topology. Since the airgap length varies around the stator circumference, the inductances of the coils in all three phases vary. It is evident that the inductances increase with smaller length of airgap; however, in the DS topology in Fig.4.9, no change in inductance is evident for the same magnetic path. This phenomenon is better clarified in Fig.4.10 showing the FEA plot of the normal component of flux density B_n using the center of the symmetric airgap as reference. Here, B_n in airgap-1 is conversely reflected in airgap-2 in the DS topology (indicated by the dotted circle for 60^o mech. position). The coils *A* and *A*' in Fig.4.1e-Fig4.1f see minimum and maximum flux linkage respectively, and the ensuing inductance from the pair remained unaffected. Thus the DS topology is electromagnetically balanced under eccentricities. Variable airgap permeance which results from eccentricities does not impair on the performance of the DS topology. This electromagnetic field behaviour is the same in all the three magnet configurations investigated.

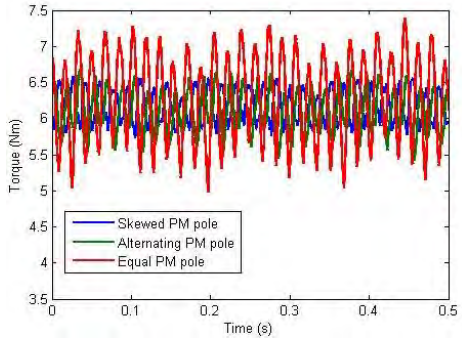

Fig.4.4. Impact of the various CTMTs on torque

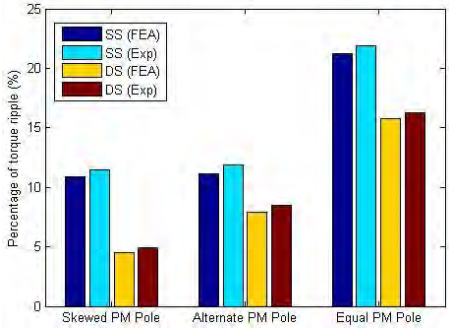

Fig.4.5. Influence of rotor topologies and CTMTs on torque ripple

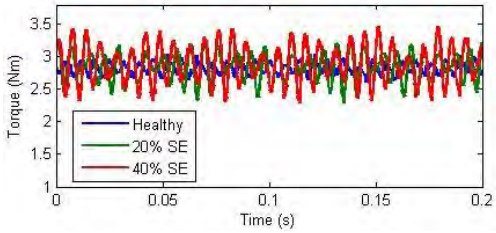

Fig.4.6. Torque pulsation under healthy and SE conditions in the SS topology

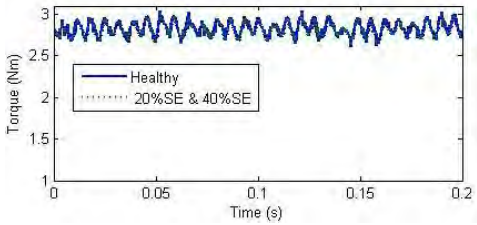

Fig.4.7. Torque pulsation under healthy and SE conditions in the DS topology

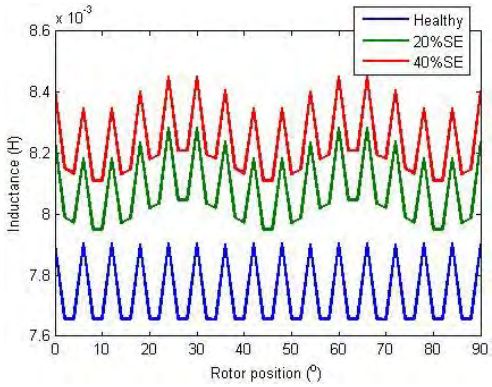

Fig.4.8. Inductance of magnetic path across rotor position with minimum airgap length in a SS topology

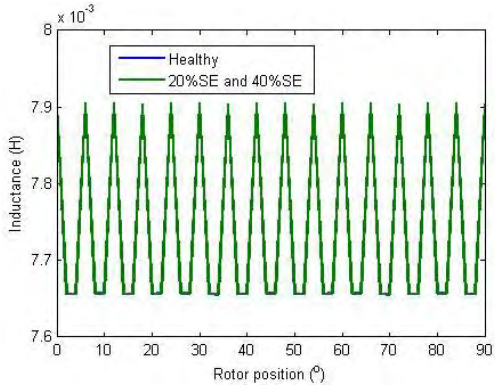

Fig.4.9. Inductance of magnetic path across rotor position with minimum airgap length in a DS topology

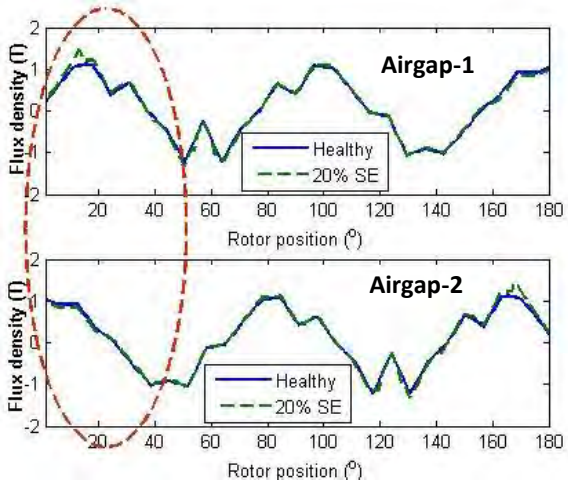

Fig.4.10. Normal component of magnetic flux density

4.5.2 Current Harmonics

4.5.2.1 Impact of CTMTs on Space Harmonics under Healthy Condition

In the FSCW configuration, the coils are spatially displaced by a limited number of slots under a high number of pole-pairs (i.e. $q < 1$) in a medium of non-sinusoidal airgap flux density distribution. Thus, space harmonics are induced in the voltages. This causes the windings to operate at current linkage harmonics defined by (4.13) [28], [33], where $m = 3$ and $k = 0, 1, 2 \ldots$, yielding $v = 1, -2, +4, \ldots$; where the sign is indicative of the direction of rotation of the harmonics based on rotating field theory. The space harmonics are of particular interest in PM machines with concentrated windings since MMF harmonics are inherently present which may cause additional rotor eddy current losses [29], [33]. Also, they are inherent regardless of the operating conditions of the machine albeit low in magnitude, especially the even order harmonics since symmetry is maintained around the poles. In Fig.4.11, the influence of the CTMT on v is obtained. It shows that the CTMTs effectively reduce their magnitudes since they cause the flux density to be more sinusoidal, thereby inducing a more sinusoidal back EMF and consequently leading to reduced current linkage harmonics. This reduction in MMF harmonics is desirable because they are the main source of torque pulsation when PM machines operate under load. Notice that the even order harmonics are lower in magnitude than the odd order harmonics since symmetry is maintained around the poles.

$$v = 1 \pm km \tag{4.13}$$

4.5.2.2 Impact of Rotor Topologies on Space Harmonics under Healthy Condition

Since the DS topology is amenable to four layers of windings, the winding factors in the double layer winding reduces from 0.067 to 0.0173, for $v = 1$. Similarly, the winding factor when $v = 2, 4, 5, 7, 8$ in the double layer configuration reduces from

0.933 to 0.9012. Consequently, the amplitudes of v are reduced by an average of 5% in the DS topology, relative to the SS topology as shown in Fig.4.12. Accordingly, lower T_{MMF} was derived from the torque response of the DS topology compared with the SS topology as shown in Fig.4.5. The decrease in amplitude is as a result of the multilayer winding in the DS topology, leading to a slightly lower distribution factor in (4.10).

4.5.2.3 Impact of Rotor Topologies and CTMTs on Space Harmonics under SE Conditions

Fig.4.13 shows the effect of SE on v using the alternate PM pole in the SS topology. The amplitudes are significantly affected by SE. The even order harmonics are largely more incited than the odd harmonics despite having been hitherto significantly reduced by the CTMTs since the space-variant airgap permeance characteristics given in (4.10) leads to asymmetric distortion of the MMF wave over a pole-pitch where the coils are displaced by a limited number of slots. Thus, the load torque in Fig.4.5 is insusceptible to SE. Furthermore, the impact of the CTMTs on v under SE in the SS topology is shown in Fig.4.14, where all the three PM configurations compared. It is revealed that the CTMTs considerably diminish the amplitudes of v, even in the presence of SE. But the amplitudes of v are unchanged in the DS topology under SE irrespective of the magnet configurations employed.

The magnitudes of v are clearly indicative of SE in the SS topology, but they may not suffice as indices for fault detection since they are largely dependent on the CTMTs employed and load variations are impactful on them as seen in Fig.4.15. Therefore the sub-harmonics in the line current are explored for fault detection.

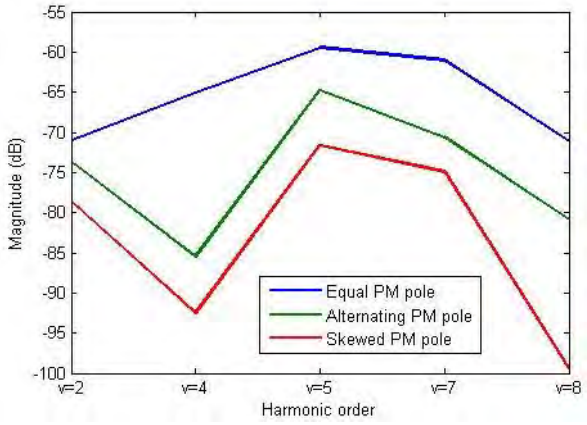

Fig.4.11. Impact of the various CTMTs on v

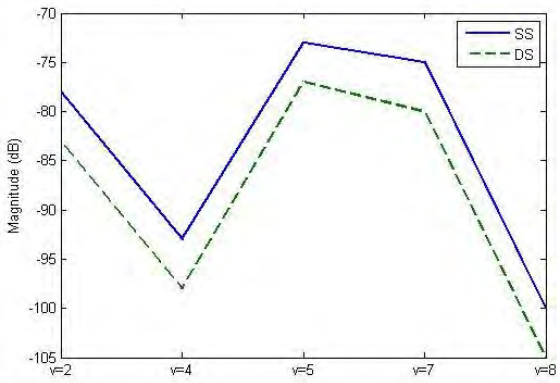

Fig.4.12. Impact of the DS topology on v

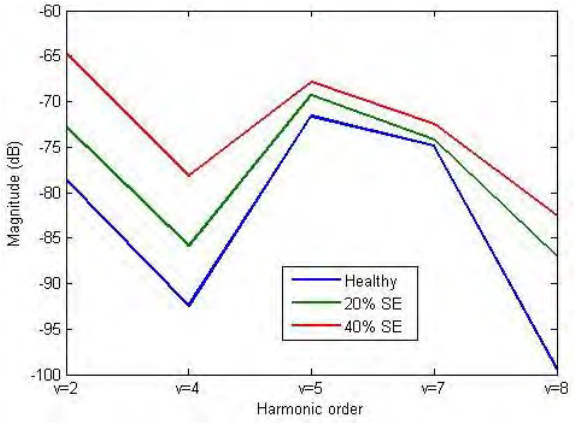

Fig.4.13. Effect of SE on v

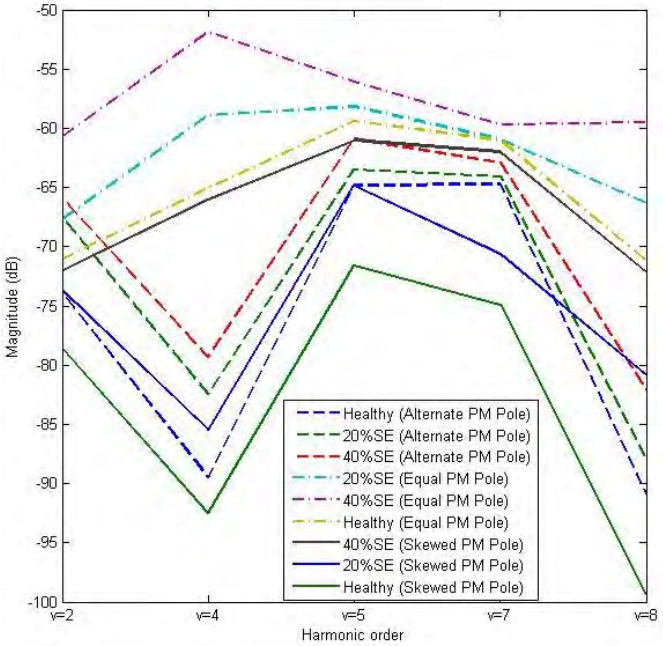

Fig.14.14 Impact of the CTMTs on v under SE

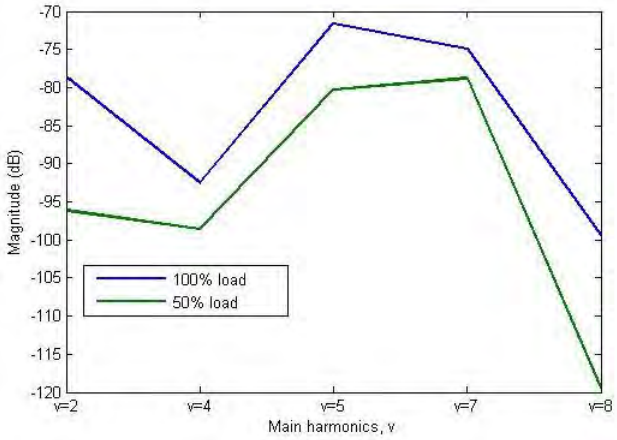

Fig.4.15. Effect of load variations on v

4.5.2.4 Sub-Harmonics under SE Condition and the Impact of CTMTs and Rotor Topologies

The amplitudes of the frequencies f_{SE} in (4.14), where f is the fundamental frequency of the line current, p is number of pole pairs and $k = 1, 2, 3 \ldots$ are extracted and proposed as indices for detection of SE in radial-flux PM machines with distributed

windings [10]-[11]. They are sidebands of the fundamental component. In the DS topology, the amplitudes of the sidebands in (4.14) are not affected and remained constant under SE conditions for the three PM configurations investigated. In the SS topology however, the sidebands significantly increased in amplitudes. The fault indices are found to be equally valid for AFPM machines in the SS topology as seen in Fig.4.16.

Unlike the space harmonics, the sub-harmonics are not significantly affected by the CTMTs under healthy and SE conditions. Their extracted amplitudes are shown in Fig.4.17. In addition, in Fig.4.18, load variations are found to have no considerable impact on their amplitudes, thereby making (4.14) a robust detection technique. However, some components in (4.13) and (4.14) overlap when v is an even order harmonic and $k = 3, 8, 13 \ldots$ respectively. Since v varies significantly in amplitudes due to load changes, the frequencies of the harmonic constants k coinciding with v are thus excluded in the detection technique and trending derived in Fig.4.16.

$$f_{SE} = f\left(1 \pm \frac{2k-1}{p}\right) \tag{4.14}$$

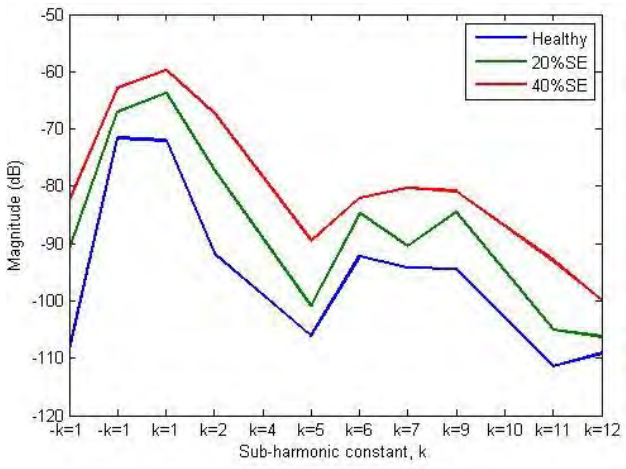

Fig.4.16. Effect of SE on frequency components with harmonic constant k

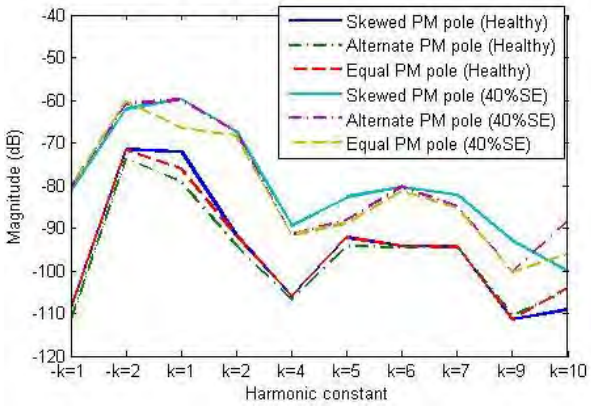

Fig.4.17. Effect of CTMTs on frequency components in (4.14)

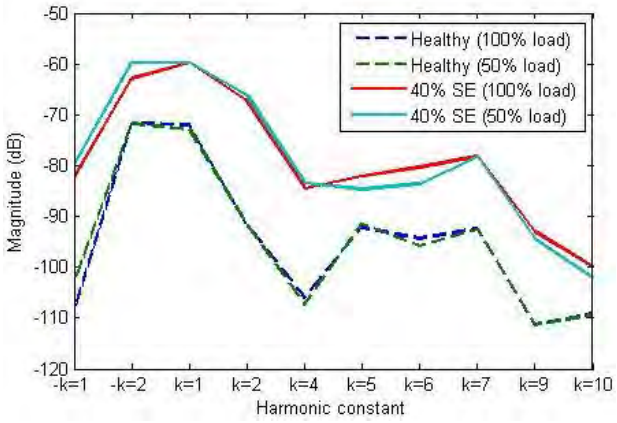

Fig.4.18. Effect load variations on frequency components in (4.14) using skewed PM pole

4.6 Current Signal Processing with ESPRIT

The standard industry technique used in processing electrical machine signals for fault diagnosis under steady-state is the FFT. It has been applied to extract the harmonics analysed. Though it is robust and simple to implement, it requires long measurement duration; typically not less than 30s is needed for high frequency resolution. However, the steady-state operation of AFPM machine is not guaranteed for such an extended time period because of load and speed variations. In addition, the hardware and/or data storage cost requirements in chapter 3 increase with

measurement duration. To overcome this, the ESPRIT parametric spectral estimation technique is proposed.

If the measured current signal is given by $x(n)$ in (4.15), where A_i, f_i and $\emptyset_i$ is the amplitude, frequency and the initial phase of the ith harmonic respectively, T_S is the sampling interval and p is the number of harmonics, parametric models which relate to the eigenvector decomposition of correlation matrix can be developed from the current signal and used to estimate the discrete part of the spectrum. An algorithm based on (4.15)-(4.20) [34]-[35] is implemented using MATLAB® programming to extract the fault harmonics. Parametric models relating to the eigenvector decomposition of the correlation matrix developed from the current signal are used to estimate the discrete part of the spectrum as described by the following steps:

1. Compute a transition matrix of $x(n)$ in (4.17)-(4.18).
2. Subsequently, construct the correlation and mutual-correlation matrix of (4.17) and (4.18) in (4.19) and (4.20) respectively, where E and Hi represents mathematical expectation and conjugation respectively.
3. Finally, sort the Eigen values from the singular-decomposition of R_{XX} and R_{XY}. Then compute the amplitudes and frequencies of the harmonic component of $x(n)$ from the resulting Eigen values.

$$x(n) = \sum_{i=1}^{p} A_i \cos(2\pi f_i n T_S + \emptyset_i) \quad n = 1, 2, \ldots, N \tag{4.15}$$

$$y(n) = x(n+1) \tag{4.16}$$

$$X(n) = [x(n) \;\; x(n+1) \;\; \ldots \;\; x(n+m-1)]^T \tag{4.17}$$

$$Y(n) = [y(n) \;\; y(n+1) \;\; \ldots \;\; y(n+m-1)]^T \tag{4.18}$$

$$R_{XX} = E\{X(n)X^{Hi}(n)\} \tag{4.19}$$

$$R_{XY} = E\{X(n)Y^{Hi}(n)\} \tag{4.20}$$

The result is seen in Fig.4.19 which shows the ESPRIT spectral estimation technique applied to the current signal under the same operating conditions as with the FFT. Close correlation of both frequencies and amplitudes is achieved with 2.5s of measurement as against 30s of measurement obtained using FFT. Using the FFT method, 60K samples of current signals were collected at 2kHz, but with ESPRIT, 5K samples were collected at 2kHz. This considerably reduces data storage requirement. However, computational time is longer using ESPRIT. The signal processing duration is 10s as against approximately 1s using FFT on the aforementioned number of samples.

4.7 Conclusions

Space harmonics are significantly reduced using CTMTs and in the DS topology under healthy condition as a result of reduced flux linkage harmonics and winding factor respectively. However, unlike the space harmonics, the sub-harmonics are not affected by the CTMTs and in the DS topology. Under SE conditions, increases in amplitudes of space and sub-harmonics are evident in the SS topology but not in the DS topology. This is effective for the three PM configurations investigated. The immunity of the DS topology is due to the opposing effect of the asymmetrical properties of its two airgap. Thus, the DS topology is a more robust and an efficient topology. It can correct the effects of rotor dissymmetry as a result of manufacturing imperfections or faults while the CTMTs can mitigate the impact of SE in the SS topology. The technique for fault detection of SE in radial-flux PM machines with distributed windings as established in literature is also applicable for the SS topology of the AFPM machine with concentrated windings if the harmonic constants which coincide with the even order space harmonics are not taken into account. The detection technique is robust against the CTMTs and load variations.

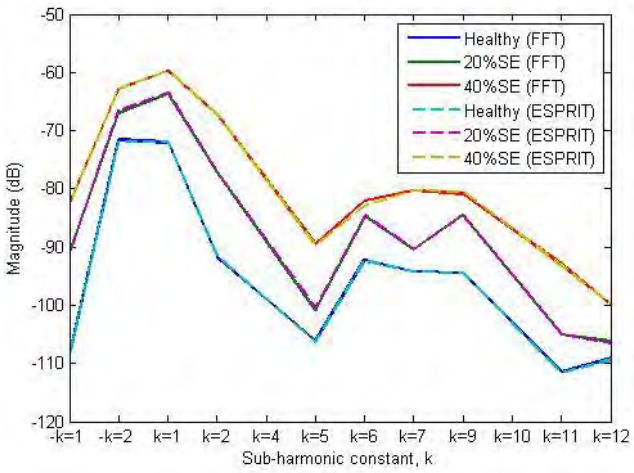

Fig.4.19. Correlation between FFT and ESPRIT using MCSA

4.8 References

[1] Giulii Capponi, F.; De Donato, G.; Caricchi, F., "Recent Advances in Axial-Flux Permanent-Magnet Machine Technology," *Industry Applications, IEEE Transactions on* , vol.48, no.6, pp.2190,2205, Nov.-Dec. 2012

[2] Okumura, Y.; Sanada, M.; Morimoto, S.; Inoue, Y., "Study of characteristics of various structures in axial-gap PM motors," *Electrical Machines and Systems (ICEMS), 2012 15th International Conference on*, vol., no., pp.1,6, 21-24 Oct. 2012

[3] Yicheng Chen; Pillay, P.; Khan, A., "PM wind generator topologies," *Industry Applications, IEEE Transactions on* , vol.41, no.6, pp.1619,1626, Nov.-Dec. 2005

[4] Kamper, M.J.; Rong-Jie Wang; Rossouw, F.G., "Analysis and Performance of Axial Flux Permanent-Magnet Machine With Air-Cored Nonoverlapping Concentrated Stator Windings," *Industry Applications, IEEE Transactions on* , vol.44, no.5, pp.1495,1504, Sept.-Oct. 2008

[5] Yicheng Chen; Pillay, P.; Khan, A, "PM wind generator topologies," *Industry Applications, IEEE Transactions on* , vol.41, no.6, pp.1619,1626, Nov.-Dec. 2005

[6] J. F. Gieras, R. J. Wang and M. J. Kamper, Axial flux permanent magnet brushless machines. Kluwer academic publishers, Dordrecht, The Netherland, 2004

[7] Pippuri, J.; Manninen, A; Keranen, J.; Tammi, K., "Torque Density of Radial, Axial and Transverse Flux Permanent Magnet Machine Topologies," *Magnetics, IEEE Transactions on* , vol.49, no.5, pp.2339,2342, May 2013

[8] Mbidi, D.N.; Van der Westhuizen, K.; Wang, R.; Kamper, M.J.; Blom, J., "Mechanical design considerations of a double stage axial-flux PM machine," *Industry Applications Conference, 2000. Conference Record of the 2000 IEEE*, vol.1, no., pp.198,201 vol.1, 2000

[9] Di Gerlando, A; Foglia, G.M.; Iacchetti, M.F.; Perini, R., "Evaluation of Manufacturing Dissymmetry Effects in Axial Flux Permanent-Magnet Machines: Analysis Method Based on Field Functions," *Magnetics, IEEE Transactions on* , vol.48, no.6, pp.1995,2008, June 2012

[10] Valavi, M.; Nysveen, A.; Nilssen, R., "Magnetic forces and vibration in permanent magnet machines with non-overlapping concentrated windings: A review," *Industrial Technology (ICIT), 2012 IEEE International Conference on* , vol., no., pp.977,984, 19-21 March 2012

[11] S. M. Mirimani, A. Vahedi, and F. Marignetti, “Effect of inclined static eccentricity fault in single stator–single rotor axial flux permanent magnet machines,” *IEEE Trans. Magn.*, vol. 48, no. 1, pp. 143–149, Jan. 2012

[12] B. Ebrahimi and J. Faiz, “Diagnosis and performance analysis of three phase permanent magnet synchronous motors with static, dynamic and mixed eccentricity,” *Electric Power Applications, IET*, vol. 4, no. 1, pp. 53 –66, January 2010

[13] Ebrahimi, B.M.; Faiz, J.; Roshtkhari, M.J., "Static-, Dynamic-, and Mixed-Eccentricity Fault Diagnoses in Permanent-Magnet Synchronous Motors," *Industrial Electronics, IEEE Transactions on* , vol.56, no.11, pp.4727,4739, Nov. 2010

[14] D. Dorrell, M. Popescu, and D. Ionel, “Unbalanced magnetic pull due to asymmetry and low-level static rotor eccentricity in fractional-slot brushless permanent-magnet motors with surface-magnet and consequent-pole rotors,” *Magnetics, IEEE Transactions on*, vol. 46, no. 7, pp. 2675 –2685, july 2010

[15] J. Li, Z. Liu, and L. Nay, “Effect of radial magnetic forces in permanent magnet motors with rotor eccentricity,” *Magnetics, IEEE Transactions on*, vol. 43, no. 6, pp. 2525 –2527, june 2007

[16] W. le Roux, R. G. Harley, and T. G. Habetler, “Detecting rotor faults in low power permanent magnet synchronous machines,” *Power Electronics, IEEE Transactions on*, vol. 22, no. 1, pp. 322 –328, jan. 2007

[17] Zhu, Z.Q.; Wu, L.J.; Mohd Jamil, M.L., "Influence of Pole and Slot Number Combinations on Cogging Torque in Permanent-Magnet Machines With Static and Rotating Eccentricities," *Industry Applications, IEEE Transactions on* , vol.50, no.5, pp.3265,3277, Sept.-Oct. 2014

[18] Jagasics, S., "Comprehensive analysis on the effect of static air gap eccentricity on cogging torque," *Robotics in Alpe-Adria-Danube Region (RAAD), 2010 IEEE 19th International Workshop on* , vol., no., pp.447,449, 24-26 June 2010

[19] Afsari kashani, S.; Heydari, H.; Dianati, B., "Cogging Torque Mitigation in Axial Flux Magnetic Gear System Based on Skew Effects Using an Improved Quasi 3-D Analytical Method.," *Magnetics, IEEE Transactions on* , vol.PP, no.99, pp.1,1, Sept.-Oct. 2015

[20] Bianchi, N.; Bolognani, S., "Design techniques for reducing the cogging torque in surface-mounted PM motors," *Industry Applications, IEEE Transactions on* , vol.38, no.5, pp.1259,1265, Sep/Oct 2002

[21] Caricchi, F.; Capponi, F.G.; Crescimbini, F.; Solero, L., "Experimental study on reducing cogging torque and no-load power loss in axial-flux permanent-magnet machines with slotted winding," *Industry Applications, IEEE Transactions on* , vol.40, no.4, pp.1066,1075, July-Aug. 2004

[22] Bianchini, C.; Immovilli, F.; Lorenzani, E.; Bellini, A.; Davoli, M., "Review of Design Solutions for Internal Permanent-Magnet Machines Cogging Torque Reduction," *Magnetics, IEEE Transactions on* , vol.48, no.10, pp.2685,2693, Oct. 2012

[23] Aydin, M.; Gulec, M., "Reduction of Cogging Torque in Double-Rotor Axial-Flux Permanent-Magnet Disk Motors: A Review of Cost-Effective Magnet-Skewing Techniques With Experimental Verification," *Industrial Electronics, IEEE Transactions on* , vol.61, no.9, pp.5025,5034, Sept. 2014

[24] Yao Duan; Toliyat, H., "A review of condition monitoring and fault diagnosis for permanent magnet machines," *Power and Energy Society General Meeting, 2012 IEEE* , vol., no., pp.1,4, 22-26 July 2012

[25] Wanjiku, J.; Khan, M.A.; Barendse, P.S.; Pillay, P., "Influence of Slot-Openings and Tooth Profile on Cogging Torque in Axial-Flux PM Machines," *Industrial Electronics, IEEE Transactions on* , vol.PP, no.99, pp.1,1

[26] A. B. Letelier, D. A. Conzalez, J. A. Tapia, R. Wallace, and M. A. Valenzuela, “Cogging torque reduction in an axial flux PMmachine via stator slot displacement and skewing,” *IEEE Trans. Ind. Appl.*, vol. 43, no. 3, pp. 685–693, May/Jun. 2007

[27] Fornasiero, E.; Bianchi, N.; Bolognani, S., "Slot Harmonic Impact on Rotor Losses in Fractional-Slot Permanent-Magnet Machines," *Industrial Electronics, IEEE Transactions on* , vol.59, no.6, pp.2557,2564, June 2012
[28] Juha Pyrhönen, Tapani Jokinen and Valeria Hrabovcova, Design of rotating electrical machines, London: Wiley 2009
[29] Magnussen, F.; Sadarangani, C., "Winding factors and Joule losses of permanent magnet machines with concentrated windings," *Electric Machines and Drives Conference, 2003. IEMDC'03. IEEE International* , vol.1, no., pp.333,339 vol.1, 1-4 June 2003
[30] Reddy, P.B.; EL-Refaie, A.M.; Kum-Kang Huh, "Effect of Number of Layers on Performance of Fractional-Slot Concentrated-Windings Interior Permanent Magnet Machines," *Power Electronics, IEEE Transactions on* , vol.30, no.4, pp.2205,2218, April 2015
[31] Hamid Toliyat, S. Nandi, S. Choi, H. Meshdin-Kelk, Electrical machines: Modeling, condition monitoring and fault diagnosis. CRC Press, Taylor and Francis Group, Boca Raton, USA, 2013
[32] J. F. Gieras, R. J. Wang and M. J. Kamper, Axial flux permanent magnet brushless machines. Kluwer academic publishers, Dordrecht, The Netherland, 2004.
[33] Nakano, M.; Kometani, H.; Kawamura, M., "A study on eddy-current losses in rotors of surface permanent-magnet synchronous machines," *Industry Applications, IEEE Transactions on* , vol.42, no.2, pp.429,435, March-April 2006.
[34] R. Roy and T. Kailath, “ESPRIT-estimation of signal parameters via rotational invariance techniques,” *IEEE Trans. Acoust., Speech, Signal Process.*, vol. 37, no. 7, pp. 984–995, Jul. 1989.
[35] Boqiang Xu; Liling Sun; Lie Xu; Guoyi Xu, "An ESPRIT-SAA-Based Detection Method for Broken Rotor Bar Fault in Induction Motors," *Energy Conversion, IEEE Transactions on* , vol.27, no.3, pp.654,660, Sept. 2012

Chapter 5
Detection of ISC Faults Using Current Analysis

5.1 Introduction

Interturn short circuit (ISC) faults are identified as the root cause of most stator winding faults which accounts for 21% of the faults occurring in electrical machines [1]. Other types of winding faults are coil-to-coil, turn-to-turn, phase open-circuit, phase-to-phase and phase-to-ground [2]. ISC is caused by copper insulation breakdown, resulting in low-power intermittent arcing, which causes erosion of the conductor until enough power is drawn to weld them. Once the welding has occurred, high induced currents in the shorted loops lead to rapid stator failure [2]. This is problematic in surface-mounted PM machine because it may produce magnetic field intensity higher than the coercivity of the magnet, thereby demagnetizing the spinning magnets permanently [3]. ISC may also aid in the acceleration of insulation breakdown due to thermal stress caused by the fault current [3]-[6]. Thus, early detection and diagnosis of this type of failure is necessary. As a result, focus of some works has been directed towards detecting ISC in rotating electric machines [3]-[15]. In [6]-[12], techniques were developed to monitor machine's health condition and make online diagnosis. The motor current signature analysis (MCSA) is the most powerful and widely used technique [10]. In [13]-[14], ISC faults are modelled both analytically and in FEA, ISC is then evaluated by calculating inductances and back EMF. In [15], reference frame and two-axis theory are used to analyse the current signal. In [7]-[8], a rigorous mathematical study of ISC is presented. In [7]-[8], [14]-[15], the knowledge of the

performance of PM machines under ISC is advanced but there are limitations in applicability of results to online detection of faults since the machines were not analysed for practical fault detection purposes or procedures. In [10]-[12], the analysis focused on the current signature using frequency and time-frequency analysis without identifying a unique frequency pattern. In [13], a frequency pattern is introduced for a radial-flux PM machine with distributed windings. It is based on the harmonics of airgap magnetic field, but it does not encompass all harmonics triggered by ISC and the frequencies overlap with that of rotor eccentricities. In AFPM machine, detection of stator winding faults is important as they become increasingly deployed in numerous applications [16]-[17]. Therefore in this chapter, detection technique for ISC faults and discrimination from SE faults in AFPM machines is sought in both steady-state and transient conditions by applying a combination of signal processing techniques on the current signal. First, AFPM machine with FSCW is modelled under ISC fault; the electromagnetic behaviour is investigated analytically and using FEA with the aim to provide insight into the pattern of fault harmonics in the current spectrum.

5.2 Modelling of the ISC Faults

PM machines with FSCW are described as fault-tolerant machines because of physical isolation among the 3-phase windings. Nonetheless, ISC may occur within turns belonging to each coil in a phase. In the electrical representation shown in Fig.5.1, the fault is on phase 'A', where subscripts 'a' and 'a1' represent healthy and faulty parts of phase 'A' respectively, V, I, L and R are the voltages, currents, inductances and resistances of each phase respectively. The transient and steady-state performance can be evaluated in (5.1). The mutual inductance M between each phase is zero since the coil windings belonging to a phase are non-overlapping and physically

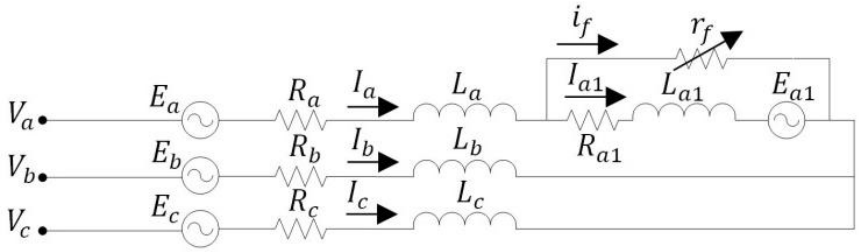

Fig.5.1. Electrical representation of the ISC fault

isolated from each other and from coils of other phases. However, under interturn fault, mutual inductance exists between the healthy and faulty part of the faulty phase. Thus under inter-turn fault, the stator voltage V_a in (5.1) can be expressed as the sum of (5.2) and (5.3), where M_1 is the mutual inductance between the healthy and faulty windings. Both transient and steady-state behaviour depends on R_a, L_a, M_1 and L_{a1}. All of these parameters are influenced by i_f, incited as $r_f \rightarrow 0$, and by the number of shorted turns; with R_a inversely proportional to the number of shorted turns, and changing with the thermal time constant of the windings due to the heating effect of i_f. It is difficult to estimate the inductances analytically, but using FEA, their quantities, as well as the influence of the number of shorted turns and saturation caused by i_f on them can be accurately evaluated.

The parameters of the prototype of the experimental machine are chosen for the field computation studies in 3D FEA using Cedrat's Flux®. Based on Fig.5.1, ISC is replicated using the geometric parameters of the prototype and the performance was determined at constant speed. In the analysis, the effect of saturation on permeance, caused by increased magnetic field due to i_f is revealed in Fig.5.2 where the stator winding inductance profile of the faulty machine is seen distorted and shifted along the vertical axis with variation in magnitude across the rotor positions where the shorted turns are located. An electromagnetic analysis using the MMF-permeance model given by (5.4) is used to further analyse this behaviour. If airgap magnetic flux density B is a product of MMF $\mathcal{F}$ and permeance Λ, at any point in the airgap the instantaneous

spatial and time variations in $B(\theta,t)$ can be determined by (5.5), where $\mathcal{F}_1$ and $\mathcal{F}_2$ are stator and rotor MMFs respectively. Since, changes in $B(\theta,t)$ is a consequence of variations in Λ, changes in permeance is the primary indicator of ISC faults. This can be evaluated with the aid of the Fourier series as an even function in (5.6) [18], where k is the number of harmonics which replace the airgap variation bounded by the stator and rotor active surfaces. The first term corresponds to the relative permeance Λ_0 of the

$$[V_{abc}] \quad = [R_{abc}][I_{abc}] + [L]\frac{d[I_{abc}]}{dt} + [E_{abc}] \tag{5.1}$$

$$\textit{where } [L] = \begin{bmatrix} L_s & 0 & 0 \\ 0 & L_s & 0 \\ 0 & 0 & L_s \end{bmatrix}$$

$$[V_a] = [E_a] + [I_a][R_a] + [L_a]\frac{d[I_a]}{dt} + [M_1]\frac{d[I_{a1}]}{dt} \tag{5.2}$$

$$[V_{a1}] = [E_{a1}] + [I_{a1}][R_{a1}] + [L_{a1}]\frac{d[I_{a1}]}{dt} + [M_1]\frac{d[I_a]}{dt} \tag{5.3}$$

$$\textit{where } [L] = \begin{bmatrix} L_s & M_{ab} & M_{ac} \\ M_{ba} & L_s & M_{bc} \\ M_{ca} & M_{cb} & L_s \end{bmatrix}$$

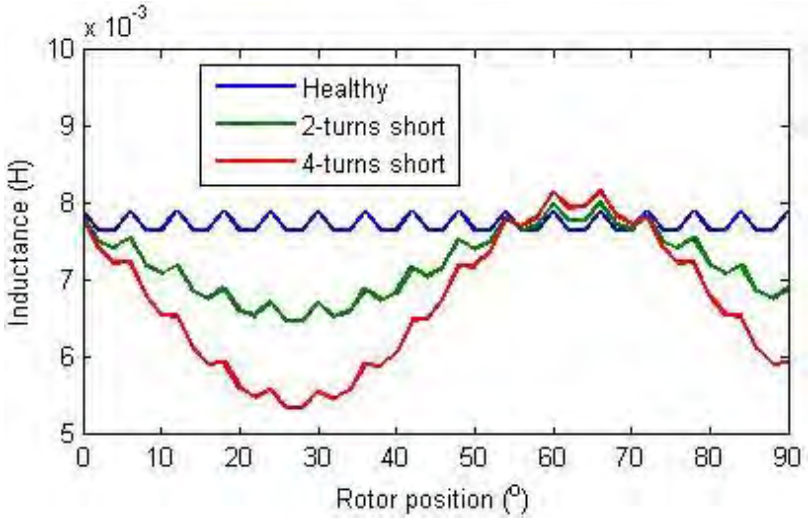

Fig.5.2. Inductance of the winding as seen from the rotor under ISC

physical airgap increased by Carter's coefficient, which takes into account stator slot openings while the second term Λ_k describes higher harmonics coefficients. At the onset of faults, change in permeance is established and the resulting asymmetric flux distribution may cause additional harmonics in the second term of (5.6). Thus the voltage induced in the windings due to space distribution of the main flux contains additional waveform component linked to the flux produced by i_f which may lead to sequence of harmonics and/or sub-harmonics in the winding linkage current.

$$B(\theta, t) = \mathcal{F}(\theta, t)\, \Lambda(\theta, t) \tag{5.4}$$

$$B(\theta, t) = [\mathcal{F}_1(\theta, t) + \mathcal{F}_2(\theta, t)\ ]\Lambda(\theta, t) \tag{5.5}$$

$$\Lambda(\theta) = \Lambda_0 + \Lambda_k = \frac{A_0}{2} + \sum_{k=1,2,3\ldots}^{\infty} A_k \cos(k\theta) \tag{5.6}$$

5.3 Implementation of ISC Fault

ISC fault as described in Fig.5.1 is replicated on the experimental machine to determine harmonics incited by i_f and extract fault features in the line current. The winding belonging to a coil in phase 'A' has been tapped to an external terminal to enable 1-6 turns to be shorted through a variable resistor so that the fault condition is controlled. The resistance is limited to ensure the current rating of the winding is not surpassed. The total resistance of each phase is approximately 0.4Ω and the resistance values across terminals corresponding to the 2 and 4 turns shorted are 0.0068Ω and 0.013Ω respectively, representing 1.67% and 3.33% fault severity respectively. Using thermal imaging, changes in temperature are measured and trended under both healthy and ISC conditions in Fig.5.3a-Fig.5.3b respectively. Abnormal temperature densities across the surface of the generator are detected with the winding fault. Hotspots are observed in Fig.5.3b in the faulty part of the stator winding; where a 13.5^{o}C rise in temperature due to i_f is observed. On the average, the winding temperature increased from 30.9^{o}C to 36.25^{o}C due to the presence of the interturn

fault (2 shorted turns). The machine was run at various speeds under several load conditions and the captured data for different scenarios were trended and analysed.

5.4 Detection of ISC Faults under Steady State Conditions

5.4.1 Feature Extraction of Faulty Components

Before applying MCSA monitoring method, an analysis and understanding of the typical harmonics in healthy AFPM machine is necessary. Regardless of faults, two sets of harmonics are immanent in the current spectrum of PM machines due to their geometric nature, design and manufacturing techniques. They are space harmonics; their harmonic order in PM machines with FSCW are given in (4.13) and slot harmonics; their frequencies of occurrence is obtained by (5.7) [20]-[21]; where f is line frequency, Q is the number of slots, $m = 3$, and p is number of pole pair. In the prototype investigated as described in section 3.3, v_{sh} overlaps with v since $Q \pm p = 2$. Other harmonics which may appear in the current spectrum are time harmonics related to the supply source. These harmonics are taken into consideration in the fault feature extraction.

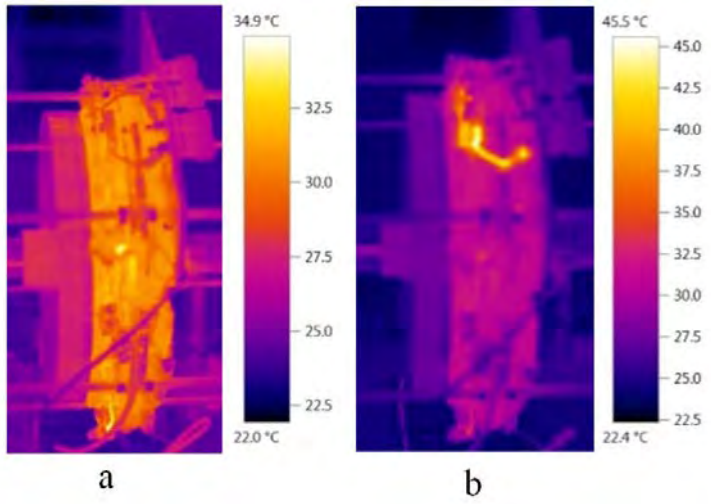

Fig.5.3. Thermal imaging of (a) healthy and (b) interturn fault conditions

Current signals are captured for duration of 1min under both healthy and ISC conditions. The rotating flux wave produced by i_f incited harmonics (f_{ISC}) which appear in the current spectrum of the stator winding in both SS and DS topologies as given in (5.8), where P is number of pole pairs, f is synchronous frequency, $n = 1, 3, 5 \ldots$ and $k = 1, 2, 3 \ldots$ are integers. The combination of k and n takes factors such as saturation and slot leakage, space and slot harmonics into account. These harmonics, shown in Fig.5.4 are identified and extracted using fast Fourier transform (FFT) and power spectra density (PSD); they are directly dependent on f. Their magnitudes increased considerably with worsening ISC but load variations have no impact on them as shown in Fig.5.5. Although the frequency pattern is robust against variations in load conditions, some frequencies coincide with harmonic components due to SE in chapter 4, because the faults harmonics induced in the line currents are a consequence of the variations in airgap permeance as per (5.3).

$$v_{sh} = f(kQ + p) \tag{5.7}$$

$$f_{ISC} = f\left(n \pm \frac{2k+1}{p}\right) \tag{5.8}$$

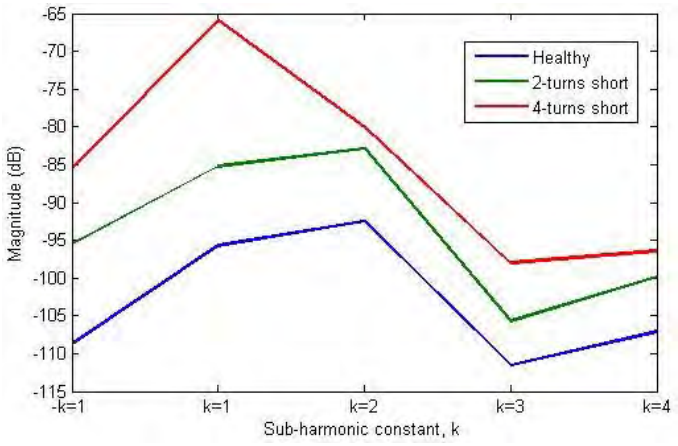

Fig.5.4. Interturn SC fault frequencies at $-k = 1$ to $+k = 4$

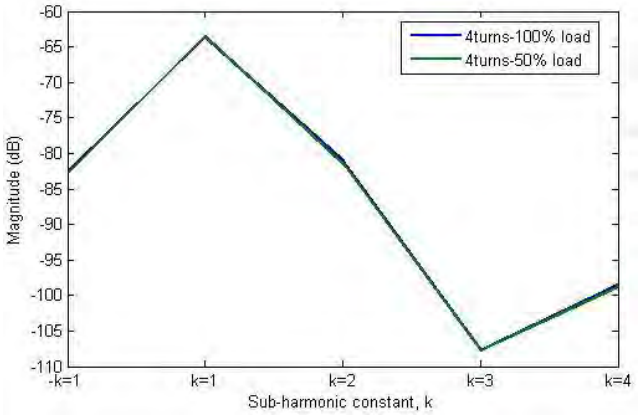

Fig.5.5. Effect of load variation on fault frequencies in (5.8)

5.4.2 Faults Discrimination under Steady State Conditions Using Park's Vector

In the previous section it is shown that MCSA is capable of detecting ISC. But the detection technique is limited at discriminating ISC from SE since some of their harmonics components overlap. This is because both faults cause variations in airgap flux density as a result of variable permeance. However, a unique feature of ISC is that it causes slight imbalance in the line current. Thus fault discriminatory feature that is based on the imbalance in the line current is examined by applying the extended Park's vector (EPV) technique. Under ideal conditions, i.e., when the current constitute a purely positive-sequence system, as a function of the main phase variables (i_a, i_b, i_c), the Park's vector (PV) has the components in (5.9)-(5.10) [24]-[25], where i_{max} is maximum value of the current positive sequence, w is angular supply frequency and t is time variable. However under abnormalities, (5.9)-(5.10) no consists of only positive-sequence but can be expressed as sum of positive- and negative- sequence components. Negative-sequence component is introduced on account of asymmetry, whose degree is direct related to the degree of asymmetry. The information on the asymmetry is contained in the current modulus of the PV in (5.11) and can be properly quantified using the EPV; a spectral analysis of the PV modulus.

The results of the EPV when applied to the current signal of the healthy and faulty machines are shown in Fig.5.6-Fig.5.7. The presence of ISC in the winding creates sags in the phase where the shorted turn is located as it rotates at angular speed w. This introduces asymmetry by impressing negative-sequence components in the current signal as manifested in the EPV signature by the presence of a spectral component at twice the fundamental frequency, whereas SE does not cause significant asymmetries in the phases. The amplitude of this component is direct related to the degree of fault as quantified in Fig.5.8 where the fault severity factor is the percentage ratio between the amplitude of the component at $2f$ to that of the dc level of the current PV. The noticeable difference in the fault severity factor at the two load levels is expected since the three phase current magnitudes increase with load. This technique is proposed to be applied to improve and complement MCSA in screening out stator winding faults from rotor eccentricities in AFPM machines.

$$i_D = \left(\frac{\sqrt{6}}{2} i_{max} sin(wt)\right) \tag{5.9}$$

$$i_Q = \left(\frac{\sqrt{6}}{2} i_{max} sin(wt - \pi/2)\right) \tag{5.10}$$

$$i_{mag} = \sqrt{{i_Q}^2 + {i_D}^2} \tag{5.11}$$

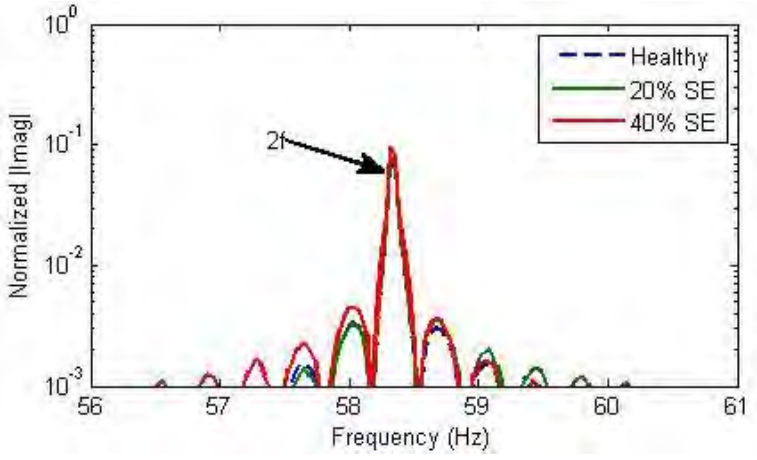

Fig.5.6. EPV signature under SE conditions

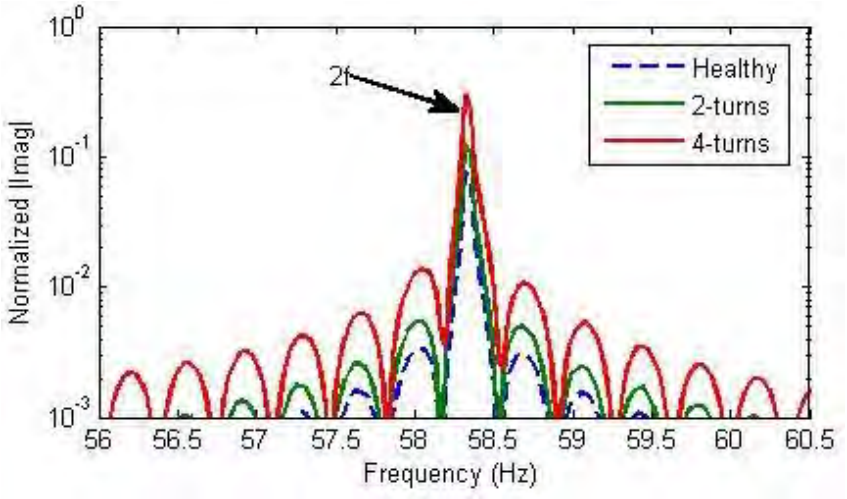

Fig.5.7. EPV signature under ISC conditions

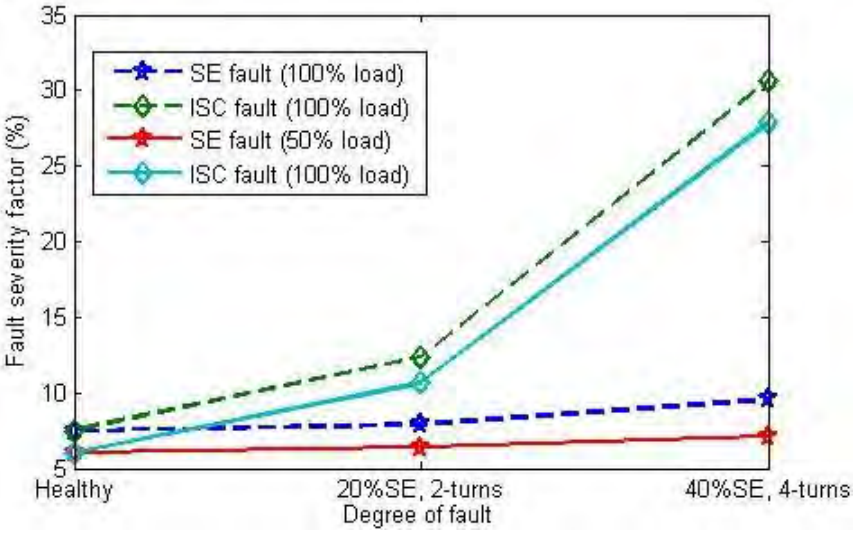

Fig.5.8. Fault severity factor

5.5 Transient State Detection of Faulty Components

The use of AFPM machines in applications characterized by transients makes it desirable to find a methodology for its transient fault detection since steady state

detection using the current signal is not definite. In these applications, transient startup operation is typical; therefore a suitable diagnostic technique is explored.

5.5.1 Typical Challenge in Extracting the Fault Related Features under Startup Transient

During startup, the fundamental frequency evolves from zero to its final steady-state value. This causes difficulty in tracking fault components in the startup transient regimes since the far larger magnitude of the fundamental harmonic overshadows the fault harmonics. This can be observed in the plot of the discrete wavelet transforms (DWT) in Fig.5.9. DWT, like any other time-frequency techniques, gives supplementary information to that obtained using frequency techniques. It is employed in analysing the signal. The fitting frequency bands for the DWT with a range that provides for the effective isolation of the fundamental from others across the various levels of the DWT are obtained using (5.12) [26], where $k = 1{:}\,n$, n is the number of decomposition level, and f_s is the sampling frequency to effectively extract the fault harmonics as they evolve. In this chapter, a high sampling rate (f_s) is used (in Table 5.1) and appropriate decimation factor is subsequently applied to the sampled current signal in the algorithm used to compute the DWT presented in Fig.5.9. The winding fault had been implemented offline before the startup. The ramp-up occurs in approximately 5s and the signal subsequently settles into steady-state in the time interval of 5-10s. The ramp-up time duration of 5s is derived from experimental knowledge and suffices for the evolution of the harmonics to be tracked. The DWT of the current signal reveals the magnitude of the fundamental harmonic (f_1) over and above all others, thus overshadowing the fault harmonics in the various decomposition levels till it reaches its peak and settles into steady-state values in *d4*. Throughout the ramp-up, as f_1 thrusts into succeeding frequency bands, the harmonics in bands *d8-d4* remained masked due to their much smaller magnitude relative to f_1. Therefore, detection of ISC is not achieved in these levels. Although the harmonics which evolved alongside f_1

Table5.1. Decomposition levels and corresponding frequency intervals

Decomposition level	D1	D2	D3	D4	D5	D6	D7	D8
Frequency band (Hz) f_s=8.5kHz	193.18-386.36	96.59-193.18	48.29-96.59	24.15-48.29	12.7-24.14	6.03-12.07	3.01-6.03	1.50-3.01

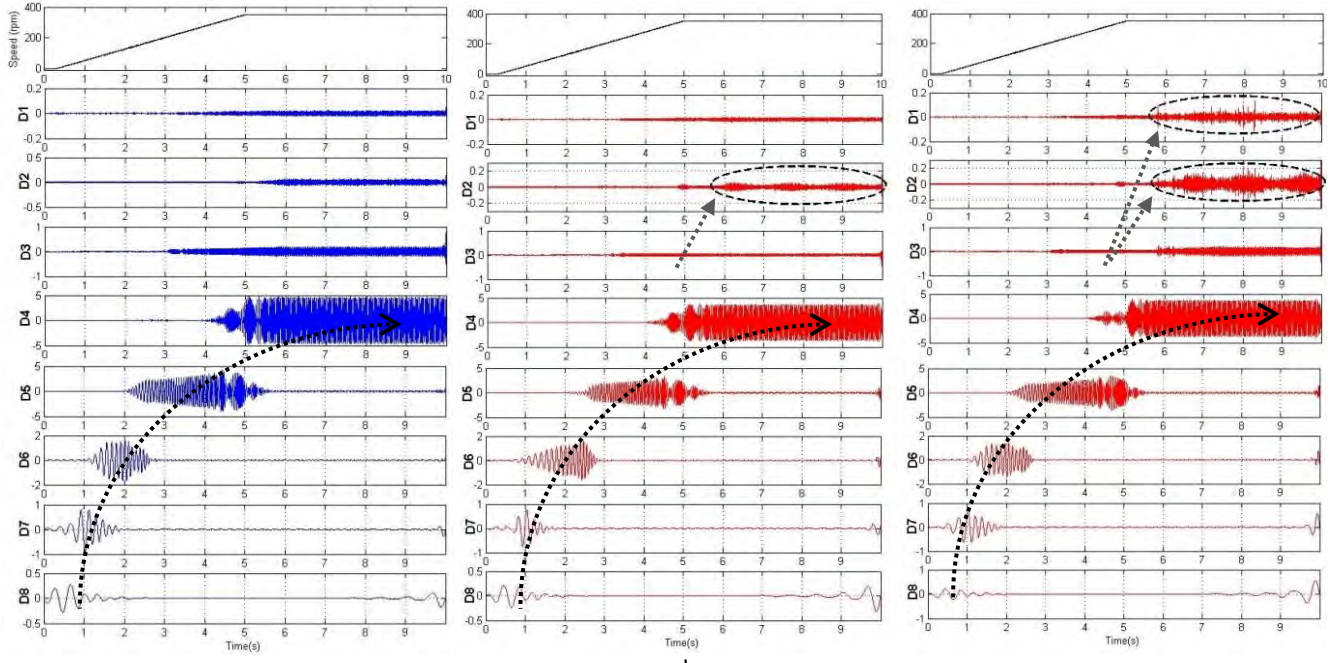

a b c

Fig.5.9. DWT of the current signal (a) healthy, (b) 2-turns short and (c) 4-turns short

had been overshadowed, undulation or oscillation appears in the decomposition level *d2-d1* (marked by dotted ellipses) due to high-order fault harmonics (i.e. $f_{ISC} > f_1$). These oscillations which are revealed after 5s when the signal has stabilized in steady state are impelled after approximately 5s. This is due to the higher-order harmonics, which depends on f_1 in (5.8), emerges with enough distance apart from the fundamental, triggering a train of oscillations to the end of the measurement duration. Nevertheless, it remains imperative to detect the presence f_{ISC} in the signal during the ramp-up time interval (i.e. 0-5s). To achieve this, the use of analytical signal in DWT is proposed.

$$f(n_k) \in \left[2^{-(k+1)}.f_s, \quad 2^{-k}.f_s\right] \tag{5.12}$$

5.5.2 Current Spectrum Analysis Using Analytical Signal

In [27]-[28], Hilbert Huang transform (HHT) is used to create an analytical signal from the current signals for broken-bar fault detection in induction machines under stationary conditions. The mathematical analysis and properties of HHT are extensively analysed in [28]-[29] as discussed in section 2.4. Fundamentally, it is a convolution of a real signal $x(t)$ with a function $1/t$ as defined in (5.13). By coupling $y(t)$ with the original signal $x(t)$ in (5.14), an analytical signal $\vec{x}(t)$ is created. The imaginary part is a version of the original signal $x(t)$ with a 90° phase shift. That is, sines are transformed to cosines and vice versa. Also, it has the same amplitude and frequency content as $x(t)$, including phase information. The instantaneous amplitude $a(t)$ is derived by obtaining the modulus of (5.15). It reflects the energy variation with time, of all frequencies in $\vec{x}(t)$ while $\theta(t)$ reflects the instantaneous phase. The Fourier transform (FT) of $\vec{x}(t)$ indicates that it is a complicated combination of dc component and other frequencies. The coupling creates a one-sided FT whereby negative frequencies are zero and the fundamental component is shifted to the dc value. This dc component can be removed by subtracting the mean of $a(t)$ from $a(t)$, whereby all harmonics except

the fundamental of the original signal $x(t)$ are represented in the spectrum. The aforementioned properties of the analytical signal are exploited in the next subsection to separate the fundamental component from other harmonics in the startup transient signal and enable fault detection using DWT. DWT is applied to perform the filtering process because it represents time-frequency spectrum understandably and it is computationally-efficient.

$$x(t) = I\sin(2\pi ft + \phi) \tag{5.13}$$

$$y(t) = x(t) \times \frac{1}{\pi t} = \frac{1}{\pi}\int_{-\infty}^{\infty} \frac{x(\tau)}{\tau - t} d\tau \tag{5.14}$$

$$\vec{x}(t) = a(t)e^{j\theta(t)} = x(t) + jy(t) \tag{5.15}$$

where

$a(t) = [x^2(t) + y^2(t)]^{1/2}$ and $\theta(t) = arctan(y(t)/x(t))$

5.5.3 Wavelet Decomposition of the Analytical Signal

Consider the current signal in (5.16), where f_1, f_v and f_{ISC} are the fundamental, space and ISC fault harmonics respectively.

$$i(t) = I_1\cos(2\pi f_1 t + \emptyset_1) + \sum_v^n I_v\cos(2\pi f_v t + \emptyset_v) + \sum_{ISC}^n I_{ISC}\cos\ (2\pi f_{ISC} t + \emptyset_{ISC}) \tag{5.16}$$

By creating an analytical signal from $i(t)$, the f_1 component which masked the evolution of f_{ISC} in Fig.5.10 can be isolated as follows:

1. Capture the start-up current signal $i(t)$
2. Compute the HHT of $i(t)$, i.e. $\hat{\imath}(t)$
3. Create the Hilbert modulus $\bar{\imath}(t)$, i.e. $\bar{\imath}(t) = i^2(t) + \hat{\imath}^2(t)$
4. Remove the dc component from the Hilbert modulus, defined by: $\bar{\imath}_a(t) = \bar{\imath}(t) - mean\ \bar{\imath}(t)$

In the spectrum of the resulting signal $\bar{\imath}_a(t)$, only f_v and f_{ISC} are present. The fundamental and spurious amplitudes at negative frequencies are eliminated. Therefore by applying the filtering abilities of the DWT on $\bar{\imath}_a(t)$, the signal can be effectively dilated and contracted using (5.12) to avoid adjacent frequency overlap from f_v so that f_{ISC} can be isolated and tracked as they develop. Their instantaneous frequencies and amplitudes can be extracted at each decomposition level where they are expressed. Detection is sought in the lower frequency bands where the energy of f_{ISC} is present isolated as follows:

1. Create a DWT of the analytical signal as per the aforementioned procedure.
2. At each decomposition level of interest, that is, where f_{ISC} is expected to evolve, track the instantaneous attributes of f_{ISC}, viz-a-viz:
   a) frequency vs time and
   b) magnitude vs time using HHT.
3. Diagnose f_{ISC} base on significant thresholds of harmonic energies.

In Fig.5.10, the results of the procedure as applied on the startup transient signal previously analysed is shown. The fault harmonics in the decomposition levels where fault harmonics at 11.65Hz and 46.6Hz (D6 and D4) are represented in the steady-state analysis are tracked for fault detection by computing their instantaneous magnitude. It reflects how much the fault harmonics energy changes with time. The energies at D6-D3 for the transient period 0-5s are also quantified in Fig.5.11 which indicates rise in magnitudes under ISC. Significant magnitudes compared to preset thresholds of the healthy machine are proposed for raising fault flag. The advantage of this technique is that whereas PSD quantifies the total energy contribution of individual harmonic component, this offers a measure of the amplitude contribution for each fault harmonic. Also, it resolves the coarseness associated with the DWT which makes the tracking of individual harmonic component difficult. In addition, there is foreknowledge of the frequencies to be tracked; distinction from noise is therefore practical.

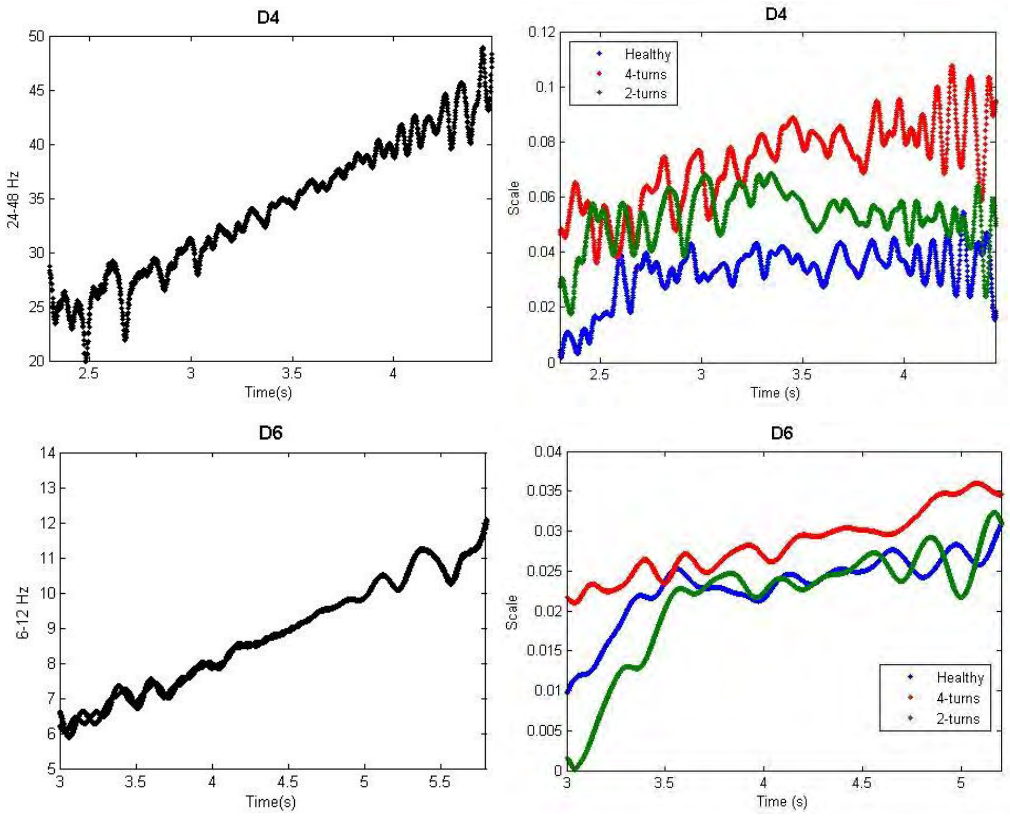

Fig.5.10. Frequency-time characteristics of f_{ISC}(left column) and magnitude-time characteristics of f_{ISC} (right column)

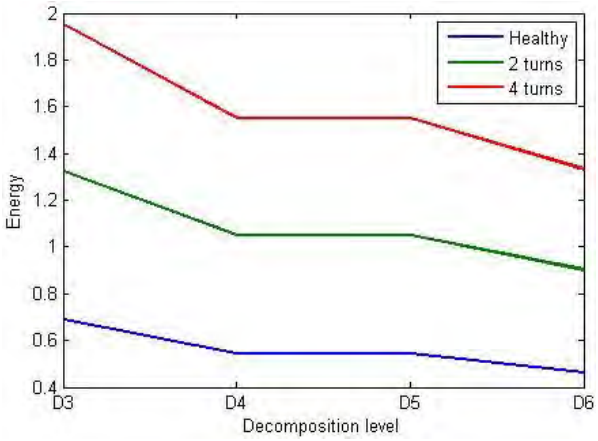

Fig.5.11. Magnitudes of the energies at D3-D6 during the transient

5.5.4 Startup Transient Faults Discrimination

The frequencies extracted using the procedure proposed in section 5.5.3 overlap with SE fault frequencies like in the steady-state scenario. Thus EPV is again proposed to discriminate between the two faults during the startup transient duration. The spectral analysis of the transient current PV is achieved in Fig.5.12-Fig.5.13 using DWT because of its effective time-frequency representation and filtering abilities. The figures show the evolution of the $2f$ components in the transient period for the healthy, ISC and SE scenarios in the bands *D5-D3*. While oscillations appear in the time-frequency spectrum under ISC conditions in Fig.5.12, none is present under SE in Fig.5.13. The energies created by the evolving $2f$ component in the bands *D5-D3* during the transient period are shown in Fig.5.14, which indicates no significant variations under SE faults.

5.6 Conclusions

The phenomenon of ISC in AFPM machines has been analysed and detection techniques proposed for both steady-state and transient conditions. ISC faults frequencies in the current spectrum are incited as a result variable airgap permeance but this behaviour is not unique to ISC. SE faults likewise causes variable airgap permeance, thus fault discrimination using MCSA is weak. However, the imbalance due to ISC faults causes distinctive twice the line frequency in the spectrum of the current PV. Thus EPV is proposed to be used to screen it from SE faults under both steady-state and transient conditions. In the transient detection, a hybrid of analytical signal obtained from HHT and wavelet decomposition is used to track the evolution of ISC fault frequencies and their harmonic energies in current spectrum to overcome the problem of large magnitudes of the fundamental component masking the fault features in startup transient operation.

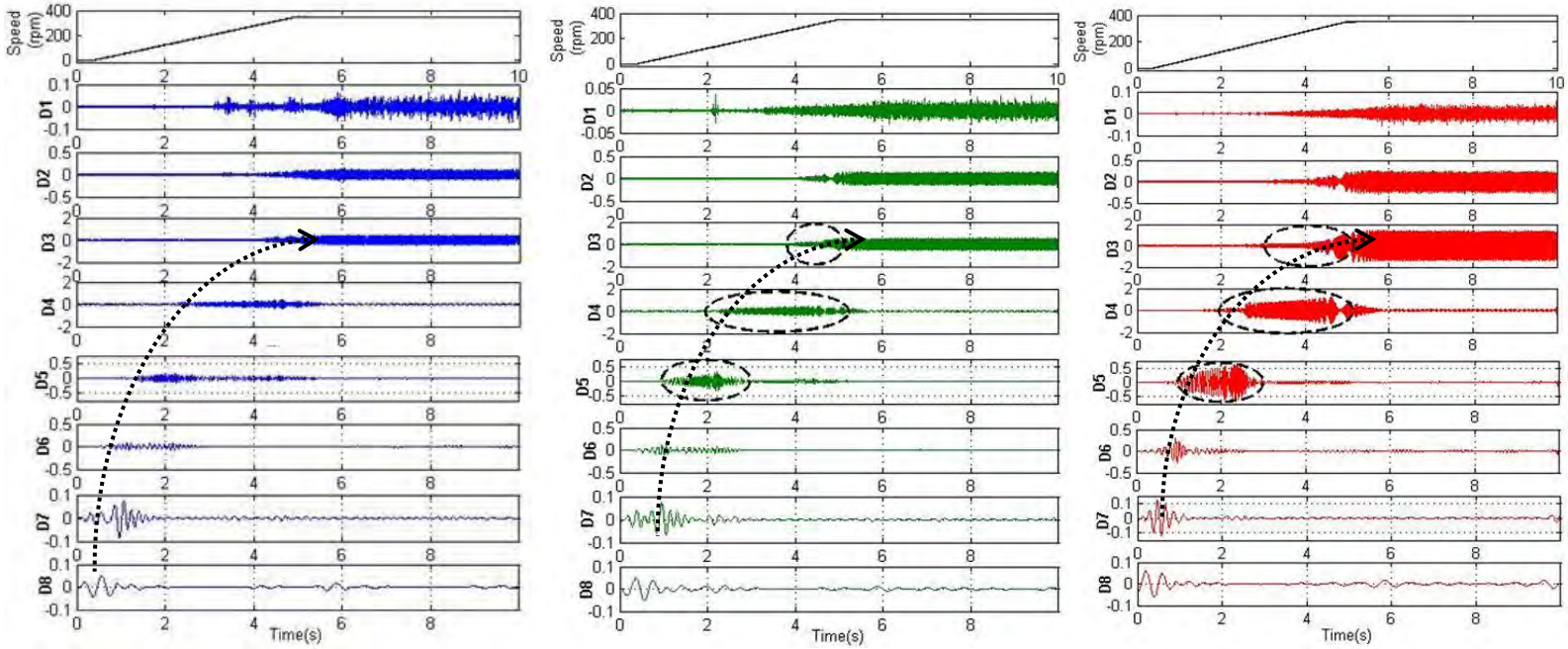

Fig.5.12. DWT of the current PV: (a) healthy, (b) 2-turns short and (c) 4-turns short

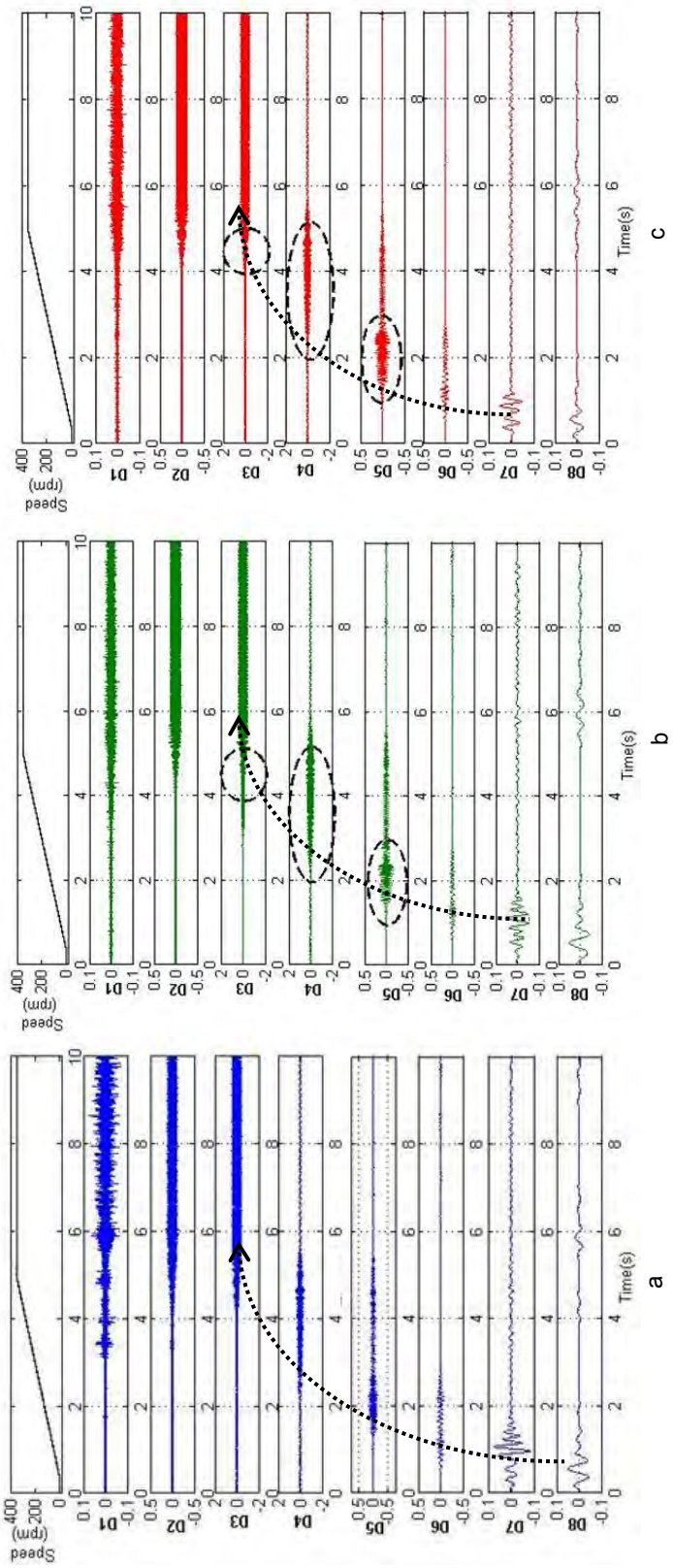

Fig.5.13. DWT of the current PV: (a) healthy, (b) 20% SE (c) 40%SE

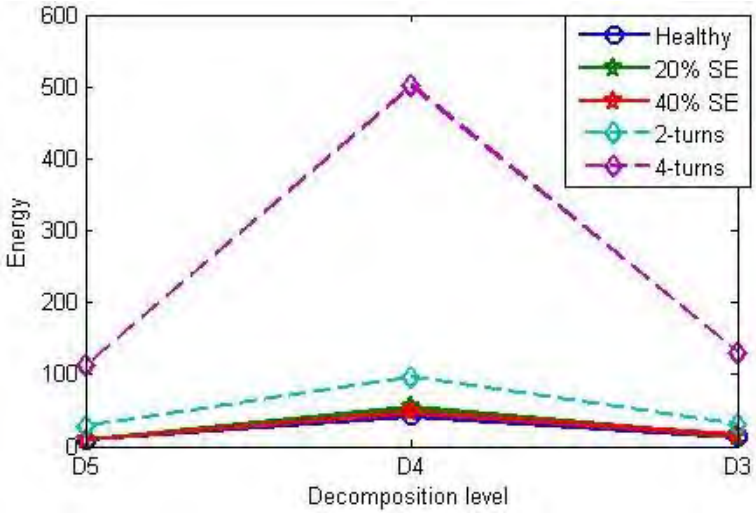

Fig.5.14. Energies of the evolving $2f$ component in the bands *D5-D3*

5.7 References

[1] A. Bonnett and C. Yung, “Increased efficiency versus increased reliability,” *IEEE Ind. Appl. Mag.*, vol. 14, no. 1, pp. 29–36, Jan./Feb. 2008.

[2] D. E Crawford, “A mechanism of motor failures”, 12th IEEE Electrical and Electronics Insulation Conference, Institute of Electrical and Electronics Engineers, Inc., New York, NY, pp. 126- 129, 1975.

[3] Gandhi, A.; Corrigan, T.; Parsa, L., "Recent Advances in Modeling and Online Detection of Stator Interturn Faults in Electrical Motors," *Industrial Electronics, IEEE Transactions on*, vol.58, no.5, pp.1564,1575, May 2011.

[4] Arumugam, P.; Hamiti, T.; Gerada, C., "Modeling of Different Winding Configurations for Fault-Tolerant Permanent Magnet Machines to Restrain Interturn Short-Circuit Current," *Energy Conversion, IEEE Transactions on*, vol.27, no.2, pp.351,361, June 2012.

[5] Bon-Gwan Gu; Jun-Hyuk Choi; In-Soung Jung, "Development and Analysis of Interturn Short Fault Model of PMSMs With Series and Parallel Winding Connections," *Power Electronics, IEEE Transactions on*, vol.29, no.4, pp.2016,2026, April 2014

[6] Romeral, L.; Urresty, J.C.; Riba Ruiz, J.-R.; Garcia Espinosa, A., "Modeling of Surface-Mounted Permanent Magnet Synchronous Motors With Stator Winding Interturn Faults," *Industrial Electronics, IEEE Transactions on* , vol.58, no.5, pp.1576,1585, May 2011.

[7] O. Mohammed, Z. Liu, S. Liu, and N. Abed, “Internal short circuit fault diagnosis for pm machines using fe-based phase variable model and wavelets analysis,” *Magnetics, IEEE Transactions on*, vol. 43, no. 4, pp. 1729 –1732, april 2007.

[8] L. Romeral, J. Urresty, J.-R. Riba Ruiz, and A. Garcia Espinosa, “Modeling of surface-mounted permanent magnet synchronous motors with stator winding interturn faults,” *Industrial Electronics, IEEE Transactions on*, vol. 58, no. 5, pp. 1576 –1585, may 2011.

[9] J. A. Rosero, L. Romeral, J. A. Ortega, and E. Rosero, “Short-circuit detection by means of empirical mode decomposition and Wigner–Ville distribution for PMSM running under dynamic condition,” IEEE Trans. Ind. Electron., vol. 56, no. 11, pp. 4534–4547, Nov. 2009.

[10] A. Espinosa, J. Rosero, J. Cusido, L. Romeral, and J. Ortega, “Fault detection by means of hilbert huang transform of the stator current in a pmsm with demagnetization,” *Energy Conversion, IEEE Transactions on*, vol. 25, no. 2, pp. 312 –318, june 2010.

[11] J. Ruiz, J. Rosero, A. Espinosa, and L. Romeral, “Detection of demagnetization faults in permanent-magnet synchronous motors under non-stationary conditions,” *Magnetics, IEEE Transactions on*, vol. 45, no. 7, pp. 2961 –2969, july 2009.

[12] M. Khan and M. Rahman, “Development and implementation of a novel fault diagnostic and protection technique for ipm motor drives,” *Industrial Electronics, IEEE Transactions on*, vol. 56, no. 1, pp. 85 –92, Jan. 2009.

[13] Ebrahimi, B.M.; Faiz, J., "Feature Extraction for Short-Circuit Fault Detection in Permanent-Magnet Synchronous Motors Using Stator-Current Monitoring," *Power Electronics, IEEE Transactions on*, vol.25, no.10, pp.2673,2682, Oct. 2010.

[14] Zhigang Sun; Jiabin Wang; Howe, D.; Jewell, G., "Analytical Prediction of the Short-Circuit Current in Fault-Tolerant Permanent-Magnet Machines," *Industrial Electronics, IEEE Transactions on*, vol.55, no.12, pp.4210,4217, Dec. 2008.

[15] B. A. Welchko, J. Wai, T. M. Jahns, and T. A. Lipo. “Magnet-Flux-Nulling Control of Interior PM Machine Drives for Improved Steady-State Response to Short Circuit Faults.” IEEE Transactions on Industry Applications, Vol.42, No.1, pp.113-120, 2006.

[16] Giulii Capponi, F.; De Donato, G.; Caricchi, F., "Recent Advances in Axial-Flux Permanent-Magnet Machine Technology," *Industry Applications, IEEE Transactions on* , vol.48, no.6, pp.2190,2205, Nov.-Dec. 2012.

[17] Pippuri, J.; Manninen, A; Keranen, J.; Tammi, K., "Torque Density of Radial, Axial and Transverse Flux Permanent Magnet Machine Topologies," *Magnetics, IEEE Transactions on* , vol.49, no.5, pp.2339,2342, May 2013.

[18] J. F. Gieras, R. J. Wang and M. J. Kamper, Axial flux permanent magnet brushless machines. Kluwer academic publishers, Dordrecht, The Netherland, 2004

[19] Ogidi, O.O.; Barendse, P.S.; Khan, M.A., "Development of a test rig for eccentricity fault studies on an axial-flux permanent magnet (AFPM) wind generator," *Electrical Machines (ICEM), 2014 International Conference on* , vol., no., pp.1562,1568, 2-5 Sept. 2014

[20] Fornasiero, E.; Bianchi, N.; Bolognani, S., "Slot Harmonic Impact on Rotor Losses in Fractional-Slot Permanent-Magnet Machines," *Industrial Electronics, IEEE Transactions on*, vol.59, no.6, pp.2557,2564, June 2012

[21] Dajaku, G.; Wei Xie; Gerling, D., "Reduction of Low Space Harmonics for the Fractional Slot Concentrated Windings Using a Novel Stator Design," *Magnetics, IEEE Transactions on*, vol.50, no.5, pp.1,12, May 2014

[22] W. le Roux, R. G. Harley, and T. G. Habetler, “Detecting rotor faults in low power permanent magnet synchronous machines,” *Power Electronics, IEEE Transactions on*, vol. 22, no. 1, pp. 322 –328, jan. 2007

[23] Yao Duan; Toliyat, H., "A review of condition monitoring and fault diagnosis for permanent magnet machines," *Power and Energy Society General Meeting, 2012 IEEE* , vol., no., pp.1,4, 22-26 July 2012

[24] Cruz, S.M.A.; Cardoso, A.J.M., "Stator winding fault diagnosis in three-phase synchronous and asynchronous motors, by the extended Park's vector approach," *Industry Applications, IEEE Transactions on* , vol.37, no.5, pp.1227,1233, Sep/Oct 2001

[25] Orcajo, G.A.; Cano, J.M.; Melero, M.G.; Cabanas, M.F.; Rojas, C.H.; Pedrayes, J.F.; Norniella, J.G., "Diagnosis of Electrical Distribution Network Short Circuits Based on Voltage Park's Vector," *Power Delivery, IEEE Transactions on* , vol.27, no.4, pp.1964,1972, Oct. 2012

[26] C. S. Burrus, R. A. Gopinath, and H. Guo, Introduction to Wavelets and Wavelet Transforms. A Primer. Englewood Cliffs, NJ: PrenticeHall, 1998

[27] Boqiang Xu; Liling Sun; Lie Xu; Guoyi Xu, "Improvement of the Hilbert Method via ESPRIT for Detecting Rotor Fault in Induction Motors at Low Slip," *Energy Conversion, IEEE Transactions on* , vol.28, no.1, pp.225,233, March 2013

[28] Puche-Panadero, R.; Pineda-Sanchez, M.; Riera-Guasp, M.; Roger-Folch, J.; Hurtado-Perez, E.; Perez-Cruz, J., "Improved Resolution of the MCSA Method Via Hilbert Transform, Enabling the Diagnosis of Rotor Asymmetries at Very Low Slip," *Energy Conversion, IEEE Transactions on* , vol.24, no.1, pp.52,59, March 2009

[29] V. Cizek, “Discrete Hilbert transform,” IEEE Trans. Audio Electroacoust., vol. 18, no. 4, pp. 340–343, Dec. 1970.

Chapter 6
Detection of SE Faults Using Vibration Analysis

6.1 Introduction

In the electromechanical design of an AFPM machine, the power output increases as a cubic function of the outer diameter [1]-[7]. This makes the structural mass account for a large percentage of the total active mass, i.e., the structural mass of the machine is as important as those of the active parts [8]-[9]. The rotor disc polar mass moment of inertia is much larger than that of the shaft. Hence, it becomes more difficult to design a rotor-shaft mechanical joint with high mechanical integrity, because the contact surface between the rotor and shaft becomes smaller in comparison to the rated power [10]. This particular structural characteristic of AFPM machine makes it predisposed to static eccentricities [8]. However, continued operation throughout the service life of electrical machines can be ensured through reliable maintenance strategies using vibration analysis (VA) [11]-[12]. Although, high cost is associated with maintenance using VA since it requires expensive sensors unlike the MCSA which makes use of the machine winding as search coil, it is nevertheless investigated in this chapter due to its effectiveness and applicability in diagnosing mechanical-related faults [11]-[12]. In addition, PM machines typically employ FSCW, a winding configuration inherently rich in current harmonics [13] which tend to overshadow the fault harmonics in the spectrum of the line current, making their extraction for fault detection using current analysis difficult.

Typically, new or healthy machines generate some level of vibration and the overall vibratory response of a machine is dependent on its structural components, structures to which it may be coupled to and the environment of operation [11], [14]-[15], however, these vibrations change due to faults. The changes can be examined for fault detection, whereby both the nature and severity may be determined [16]. The defective and natural frequencies of the machine is identified through an analysis of the frequency spectrum of vibration signal using signal processing techniques [14]-[19]; in these papers induction machines are mostly investigated. In [17], detection of broken-bars in induction machines by principal slot harmonics sidebands using transient vibration is investigated. Signatures associated with the harmonics are tracked. In [18], complex wavelets are used to detect multiple faults in variable frequency drives. Simple threshold of the wavelets energies is used as fault indices, and feature extraction and classifier modelling using wavelets are applied for detection of faults while in [19], the optimum network size of probabilistic neural network using orthogonal least square regression algorithm is obtained in an effort to reduce computation in dual tree complex wavelets feature extraction. The 'twice the line' frequency is proposed as an index for fault detection in induction machines using vibration analysis in [16] but the index is not specific to any type of fault. In [20]-[25], magnetic forces in PM machines are investigated and characterized but not for fault detection purposes. In [20]-[21], a strong magnetic force of attraction exists between the rotor magnets and the stator core in PM machines; therefore, a slight rotor dissymmetry could cause an unbalance magnetic pull (UMP) and consequently, induce vibration. In [22]-[25], the magnetic forces in PM machines with concentrated windings are investigated. They are found to have more vibration problems than machines with distributed windings due to larger MMF harmonics content and stator slot and pole combination. The magnetic forces and dominant modes of vibration are identified, and their mitigation techniques through improved design methods are proposed.

In literature, there are no clearly defined vibratory frequencies associated with

specific faults nor any detailed information available on the vibration behaviour of PM or AFPM machine topologies for application in fault detection strategies. Thus, this chapter explores the applicability of VA in reliably detecting SE in AFPM machines in both steady-state and transient regimes.

6.2 Vibration Harmonics in PM Machines

6.2.1 Sources of Vibration

Vibrations produced by electrical machines originate from four sources namely; electromagnetic, mechanical, aerodynamic and electronic [26]. Mechanical vibration depends on mass, rigidity and elasticity of the stator and rotor structure. Aerodynamic and electronic sources are from fans used for forced air cooling while solid-state converters respectively. Vibrations from electromagnetic sources originate from electromagnetic forces caused by MMF harmonics and permeance waves in the airgap. If these electromagnetic forces enter into the natural (mechanical) vibrating frequencies, resonance may occur. The prominent reason for electromagnetic vibration is due to the presence of PMs. The magnetic forces produced in them are computed using Maxwell's stress tensor. These forces comprise the normal (F_n) and tangential (F_t) components in (6.1)–(6.2), where $j = 1, 2, 3 \ldots N$ [22], [27]-[28]. While F_t produces the useful electromagnetic torque, F_n causes the vibration and noise of electromagnetic origin. Practically, the conversion of F_t to electromagnetic torque may not be very efficient and the remaining magnetic energy might cause vibration, but this will be fringe and is assumed negligible for the reason being that it is much smaller in magnitude than the normal component of force as evident in (6.2). Therefore in this chapter the source of electromagnetic vibration is assumed to arise mainly from F_n.

$$F_n = \frac{1}{2\mu_0}\left[\sum_j^N \left({B_{nj}}^2 - {B_{tj}}^2\right)\right] \tag{6.1}$$

$$F_t = \frac{1}{\mu}\left[\left(\sum_j^N {B_t}^2\right)\right] \tag{6.2}$$

6.2.2 Analysis of Electromagnetic Exciting Force Harmonics

In a closed circuit, only the fundamental harmonic of the PM field interacts with the fundamental harmonic of the armature reaction field to produce the useful electromagnetic torque. Other harmonics of the PM field interact with themselves and the armature reaction fields, while some armature reaction fields (including the fundamental) interact with each other to produce the even modes of normal component of force, F_n in (6.3), which in turn produces vibration, noise and may induce additional eddy current loss [24]-[25], [30]. However, F_n as described by (6.3), where superscripts pm and v denote PM and armature reaction fields respectively, does not necessarily produce larger fields in a closed circuit. The magnitudes of the fields depend on the winding configuration employed. For example, in a concentrated winding configuration, the armature reaction fields consist of forward- and backward-rotating harmonics whose resultant may not be additive [31]. Also, not all the modes of F_n are important to machine vibration [20]-[24]. The lowest mode has a far greater magnitude than other even modes [24], [27]. In open circuit, since the main field contents of B_n in surface PM machines differ based on pole/slot combination [23], [29], the lowest mode of F_n given in (1) differs. It is the greatest common divisor (GCD) of the number of slots and poles [23]-[24], [27]-[30]. To determine the modes and frequencies of occurrence of F_n, (1) is further analysed in (6.4)-(6.5) using the analytical expression of B_n, where $n, l = 0,1,2, \ldots, k = n$ ($n = 0,1,2 \ldots$) and $u = 2n + 1$ [23]-[24], [27]-[28]. The force modes and corresponding frequencies are obtained from the second and first term in (6.5) respectively. Another important electromagnetic harmonic component is the 'twice the line' frequency which is equally present in the vibration spectrum with a constant amplitude under various load conditions [16], [32]. This component is induced by the rotating flux waves from the line voltage or current. The effects of SE on these harmonics are further examined in this chapter.

$$F_n = \frac{1}{2\mu_0}\left[\sum_{ji}^{N} {B_j}^{pm} {B_i}^{v}\right] \tag{6.3}$$

$$F_n \propto \{\sum_u \sum_k B_{muk} \cos[upw_r t - (up \mp kN_s)\theta]\}^2$$

$$= \sum_u \sum_k F_{nl} \cos[2npw_r t - (2np \mp lN_s)\theta] \quad (6.4)$$

$$[2npw_r \quad - 2np \pm kN_s] \quad (6.5)$$

6.3 SE and its Effects on Magnetic Forces

The electromagnetic effects of SE have been described using FEA in chapter 4. The normal component of magnetic flux density obtained under the same no-load and nominal speed for both healthy and SE conditions using the same reference point for the rotor positioning is shown in Fig.6.1. Notice the region marked with the red ellipse corresponding to 0-45 mechanical degrees. The flux density increased due to minimum reluctance of the magnetic circuit, but gradually decreased across the remaining part of the airgap as referred to by the rotor position. Since B_{nj} in (6.1) is a product of the airgap MMF and airgap permeance, in uneven permeance the rotating airgap MMF becomes unbalanced, thereby exciting the harmonics j, which when interacted with each other and/or armature reaction fields may incite F_n and other electromagnetic harmonics, giving rise to tones which may result in the vibration of the stator and machine housing.

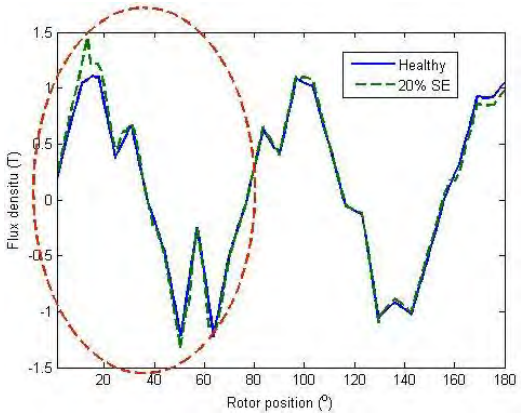

Fig.6.1. Magnetic flux density in the airgap

6.4 Experimental Setup and Procedures

The SS topology is the prototype investigated because of its susceptibility to SE, alongside the skewed PM pole. The skewed magnetic pole produces the least MMF harmonics among the three PM configurations as revealed in chapter 4. In addition, it reduces inherent cogging torque associated with the experimental machine by 70% [33]; otherwise additional vibration due to excessive cogging may be induced. In this way, vibrations due to cogging are isolated. The ceramic shear piezoelectric accelerometer and NI 9234 are the sensors and data acquisition devices respectively used to capture the vibration data. The accelerometers were mounted on the stator housing at the drive end of the machine; their directions and locations are illustrated in Fig.6.2 and detailed in Table 6.1. The machine was operated at various loads and speeds under healthy and SE scenarios. It was driven in generator mode so as to eliminate the contributions of vibrations from electronic sources which may emanate from the switching of solid-state converters. Proper location and mounting of the acce-

Table 6.1. Location of accelerometers

Accele-rometers	**Direction**	**Location**
A	Pr: Axial (parallel to the shaft)	Machine housing
B	T: Tangential (perpendicular to the shaft)	Machine housing
C	R: Radial (⊥ to the shaft but at 90^0 to the tangential)	Machine housing
D	Pr: Axial (parallel to the shaft)	Stator core

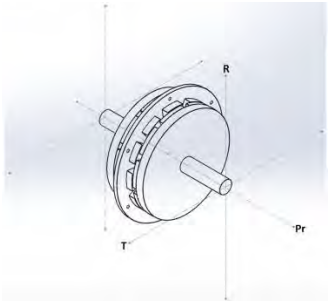

Fig.6.2. Positioning of accelerometers for vibration measurement

lerometers is critical to capturing vibration data. The locations were clearly marked to ascertain repeatability of measurements at the same location during successive measurements. Since accuracy is prime, the procedures described by the international standards ISO-13373-1 and ISO-13373-2 [34]-[35] which encompass the measurement point and measurement equipment discussed in subsection 3.3.3 were followed. In order to establish baseline data, it was monitored in its healthy state over an extended period of time and the characteristics of the data trends were correlated for uniformity. The signals are acquired at 4kHz and 120K samples are collected for steady-state analysis and at 2kHz with 5K samples for start-up transient analysis.

Fast Fourier transform (FFT) is the industry standard tool applied in steady-state to extract harmonics or frequency components from the vibration signals [35]. But it has some demerits which are discussed in detail in chapter 2. It is unable to accurately represent signals that have non-periodic components that are localized in time or space, such as transient impulses. Another of its shortcoming is the inability to provide information about the time structure of a signal. Therefore a Cohen class distribution, ZAM distribution is explored alongside the FFT to detect the presence of SE under non-stationary conditions. It is preferred over other Cohen class distributions because it resolves the problem of signature spattering [37]-[38]. This is important to the analysis of the vibration spectrum since vibration signals are inherently rich in energy density.

6.5 Results and Discussion

6.5.1 Frequency Analysis

6.5.1.1 Determination of Natural Frequencies

The natural frequencies formula in (6.6)-(6.7) [26]-[27], [39], where $m_0 = 0, 2, 4 \ldots$, k is a constant which depends on the geometrical parameters of the machine, are used to calculate the natural modes. Results derived are presented in Table 6.2, mode 2 critical frequency closely correlates with the result of the resonance test which reveals

significant low-frequency tones picked-up by the accelerometers at 48.2Hz, as shown in Fig.6.3. Although, identification of natural frequencies is typically done in the design stage to prevent resonance and noise, they have been obtained in this paper to identify and isolate the sources of the harmonics in the vibration signal and to establish that the natural frequencies of the machine do not coincide with its electromagnetic vibratory response of the experimental machine.

$$f_0 = \frac{1}{2\pi}\sqrt{\frac{K_r}{M_r}} \tag{6.6}$$

$$f_{m_0} = f_0 \frac{m_0({m_0}^2-1)k}{\sqrt{{m_0}^2+1}} \tag{6.7}$$

6.5.1.2 Extraction of Fault Frequencies

Higher magnitudes of vibration is measured and trended from accelerometers, 'A' and 'D' rather than 'B' and 'C'. The higher vibratory magnitudes are connected with the location of the accelerometers (Table 6.1); the axial direction of magnetic flux.

Table 6.2. Modes of vibration

$\boldsymbol{m_0}$	0	2	4	6	8	10
$\boldsymbol{f_{m_0}}$ **(kHz)**	0.21	0.051	0.54	0.62	1.1	1.76

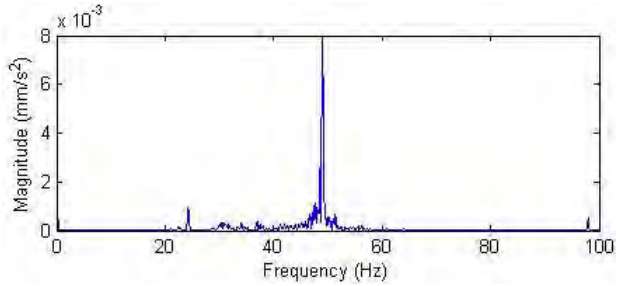

Fig.6.3. Mode 2 natural frequency of the machine

Thus, the signals acquired from 'A' and 'D' are deemed better indicators of vibratory patterns due to electromagnetic origin in AFPM machines. Using the Fourier transform and power spectrum density (PSD), the harmonics present in the signals are extracted for both healthy and SE scenarios at various speeds under steady-state condition. Attention is paid to modes and frequencies of occurrence of F_n as given in (6.5) since they are the main source of vibration. For the prototype investigated, the only mode of F_n on open circuit is 2; the GCD of the slot/pole combination of the prototype. And in a closed circuit, though F_n consists of all even modes (2^{nd}, 4^{th}, 6^{th}…), the lowest, i.e., the 2^{nd} is the most important to machine vibration because of its much higher magnitude relative to others and its frequency of occurrence in the vibration spectrum, i.e., below 1kHz. Therefore, the second magnetic force harmonic F_2 is the most dominant in the vibration spectrum for all load conditions. Analysis of the spectrum reveals that the UMP due to SE exacerbated the amplitude of F_2 alongside the amplitudes of harmonics at the multiples of the line frequencies given by (6.8), where $n = 1, 2, 3$ … and f is the fundamental frequency of the line current, (i.e., $2f, 4f$ etc.). Thus the locations of all the identified fault-frequencies are dependent on w_r. Their extracted values for operating speed condition are shown in Fig.6.4, where the magnitudes of the harmonic at F_2 under various degrees of SE rise above zero decibels, relative to the healthy signal; to 0.48dB and 0.8dB for 20%SE and 40%SE under no load condition respectively. Therefore the absolute vibration at F_2 is shown in Fig.6.5 to indicate the increase in amplitude. For the F_{line} harmonics, vibration amplitudes significantly increased with worsening SE though their effective amplitudes decreased with increasing order of n. The tones are a train of pulsations induced by electromagnetic flux waves caused by the line current or voltage revolving at the synchronous speed. As SE triggers increases in magnitudes of the space and sub-harmonics of the line current, it consequently incites the waves giving rise to significant increases in their amplitudes. The more prevailing components are the $2f$ and $8f$ frequencies with larger tones. Marginal change in amplitudes of the F_2 and F_{line} is obtained under load conditions as

seen in Fig.6.6; the armature reaction fields have little influence on the magnetic force at F_2. This is because as the magnitudes of the space harmonics v increased under load, they are cancelled out as they interact with each other and components of magnetic flux density, due to their opposing rotating effect. Since the resulting magnitudes of harmonics investigated are directly proportional to the eccentricity, indices for fault detection of SE in AFPM machine using vibration monitoring are proposed to be built on the vibratory magnitudes at their frequencies.

$$F_{line} = 2^n f \tag{6.8}$$

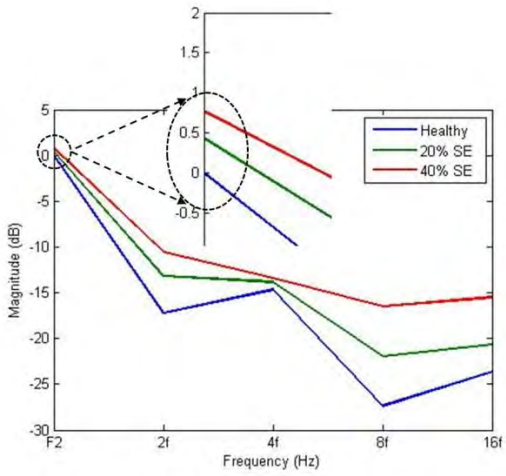

Fig.6.4. Vibration harmonics at different fault frequencies

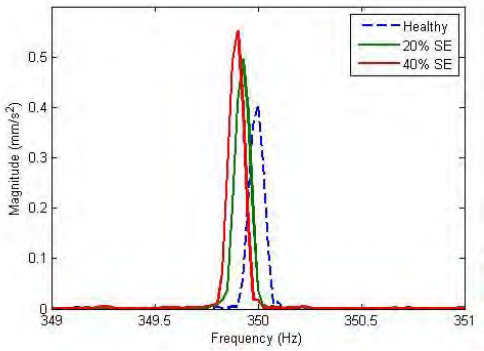

Fig.6.5. Absolute vibration at F_2

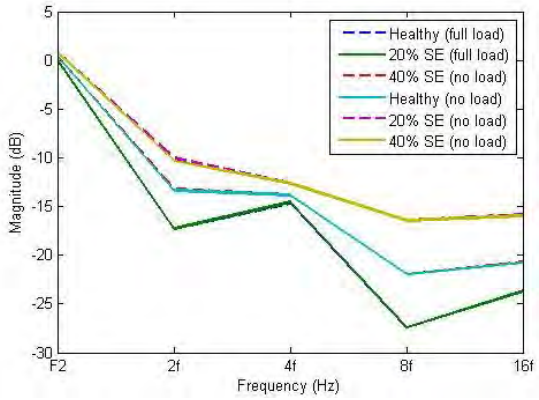

Fig.6.6. Amplitudes of vibration harmonics under load

Although SE was replicated by skewing the stator with respect to the rotor symmetry to prevent the development of other faults during experimentation, the occurrence of dynamic eccentricities (DE) cannot be completely eliminated due to the UMP caused by SE. Under DE, the rotor displacement and airgap length in Fig.4.2 is time-dependent as the rotational axis of the rotor disc is no longer in equilibrium with the rotor symmetrical axis while rotating with the rotor disc. The disequilibrium, though minimal, causes an alternation of the UMP from minimum to maximum in the region of maximum and minimum reluctance respectively as the rotor revolves around the stator. This variation in magnetic reluctance results in the excitation of frequencies contiguous to F_2 as seen in Fig.6.7-6.8. They are forward and backward frequencies at variance with F_2 by the rotational frequency, $\pm w_r$. Aggravated magnitudes of these frequencies may modulate F_2 and cause structural instability in the presence of a slight offset in the centre of mass of the machine.

6.5.1.3 Vibration Signal Processing with ESPRIT

Fig.6.9 shows the result from the ESPRIT spectral estimation technique applied to the vibration signal under the same operating conditions as with the FFT. Close correlation of both frequencies and amplitudes, like the case of current analysis in chapter 4 is achieved with 2.5s of measurement duration as against 30s of measurement time obtained using FFT.

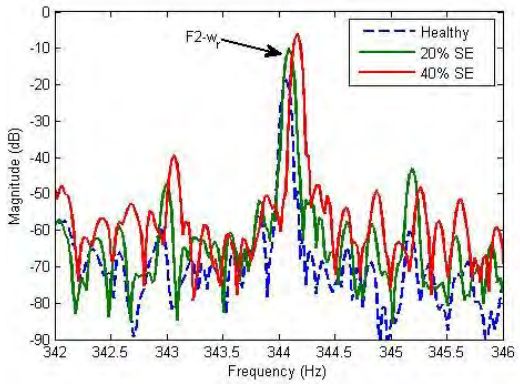

Fig.6.7. Vibrations due to DE as induced by SE; $F_2 - w_r$

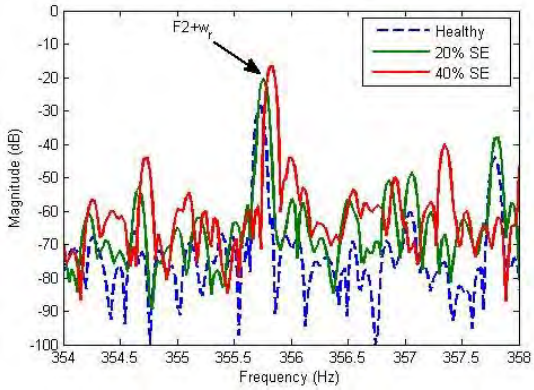

Fig.6.8. Vibrations due to DE as induced by SE; $F_2 + w_r$

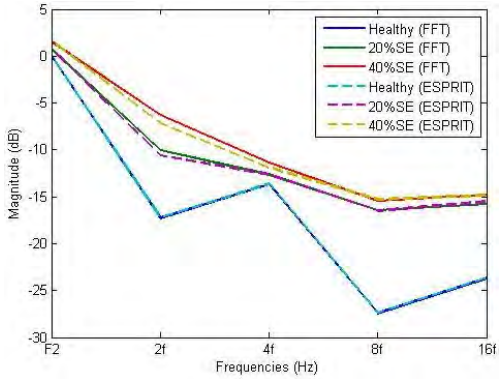

Fig.6.9. Comparison between FFT with ESPRIT using VA

6.5.2 Time-Frequency Analysis

The steady-state operation of AFPM machines is not guaranteed for an extended period of time. The various operating conditions (e.g. change in load or speed) in its applications cause non-stationarity vibration signals. Hence, the harmonics extracted in the previous subsection are tracked using ZAM distribution. The theoretical background is discussed in chapter 2. The vibration signal is obtained from start-up transients for both healthy and various SE conditions. Fig.6.10-6.12 presents the ZAM distribution plots for transient start-up condition. In these plots, time-varying spectral energy indicates the vibratory harmonics in the time-frequency domain. The healthy vibration signal in Fig.6.10 shows the energy concentration at the period, t>2s, corresponding to the stationary state region where F_2 is revealed after the machine settled down to constant speed operation. In Fig.6.11-6.12, under SE, increased vibratory level emerged during the transient interval, specifically at the period shortly before the steady-state interval, t<2s in the 50–60Hz frequency range. The engravings on the spectrogram, indicated in both figures are caused by the harmonic at $2f$. Other harmonics relating to the $2^n f$ order are not revealed due to their much smaller amplitudes relative to that at F_2. The same behaviour is also observed for the DE related harmonics; they are overshadowed by the evolving magnitudes of F_2. On close inspection, in the 300–360Hz frequency range, the vibration energy at F_2 becomes intense at the same time of appearance of the $2f$ harmonics. The spectrum in Fig.6.13 shows that these harmonics are revealed at the time the peak vibration acceleration is reached, shortly before coasting to steady state. Both harmonics at F_2 and $2f$ are further revealed in Fig.6.14 which quantifies the energy spectral density of the start-up vibration signal at the aforementioned point where they are revealed. The derived energy of the harmonics significantly increased in the presence of SE, by 4.5dB and 8dB at F_2in both 20%SE and 40%SE conditions respectively, relative to the healthy state, while a 4-6dB increase in the $2f$ harmonic is derived for 20-40%SE. These magnitudes are greater than in the steady state; thus, alongside the extracted supplementary

information on the time of appearance of the harmonics, it makes the start-up transient diagnosis more advantageous and reliable than the steady-state analysis. A transient start-up diagnostics check can be performed during cutting-in of wind turbines and start-up mode in electric vehicles; applications where the deployment of AFPM machines are growing and continually emerging [4].

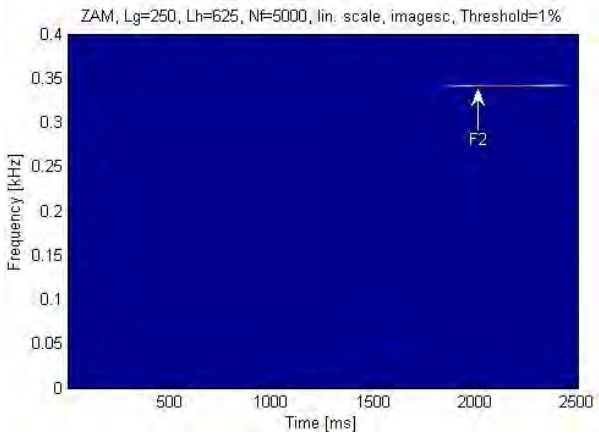

Fig.6.10. ZAM analysis plot showing healthy scenario

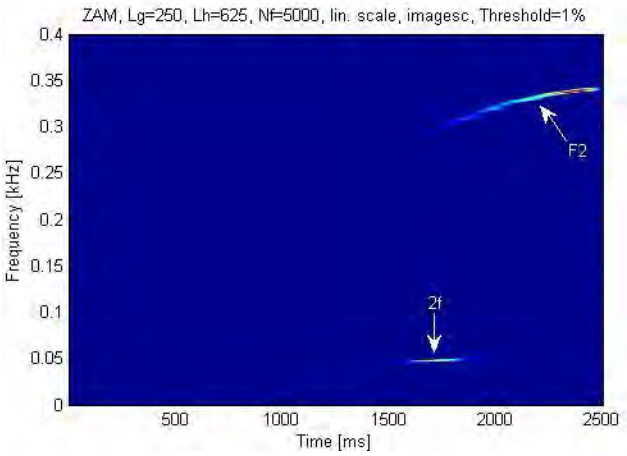

Fig.6.11. ZAM analysis plot for 20% SE

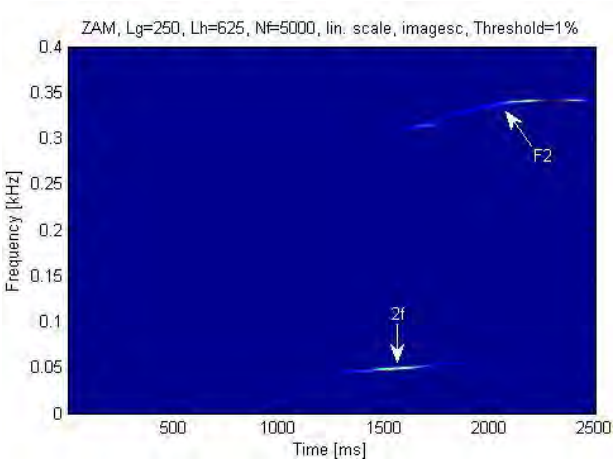

Fig.6.12. ZAM analysis plot for 40% SE

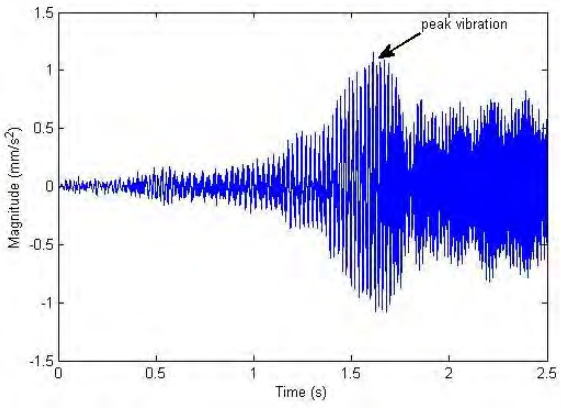

Fig.6.13. Waveform of captured vibration acceleration

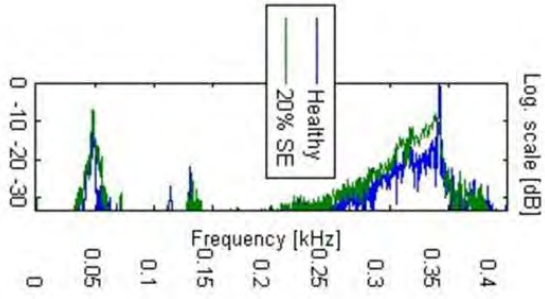

Fig.6.14. Energy spectrum for both healthy and 20% SE conditions

6.6 Conclusions

This chapter proposes a technique for the detection of SE in AFPM machines using VA. Analysis of the vibration signature acquired from an AFPM machine for detection of SE has been presented using frequency and time-frequency techniques for steady and transient states respectively. It is shown that there is a direct link between SE and vibratory levels but the location of transducers is important in achieving effective and resolute measurement of the vibrations. The experimental approach carefully isolates electromagnetic vibrations from other types of machine vibrations. The richness of electromagnetic information and degree of accuracy of fault indicators obtained from vibration monitoring is high, thus, it is a reliable SE faults diagnostic strategy for AFPM machines. The proposed fault index is robust against load variations for the pole/slot combinations investigated. The sensors can be non-invasively mounted, measurement mode can be either offline or online and the signals acquired can be analysed in both steady state and transient state using standard signal processing techniques.

6.7 References

[1] M Aydin, S. Huang and T. A. Lipo, “Design, analysis and control of a hybrid field-controlled axial-flux permanent magnet motor,” *IEEE Trans. Ind. Electron*., vol. 57, no 1., pp. 78-87, Jan. 2010

[2] Y. Kano, T. Kosaka, and N. Matsui, “A simple nonlinear magnetic analysis for axial-flux permanent-magnet machines,” *IEEE Trans. Ind. Electron.*, vol. 57, no. 6, pp. 2124–2133, Jun. 2010

[3] W. Fei, P. C. K. Luk, and T. S. El-Hasan, “Rotor integrity design for a high-speed modular air-cored axial-flux permanent-magnet generator,” *IEEE Trans. Ind. Electron.*, vol. 58, no. 9, pp. 3848–3858, Sep. 2011

[4] Giulii Capponi, F.; De Donato, G.; Caricchi, F., "Recent Advances in Axial-Flux Permanent-Magnet Machine Technology," *Industry Applications, IEEE Transactions on* , vol.48, no.6, pp.2190,2205, Nov.-Dec. 2012

[5] F. Crescimbini, A. Lidozzi, and L. Solero, “High-speed generator and multilevel converter for energy recovery in automotive systems,” *IEEE Trans. Ind. Electron.*, vol. 59, no. 6, pp. 2678–2688, Jun. 2012

[6] Di Gerlando, G. Foglia, M. F. Iacchetti, and R. Perini, “Axial-flux PM machines with concentrated armature windings: Design analysis and test validation of wind energy generators,” *IEEE Trans. Ind. Electron.*, vol. 58, no. 9, pp. 3795–3805, Sep. 2011

[7] T. D. Nguyen, K.-J. Tseng, S. Zhang, and H. T. Nguyen, “A novel axial flux permanent-magnet machine for flywheel energy storage system: Design and analysis,” *IEEE Trans. Ind. Electron.*, vol. 58, no. 9, pp. 3784–3794, Sep. 2011

[8] D. N. Mbidi, K. van der Westhuizen, R. Wang, M. J. Kamper, and J. Blom, “Mechanical design considerations of a double stage axial-flux PM machine,” *IEEE IAS Conf*., vol. 1, pp. 198–201., 2000
[9] A. S. McDonald, M. A. Mueller, and H. Polinder, “Structural mass in direct-drive permanent magnet electrical generators,” *IET Renew. Power Gener*. vol. 2, no. 1, pp. 3–15, 2008.
[10] J. F. Geiras, R. J. Wang and M. J. Kamper, Axial-flux permanent magnet brushless machines, London: Kluwer academic publishers 2004
[11] P. Tavner, L. Ran, J. Penman and H. Sedding, “Condition monitoring of rotating electrical machines,” *IET Power and Energy series*, London, UK, 2008
[12] Zhang, P.; Neti, P., "Detection of Gearbox Bearing Defects using Electrical Signature Analysis for Doubly-fed Wind Generators," *Industry Applications, IEEE Transactions on* , vol.PP, no.99, pp.1,1, Dec. 2014
[13] Reddy, P.B.; El-Refaie, A.M.; Kum-Kang Huh, "Effect of Number of Layers on Performance of Fractional-Slot Concentrated-Windings Interior Permanent Magnet Machines," *Power Electronics, IEEE Transactions on* , vol.30, no.4, pp.2205,2218, April 2015
[14] R. Lisner and P. L. Timar, “A new approach to electric motor acoustic noise standards and test procedures,” *IEEE Trans. Energy Convers.*, vol. 14, no. 3, pp. 692–697, Sep. 1999
[15] G. H. Jang and D. K Lieu, “Vibration reduction in electric machine by interlocking of the magnets,” IEEE Trans.Magn., vol. 29, no. 2, pp. 1423– 1426, Mar. 1993
[16] M. Tsypkin, “Induction motor condition monitoring: vibration analysis technique - a twice line frequency component as a diagnostic tool,” IEEE International Electric Machines & Drives Conference (IEMDC), 2011
[17] Climente-Alarcon, V.; Antonino-Daviu, J.A.; Vedreno-Santos, F.; Puche-Panadero, R., "Vibration Transient Detection of Broken Rotor Bars by PSH Sidebands," *Industry Applications, IEEE Transactions on* , vol.49, no.6, pp.2576,2582, Nov.-Dec. 2013
[18] Seshadrinath, J.; Singh, B.; Panigrahi, B.K., "Investigation of Vibration Signatures for Multiple Fault Diagnosis in Variable Frequency Drives Using Complex Wavelets," *Power Electronics, IEEE Transactions on* , vol.29, no.2, pp.936,945, Feb. 2014
[19] Seshadrinath, J.; Singh, B.; Panigrahi, B.K., "Vibration Analysis Based Interturn Fault Diagnosis in Induction Machines," *Industrial Informatics, IEEE Transactions on* , vol.10, no.1, pp.340,350, Feb. 2014
[20] Valavi, M.; Nysveen, A.; Nilssen, R., "Analysis of a low-speed PM Wind generator with concentrated windings in eccentricity conditions," *Electrical Machines and Systems (ICEMS), 2013 International Conference on* , vol., no., pp.1266,1270, 26-29 Oct. 2013
[21] Zhu, Z.Q.; Ishak, D.; Howe, D.; Jintao Chen, "Unbalanced Magnetic Forces in Permanent-Magnet Brushless Machines With Diametrically Asymmetric Phase Windings," *Industry Applications, IEEE Transactions on* , vol.43, no.6, pp.1544,1553, Nov.-dec. 2007
[22] Chin, R.; Kanninen, P., "The Phenomenon of Magnetic Force: Estimating its Effects on Wind Turbine Generators," *Industry Applications Magazine, IEEE* , vol.19, no.4, pp.39,46, July-Aug. 2013
[23] Haodong Yang; Yangsheng Chen, "Influence of Radial Force Harmonics With Low Mode Number on Electromagnetic Vibration of PMSM," *Energy Conversion, IEEE Transactions on* , vol.29, no.1, pp.38,45, March 2014
[24] Zhu, Z.Q.; Xia, Z.P.; Wu, L.J.; Jewell, G.W., "Analytical Modeling and Finite-Element Computation of Radial Vibration Force in Fractional-Slot Permanent-Magnet Brushless Machines," *Industry Applications, IEEE Transactions on* , vol.46, no.5, pp.1908,1918, Sept.-Oct. 2010
[25] W. Zhu, S. Pekarek, B. Fahimi, and B. J. Deken, “Investigation of force generation in a permanent magnet synchronous machine,” *IEEE Trans. Energy Convers.*, vol. 22, no. 3, pp. 557–565, Sep. 2007

[26] P. Vijayraghavan and R. Krishnan, “Noise in electric machines,” *IEEE Trans. Ind. Appl.*, vol. 35, no. 5, pp. 1007–1014, Sep. 1999.
[27] J. F. Geiras and M. Wing, Permanent magnet motor technology, design and applications, second edition, Marcel Dekker, Inc. New York 2002
[28] Z. P. Xia, Z. Q. Zhu, L. J Wu and G. W. Jewell, "Comparison of radial and vibration Forces in 10-pole/12-slot fractional-slot surface-mounted and interior pm brushless AC machines," *International Conference on Electrical Machines*, Italy, September 2010
[29] Valavi, M.; Nysveen, A.; Nilssen, R., "Magnetic forces and vibration in permanent magnet machines with non-overlapping concentrated windings: A review," *Industrial Technology (ICIT), 2012 IEEE International Conference on* , vol., no., pp.977,984, 19-21 March 2012
[30] Z. Q. Zhu, Z. P. Xia, L. 1. Wu and G. W. Jewell, "Influence of slot and pole number combination on radial force and vibration modes in fractional slot PM brushless machines having single- and double-layer windings," *IEEE Energy Conversion Congress and Exposition (ECCE),* USA, September 2009
[31] Amara, Y.; Jiabin Wang; Howe, D., "Analytical prediction of eddy-current loss in modular tubular permanent-magnet machines," *Energy Conversion, IEEE Transactions on* , vol.20, no.4, pp.761,770, Dec. 2005
[32] Finley, W.R.; Hodowanec, M.M.; Holter, W.G., "An analytical approach to solving motor vibration problems," *Industry Applications, IEEE Transactions on* , vol.36, no.5, pp.1467,1480, Sep/Oct 2000
[33] J. G. Wanjiku, H. Jagau, M. A. Khan and P. S. Barendse. “Minimization of cogging torque in a small axial-flux PMSG with a parallel-teeth stator,” *IEEE Energy Conversion Congress and Exposition* 2011
[34] ISO13373-1:2002, Condition monitoring and diagnostics of machines, vibration condition monitoring, part 1: general procedures
[35] ISO13373-1:2005, Condition monitoring and diagnostics of machines, vibration condition monitoring, part 2: processing, analysis and presentation of vibration data
[36] Henao, H.; Capolino, G.-A.; Fernandez-Cabanas, M.; Filippetti, F.; Bruzzese, C.; Strangas, E.; Pusca, R.; Estima, J.; Riera-Guasp, M.; Hedayati-Kia, S., "Trends in Fault Diagnosis for Electrical Machines: A Review of Diagnostic Techniques," *Industrial Electronics Magazine, IEEE* , vol.8, no.2, pp.31,42, June 2014
[37] Rajagopalan, S.; Habetler, T.G.; Harley, R.G.; Restrepo, J.A.; Aller, J.M., "Non-Stationary Motor Fault Detection Using Recent Quadratic Time-Frequency Representations," *Industry Applications Conference, 2006. 41st IAS Annual Meeting. Conference Record of the 2006 IEEE* , vol.5, no., pp.2333,2339, 8-12 Oct. 2006
[38] Y. Zhao, L. E. Atlas, and R. J. Marks II, “The use of cone-shaped kernels for generalized time-frequency representations of nonstationary signals,” IEEE Trans. on Acoustics, Speech, and Signal Process., vol. 38, no. 7, pp. 1084-1091, 1990
[39] A. Grabner, “Analytical and numerical calculation of natural resonance frequencies in case of concentrated coil armature windings,” Canadian Conference on Electrical and Computer Engineering, Saskatoon, Sask. May 2005

Chapter 7
Detection of ISC Using Electrical Impedance Spectroscopy

7.1 Introduction

Failures which result from ISC faults may be very costly. Thus the advantage of the lead time between interturn faults and failure is the basis for the development of fault detection techniques to monitor the state of healthy of stator windings. A variety of online techniques have been developed and proposed as shown in chapter five. The demerits of these techniques are the complex calculations and feature extraction processes involved. Therefore in this chapter, to detect the presence of ISC in the experimental machine, a simple technique using input impedance spectroscopy is sought. The input impedance of electrical machines have been studied in literature due to increasing use of fast switching inverters at high frequencies (HFs) in variable speed drives. In [1]-[3], the problems of winding insulation damage, bearing current and electromagnetic interference caused by such HF switching are investigated. Impulse responses of low voltage machines at HFs are examined in [4]-[5]. Experimental input impedance model for electrical machines have also been presented in [4], [6]-[7]. The purpose of the models is to act as termination impedance when simulating voltage oscillations in the feeder cable between inverter and machine. Options for signal coupling in experimental measurements are also presented in [4]-[8], they are; *phase-phase, phase-neutral, phase-ground, three phase-ground and two phase-phase*. In [5], the following conclusions are made:

1. Input impedance is inductive and increases linearly as a function of frequency.

2. Skin effect affects the impedance at HFs.
3. Parallel resonance is reached at the highest input impedance.
4. Beyond the parallel resonant frequency f_0, input impedance becomes capacitive.

In this chapter, an impedance model is applied to analyse the effect of ISC at HFs. Input impedance is estimated by applying broadband multisine signal in an electrical impedance spectroscopy (EIS) scheme. Deviations of the measured impedance under ISC condition from reference impedance (healthy) is perused for fault indications.

7.2 Winding Impedance Model

It is imperative to note that there is a distinction between winding insulation monitoring to diagnose degradation prior to winding faults in high voltage (>3.3kV) machines and condition monitoring to detect ISC in low voltage (<600V) machines. In practice, the pre-warning of insulation degradation in low voltage machines is not diagnosed via online measurements but the resulting ISC fault is usually detected before failure sets in [9]. Thus in this chapter, the developed model does not evaluate turn-turn insulation degradation, a complex physical phenomenon, but forms the basis for analysing the input impedance response under turn-turn fault for detection purposes.

7.2.1 Coil Winding

In high voltage machines, the windings are made from form-wound coils and their positions in slots are well defined but the windings in low voltage machines may not be regularly defined making the position difficult to determine. Therefore an approximation of turn positioning in the stator core is used. The coil winding model is shown in Fig.7.1 based on physical placement of coils in stator slots. The consequence of insulation breakdown which leads to ISC is used to derive the model. Each turn (consists of resistive and inductive components) is isolated from other turns through

high resistance insulation although mutual inductive coupling and turn-turn capacitance exist between turns. Similarly, each turn is isolated from the stator core (ground) through high resistance insulation and there exists turn-ground capacitance between each turn and ground. Under ISC, electrical parameters related to turn-to-turn deviate from healthy to faulty conditions under ISC. The parameters in the model are listed in Table 7.1, where the units express their behaviour for both healthy and faulty scenarios. At the onset of ISC, as $R_{t1-t2} \rightarrow 0$, the effective per phase resistance decreases and a stronger mutual inductive coupling M_{t1-t2} between the healthy and shorted turns sets in. The consequence and overall effect of this behaviour is better determined by measuring the machine input impedance where that of a faulty machine may deviate from the healthy one.

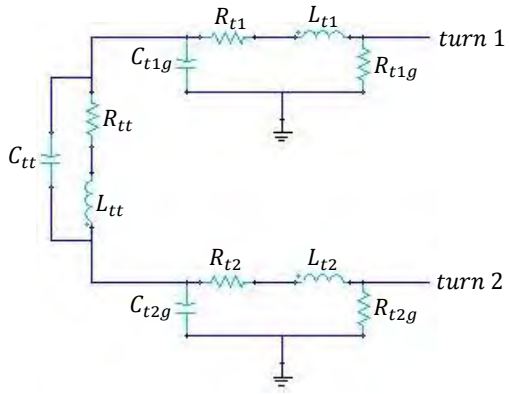

Fig.7.1. Coil winding model

Table7.1. Coil winding model parameters

Parameters	**Nomenclature**	**Unit (Healthy)**	**Unit (ISC)**
Resistance of each turn	R_{t1}, R_{t2}	mΩ	mΩ
Inductance of each turn	L_{t1}, L_{t2}	µH	µH
Resistance of turn to ground (stator core)	R_{t1g}, R_{t2g}	MΩ	MΩ
Capacitance of turn to ground (stator core)	C_{t1g}, C_{t2g}	pF	pF
Resistance between turns	R_{tt}	MΩ	mΩ
Mutual inductance between turns	L_{tt}	µH	mH
Capacitance between turns	C_{tt}	pF	pF

7.2.2 Input Impedance

Stray capacitances and leakage inductances start to affect the input impedance of electrical machines at HFs [5]. The stray capacitances are formed by the capacitance between adjacent coil turns C_{tt}, capacitance between a phase winding and the stator core and capacitance between phase windings of two phases. Correspondingly, leakage inductances are formed by mutual inductance between coil turns and mutual inductance between phase windings of two phases. The HF stray capacitances may produce sufficient reactance to nullify the magnitude of inductive reactance such that pure resistance is achieved at resonance. The equivalent circuit in Fig.7.2, where R_{hf} is HF winding resistance, L_{hf} is HF winding inductance C_{hf} is HF winding capacitance and R_c is the resistance of the magnetic core at high frequencies is thus derived to analyse HF resonance and the effect of ISC on input impedance. From the equivalent circuit, parallel resonance occurs in (7.1) when $wC = wL$; therefore since stator resistance increases with frequency and is inversely proportional to the number of shorted turns, significant change in impedance under ISC may become substantial at HF resonance.

$$Z^2 = \frac{R}{1+jR\left(wC-\frac{1}{wL}\right)} \tag{7.1}$$

7.3 Input Impedance Estimation Using Broadband Spectroscopy

Impedance measurement by injecting a carrier frequency into the machine and extracting information from the phase and amplitude of the impedance response has been used in several condition monitoring and control schemes [10]-[12]. Typically, the carrier frequency of the inverter drive which is much higher than the fundamental is used [11]. A major disadvantage of this method is the complex demodulation of the

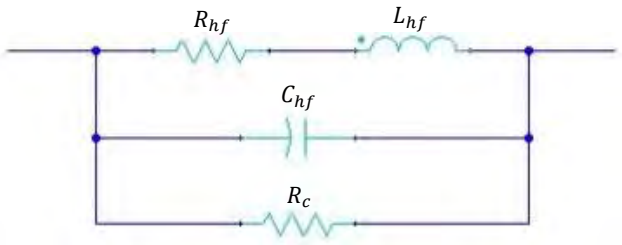

Fig.7.2. HF equivalent circuit

carrier frequency and the digital filtering involved. Also, the HF switching of the inverter needs to be continuously modified, making the method practically limited. The setup in Fig.7.3 is proposed to avoid the problems. It makes use of an external circuitry or source for HF excitation of the machine windings. In this way, the HF signal is decoupled from drive and is independent of inverter switching. The modification of the PWM pattern can be avoided and broadband EIS can be performed using periodic excitations. In addition, the signal to noise ratio is improved. The procedure for the broadband EIS is as follows:

1. Generate HF signal using a signal generator.
2. Amplifier the signal.
3. Inject the amplified signal into the windings.
4. Acquire v_{HF} and i_{HF} shown in Fig.7.4 using DAQ devices with sufficient bandwidth.
5. Determine the impedance magnitude, phase, real and imaginary components from the acquired information using the impedance-frequency (Z-f) response algorithm. An overview of the algorithm as implemented in LabVIEW® programming environment is described in Fig.7.4.

The generated HF signals are harmonically unrelated to the line frequency and are much smaller (70-80dB smaller) than the line voltage. This will ensure that the machine operation is not disrupted in an online scheme and to prevent signal saturation at high frequencies.

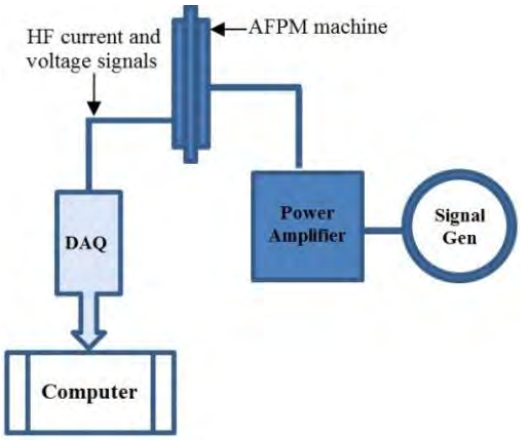

Fig.7.3. Schematic for the EIS test

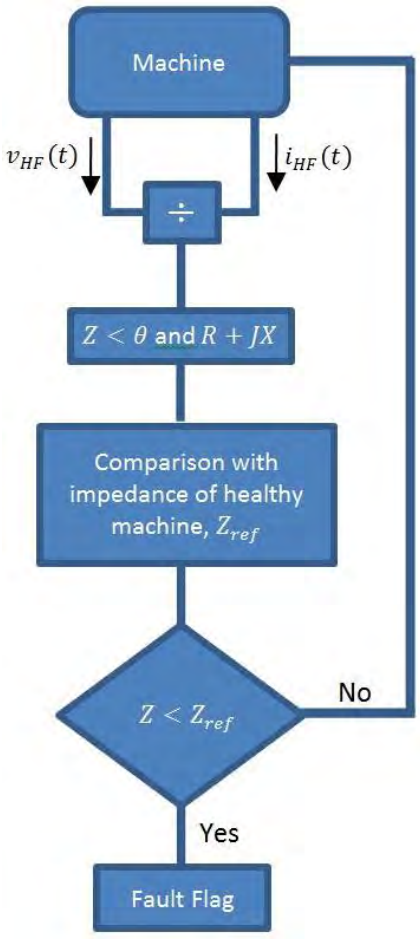

Fig.7.4. Impedance-frequency response algorithm

7.3.1 Multisine Excitation

The broadband EIS requires measurements and acquisition for each of the frequency points of interest. This takes considerable time and may be practically limited for real-time monitoring. A solution as proposed in electrochemical applications is to design a multisine signal to provide excitation at desired frequencies [14]-[15]. Multisine excitation has also been applied in power systems application; the power grid in the Western United States is probed with a multisine signal in order to validate their system models using ID on the measured response to the multisine probe [16]. This will reduce the measurement duration by exciting all desired frequencies simultaneously [15]. The time signal expression for a real-valued multisine signal can be represented by a trigonometric sum order in (7.2) [15], where N is the number of exciting frequencies, a_n are the fundamental amplitudes and φ_n are the phases. A broadband multisine excitation signal with flat amplitude spectrum and a bandwidth which covers the windings HF resonance was designed and coupled to the windings in an offline scheme.

$$x(t) = \Re e\left\{\sum_{n=1}^{N} a_n e^{j(2\pi f_n t+\varphi_n)}\right\} \tag{7.2}$$

7.4 Experimental Results

HF signals are applied to the machine and from measured HF voltages and currents, impedances are determined. From the impedance model, the feasibility of significant variations in impedance under ISC is expected at resonance; therefore it will be efficient to target frequencies in the vicinity of resonance rather than a wide range of frequencies. Also, targeting specific frequencies that are of interest in the input impedance spectrum is needed for an effective periodic multisine since the minimum frequency determines the signal length. To define this frequency distribution, a prior knowledge of the Z-f response of the machine is required. This is determined by sequentially exciting sinusoids over a wide range of frequencies. Fig.7.5 shows the Z-f

response as obtained by exciting frequencies between 50Hz-150kHz in a *phase-neutral* signal coupling mode. Notice that the variations in Z due to ISC are large in the bandwidth 10-50kHz, i.e., the vicinity of the parallel resonant frequency, as revealed in the phase information. Above and below the resonant region, no significant deviations are obtained.

In Fig.7.6, the result of the multisine excitation for the *phase-neutral* HF signal coupling is shown. It indicates that Z is a linear function of frequency before the resonant frequency at approximately 30kHz where the phase is zero. At f_0, HF capacitances stray in and a strong capacitive reactance builds up to cancel the inductive reactive components, thus Z becomes purely resistive as revealed in the Nyquist plot in Fig.7.7. Below f_0, Z is inductive and above f_0, it becomes capacitive. The magnitude of Z at resonance is at maximum, thereafter it drops in the capacitive region. Under ISC conditions, considerable decrease in Z is obtained; average of 10.95% and 20.01% for both 2turns and 4turns respectively. The decrease becomes substantial as f increases since winding resistance increases due to skin effect. Thus changes in Z at HF resonance can be used to determine the state of health of stator winding and detect the presence of ISC.

The Z-f responses for two other signal coupling options are presented in Fig.7.8-Fig.7.9. The Z-f characteristics derived for both are similar to that of *phase-neutral*. The only difference being the larger impedance magnitudes obtained. Among these options, *phase-neutral* is deemed best amenable to faulted phase identification because each phase can be tested independent of the others and also for online implementation since it is not intrusive. The tests are repeatable without significant deviation in results for both impedance and angle measurements.

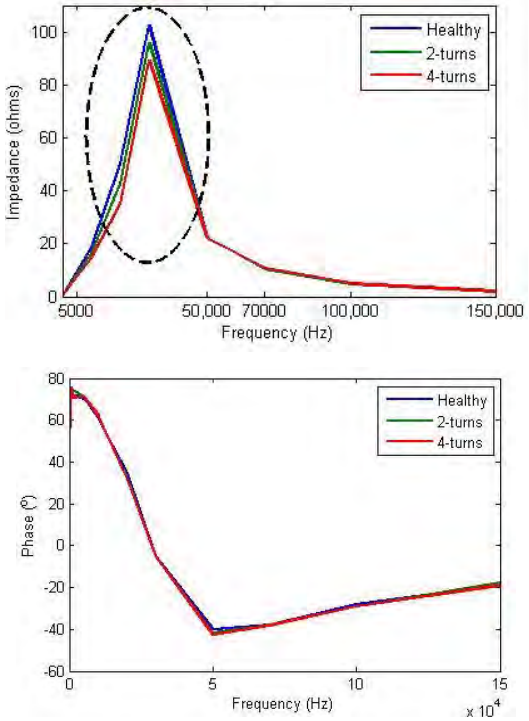

Fig.7.5. Input impedance in the signal coupling *phase-neutral*

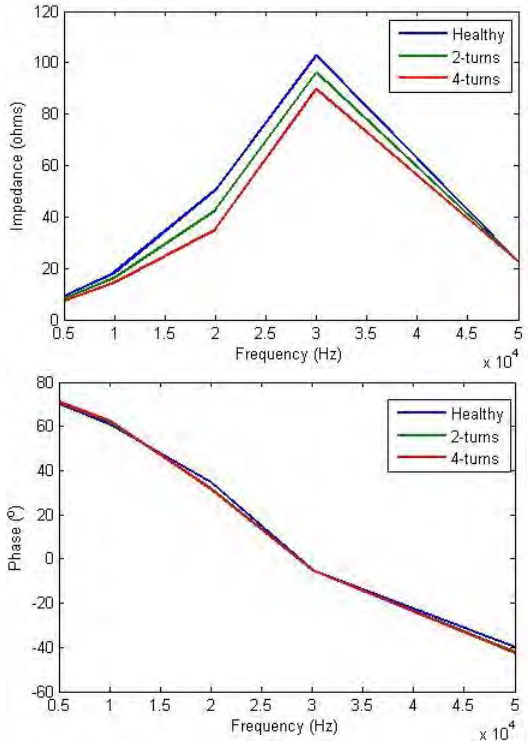

Fig.7.6. Input impedance in the resonant region for the signal coupling *phase-neutral*

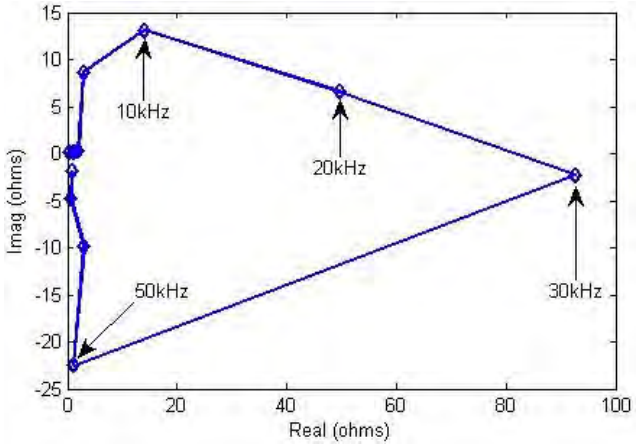

Fig.7.7. Nyquist plot of the input impedance

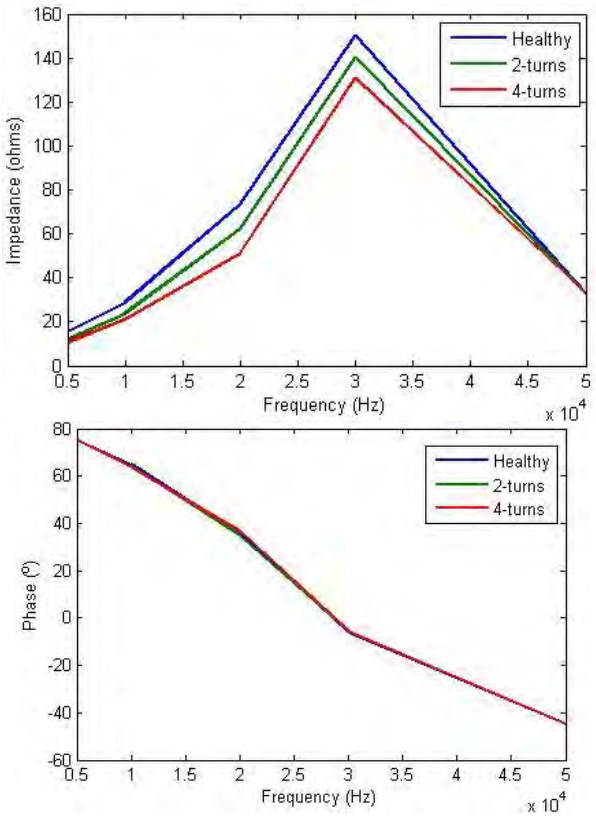

Fig.7.8. Input impedance in the resonant region for the signal coupling *phase-phase*

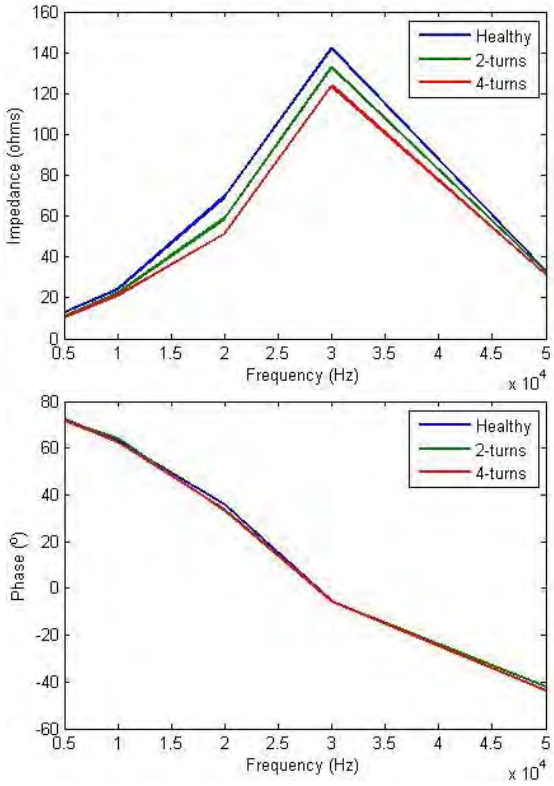

Fig.7.9. Input impedance in the resonant region for the signal coupling across *two phase to another phase*

7.5 Conclusions

A scheme to implement EIS and a model to analyse the result obtained from the EIS is presented. From the EIS, input impedance and its parameters are derived using a Z-f response measurement algorithm. Based on significant variations from a comparison of measured impedance with the reference impedance (healthy), stator winding faults can be detected. The method is simple; it avoids the complex feature extraction process involved using signal processing techniques.

7.6 References

[1] L. Saundm, G. S!4blinski, S. Evon, D. Kempkes, "Riding the Reflected Wave -IGBT Drive Technology Demands New Motor and Cable Considerations", IEEE Penoleurn and Chemical Indusny Confermce, Philadeplhia, PA, September 23-26, 1996, pp 75-84.

[2] T. Takahashi, M. Termeyer. H. Tsai, T. Lowery, "Motor Lead Length Issues for IGBT PWM Drives", EEE Pulp and Poper Conference, 1995, pp. 21-27.
[3] J.L. Guardado and K.J. Cornick, “Calculation of machine winding electrical parameters at high frequencies for switching transient studies”, IEEE Trans. Energy Conv., Vol. 11, pp. 33-40, 1996.
[4] J.L Guardado, J.A Flores, V. Venegas, J.L. Naredo and F.A. Uribe, “A machine winding model for switching transient studies using network synthesis”, IEEE Trans. Energy Conv., Vol. 20, pp.322-328, 2005.
[5] Ahola, J.; Lindh, T.; Partanen, J., "Simulation model for input impedance of low voltage electric motor at frequency band 10 kHz-30 MHz," *Electric Machines and Drives Conference, 2003. IEMDC'03. IEEE International* , vol.2, no., pp.1127,1132 vol.2, 1-4 June 2003
[6] Metwally, I.A., "Simulation of the impulse response of electrical machines," *Energy Conversion, IEEE Transactions on* , vol.14, no.4, pp.861,867, Dec 1999
[7] E. Zhong, T. Lip, "improvements in EMC Performance of Inverter-Fed Motor Drives", IEEE Transaction on Industry Applications, Vol. 21,No.6,Nov./Dec. 1995.
[8] D. Schlegel, G. WraIe, R. Kerlunan, G. Skibinski, "Rmant Tank Motor Model For Voltage Reflection Simulations With PWM Drivcs", Proceedings of the IEEE International Electrical machines and Drives Conference, Seattle, USA, 9-12 May 1999, pp- 463465
[9] Thomson, W.T.; Fenger, M., "Current signature analysis to detect induction motor faults," *Industry Applications Magazine, IEEE* , vol.7, no.4, pp.26,34, Jul/Aug 2001
[10] Perisse, F.; Werynski, P.; Roger, D., "A New Method for AC Machine Turn Insulation Diagnostic Based on High Frequency Resonances," *Dielectrics and Electrical Insulation, IEEE Transactions on* , vol.14, no.5, pp.1308,1315, October 2007
[11] Arellano-Padilla, J.; Sumner, M.; Gerada, C., "On-line detection of stator winding short-circuit faults in a PM machine using HF signal injection," *Electrical Machines, 2008. ICEM 2008. 18th International Conference on* , vol., no., pp.1,8, 6-9 Sept. 2008
[12] Seilmeier, M.; Ebersberger, S.; Piepenbreier, B., "HF Test Current Injection-Based Self-Sensing Control of PMSM for Low- and Zero-Speed Range Using Two-Degree-of-Freedom Current Control," *Industry Applications, IEEE Transactions on* , vol.51, no.3, pp.2268,2278, May-June 2015
[13] Shih-Chin Yang, "Saliency-Based Position Estimation of Permanent-Magnet Synchronous Machines Using Square-Wave Voltage Injection With a Single Current Sensor," *Industry Applications, IEEE Transactions on* , vol.51, no.2, pp.1561,1571, March-April 2015
[14] de Beer, C.; Barendse, P.S.; Pillay, P., "Fuel Cell Condition Monitoring Using Optimized Broadband Impedance Spectroscopy," *Industrial Electronics, IEEE Transactions on* , vol.62, no.8, pp.5306,5316, Aug. 2015
[15] B. Sanchez, G. Vandersteen, R. Bragos, and J. Schoukens, “Basics of broadband impedance spectroscopy measurements using periodic excitations,” Meas. Sci. Technol., vol. 23, no. 10, pp. 105501–105515, Aug. 2012
[16] J. W. Pierre, N. Zhou, F. K. Tuffner, J. F. Hauer, D. J. Trudnowski and W. A. Mittelstadt, "Probing Signal Design for Power System Identification," in *IEEE Transactions on Power Systems*, vol. 25, no. 2, pp. 835-843, May 2010.

Chapter 8
Conclusions and Recommendations

8.1 Overview of the Thesis

The findings from this thesis provide valuable insight into fault patterns in AFPM machines. The contributions made are disseminated in each chapter of the thesis. Specific attention was given to development of online fault detection techniques by overcoming challenges in the signal-based monitoring method. This was achieved by conducting detailed analysis of key fault signatures. To aid in the analysis, fault models that can be implemented in FEA and experimentation were developed. The models were tailored to accommodate healthy and faulted conditions while minimizing complexity and error. Implementation of signal processing techniques facilitated in establishing accurate fault detection techniques.

8.2 Conclusions

Based on the results and analyses presented, the following conclusions are drawn:

In chapter 2 the signal-based method of analyzing fault-indicators in electric machines is identified as best suited for online fault detection and consequently proposed to be applied in this thesis. Others methods such as the model/simulation-based and machine-theory-based are suitable for performance analysis of electrical machines under both healthy and faulty conditions but not in real-time. AI may recognize faults in real-time but fault characteristics and patterns must have been initially determined and set to train its network for successful online implementation,

hence its applications were limited in this thesis since the objectives are to identify fault patterns.

Chapter 3 presents the common faults associated with AFPM machines and the development of a test-rig for CM and the experimental work in this thesis. The test-rig serves as a platform for accurate and reliable fault replication, investigations and online CM system.

In chapter 4, various topologies of AFPM are investigated for performance under SE. It is shown in FEA and verified experimentally using torque and current signal that the DS topology is immune to SE while the SS topology is susceptible to it. It is also shown that under SE the CTMTs may limit the magnitudes of space harmonics in the SS topology. Fault detection technique which is robust against the CTMTs and load variations is established for the SS topology using the amplitudes of sub-harmonics frequencies as fault indicators. Finally, ESPRIT is applied as an alternative to FFT in extracting the fault harmonics to overcome the problem of long measurement duration which is characteristic of FFT.

Chapter 5 investigates the behaviour of ISC in AFPM machine using FEA. The results are verified experimentally. The DS topology is not immune to ISC faults unlike the case of SE. Fault features under steady-state and startup transient conditions are extracted from the line current. EPV is used to overcome the problem of poor fault discrimination of ISC from SE due to fault-frequency overlap in the line current.

In Chapter 6 VA is used as an alternative to MCSA in detecting SE since vibration signal is amenable to mechanical related faults. It is shown that there is a direct link between SE and vibratory levels and the location of transducers is important in achieving effective and resolute measurement of the vibrations. Vibratory tones excited by electromagnetic forces due to SE under both steady-state and transient conditions are identified and detection techniques are proposed.

In chapter 7, a model to analyse the input impedance of stator windings using EIS is presented. Qualitative information on the state of health is obtained. Diagnosis based

on the input the impedance and the parameters derived from frequency response measurement algorithm is proposed for ISC faults. The technique is advantageous because of its simplicity over signal processing techniques.

8.3 Recommendations and Future Work

The experimental work conducted in this thesis was done across steady-state and non-stationary conditions in order to cover possible scenarios that can occur during machine operation. It is possible to further the research by extending the conditions in future work and improve our understanding under more severe conditions. The concepts presented were verified and on small machine prototypes to provide a basis at a fundamental level without considering the dynamics in medium to large machines. Some further work might be required to apply the proposed diagnostic techniques in high-powered machines. It is also recommended that the EIS technique be further developed for online implementation.

8.4 Concluding Remarks

The condition monitoring of electrical machines has become part of industrial asset management. Thus the development of fault detection techniques for AFPM machines will provide a basis for prognostics and state of health monitoring that allow for reliable operation and life cycle extension in applications where AFPM machines are deployed.

Appendix A

Table A1. Server motor data

Specification	**Value**
Rated speed (rpm)	1500
Maximum speed (rpm)	3000
Rated torque (Nm)	19.1
Maximum torque (Nm)	57.29
Rated current (A)	19.4
Maximum current (A)	58.2
Torque constant (Nm/A)	0.98
Voltage constant (mV/rpm)	35
Encoder resolution (°)	0.0036
Weight (kg)	18.5

Table A2. Accelerometer parameters

Performance Parameter	**Value**
Sensitivity (±10 %)	101.9mV/g (10.392 mV/(m/s²))
Measurement range	±4900 m/s² pk
Frequency range (±5 %)	0.5 to 10000 Hz
Frequency range (±10 %)	0.3 to 15000 Hz
Resonant frequency	≥50 kHz
Broadband resolution (1)	0.005 m/s² rms

Appendix B

Experimental Procedure for Fault Investigation of Axial-Flux Permanent Magnet Machine

Date:

Researcher: Supervisor:

No load operation

To obtain the voltages signals from the machine in the absence of the load:

1. Ensure that the main isolator of the drive is de-energised, and then switch-off the loads from the machine terminals.
2. Energise the main isolator of the drive, press the start buttons on the control panel, then select the speed mode using the selector switch on the touch panel. Wait for the machine to run-up to maximum speed.
3. Then run the *LabView VI* to record the voltage signals for $30s$ and then save.

Loaded operation

For consistency, run the machine for approximately $15mins$ to warm-up on no-load. Once warmed-up, the load level can be adjusted by varying its resistance with the switches. The current flowing into the resistor is used to confirm the loading level. The load levels and current values are shown in Table

1. Switch-on the loads at the machine terminals as desired and energise the main isolator the main isolator of the drive.
2. Press the start buttons on the control panel, and then select the speed mode using the selector switch on the touch panel. Wait for the machine to run-up to maximum speed.
3. Then run the *LabView VI* to record the voltage signals for $30s$ and then save.

Table B1. Loading levels and current

Loading (%)	**Torque (Nm)**	**Current (A)**
100		
50		
0		

For each operation described, the following procedure is repeated for all loading levels. The procedure is applied to the steady state and transient operation.

Steady state operation

Run the *LabView VI* to record the signals for approximately $30s$ and then save.

Start-up transient operation

Adjust the drive acceleration duration to 10s. Run the *LabView VI* to record the signals acquired for approximately during that period.

Note: The following documentation is linked to this procedure:

Hazard identification and risk assessment form

3kW Servo Wind Generator Drive Manual

Assembly and Disassembly Procedure for AFPM Machine

Appendix C

Assembly and Disassembly Procedure for the Axial-Flux Permanent Magnet Machine

This documentation describes the procedure for assembling, disassembling the AFPM machine and storage of the high energy magnets

Disassembly Procedure

1. Loosen the screw on the rotor-shaft joint.
2. Loosen the coupling on the drive-machine joint.
3. Use the long bolts to hold both sides of the rotor discs, locking them firmly into the threaded holes of the discs, through the holes in the stator external frame. N/B: Place two nuts on a bolt such that they will be on opposite sides of the stator external frame when the bolt is fastened.
4. Use spanners to gradually and simultaneously tighten the nuts on the outer sides of both stator external frames so as to apply outward force/pull on both discs. As this is being done, constantly loosen the bolts on the inner side of stator external frames onto the discs to give allowance for further 'pulling apart' of the discs.
5. Observe for changes after a few pressures to be sure the rotor discs are pulling apart evenly away from the stator.
6. When the discs are between 5-7 cm away from the stator, loosen one of the stator external frames so as to enable the removal of either disc.

Assembly Procedure

1. Place the discs and stator external frames in the proper position as shown in Figure 1 with the bolts and nuts in positions as described in the *Disassembly Procedure* above.
2. Use spanners to gradually and simultaneously tighten the nuts on the inner sides of both stator external frames so as to apply inward force/push on both discs. As this is being done, constantly loosen the bolts on the outer side of stator external frames onto the discs to give allowance for further 'pulling together' of the discs.
3. Ensure that the bolts are holding the discs firmly despite the attractive force between rotor and stator.

4. Ensure that the discs are properly sited on the lips on the shaft by observing that mechanical clearance exists between the stator and discs.
5. When (4) is observed, remove the bolts and nuts.

Magnets/Rotor Discs Storage Procedure

Line up all the magnets by placing small sections of wood/plastic between two pieces. For the rotor discs, place them face-up on top of each other, with each surface covered with wooden boards. Store both in a safe box (carton) and keep both away from ferromagnetic materials (iron, steel etc.).

Note: The following documentation is linked to this procedure:

Hazard identification and risk assessment form

3kW Servo Wind Generator Drive Manual

Assembly and Disassembly Procedure for AFPM Machine